Gold nanoparticle arrays for biosensing

BIOS, EEMCS, University of Twente

Julia Kaptein

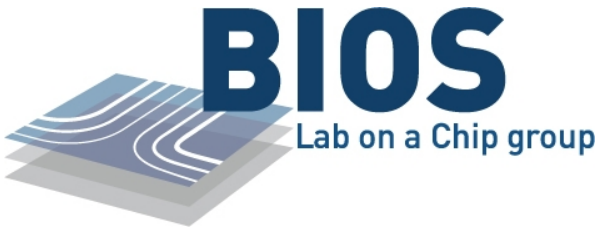

PROF.DR.IR. L.I. Segerink & J.T.W. Berendsen &
PROF.DR. S.M. García Blanco & J.E Van Dongen
BIOS, EEMCS
Netherlands
25-06-2020

UNIVERSITY OF TWENTE.

Abstract

Gold nanoparticles are increasingly used for biosensing purposes. This is because of the concept of localized surface plasmons which induces an enhancement in the electric near-field of gold nanoparticles and yields an oscillation of electrons in the visible range. In this case the purpose is early cancer detection, from urine, by looking at the red-shift of coupled gold nanoparticles. The scattering cross section and near-field enhancement of various shape size combinations is gathered and for shape size combinations that meet the requirements the scattering cross section upon coupling with nano spheres is gathered. Different distances from the spheres to the particles will be simulated. The simulations are done using the MNPBEM toolbox in MATLAB. This toolbox employs the boundary element method. The boundary method is a way of solving Maxwell equations only at the boundaries of particles which makes it fast in comparison to other toolboxes. It is found that multiple shape size combinations are valid for the purpose of this project, however a rod with a 60 nm diameter and a height of 100 nm is found to be the best suited since it shows a clear red-shift and has high peak wavelengths when both coupled and uncoupled. But most importantly it shows a strong near-field enhancement for the uncoupled particle.

Contents

1 Introduction

In the Netherlands, every hour, approximately 13 people are confronted with the diagnosis cancer. That is about 118.000 new patients every year in the Netherlands solely. The number of survivors has increased over the years, however in 2018 still approximately 45.000 people passed away [1]. The international numbers are even more dreadful. In 2018 over 17 million people got the diagnosis cancer and approximately 9.6 million passed away. This is more than half of the diagnosed patients [2]. In order to decrease the number of deaths by cancer, early detection is vital. Research into early detection of cancer is therefore taking off.

1.1 Cancer research with the use of gold nanoparticles

One of the projects looking into the early detection of (pre-)cancer is the Weijerhorst project. The project aims at early (pre-)cancer detection, using bio markers in urine. Precancerous cells are cells that partially behave like cancer cells. They, however, are not (yet) dangerous for the functioning of the body. A tumor consisting of precancerous cells is therefore called a benign tumor. The cells divide exceptionally fast, this is obvious since they lack the time to properly develop. An example is that some of these cells can have an extra nucleus. In the DNA it can be seen that tumor cells are divergent. They become malignant when they grow into tissue or metastases form[3]. Methylation of DNA is a process where methyl groups are added to a DNA molecule. This can change the activity of the DNA while the sequence remains unchanged. The methyl groups, that bind to the DNA, can disable certain genes. Methylation is a standard process in the body, since different cells need different parts of the DNA. When a person has (pre-)cancer, hypermethylation happens which disables the so called tumor suppressor genes that prevent cancer[4]. Research has shown that (pre-)cancer can be detected by looking at the hypermethylation, in this case from urine. The presence of one or more specific methylation markers can be an indicator of a type of (pre-)cancer an individual is likely to suffer from. By looking at hypermethylated DNA, multiple types of cancer can be detected. The type of methylation markers can tell which type of cancer is found in the sample. However, there are also markers that can indicate multiple kinds of cancer. These markers are called common markers. [3].

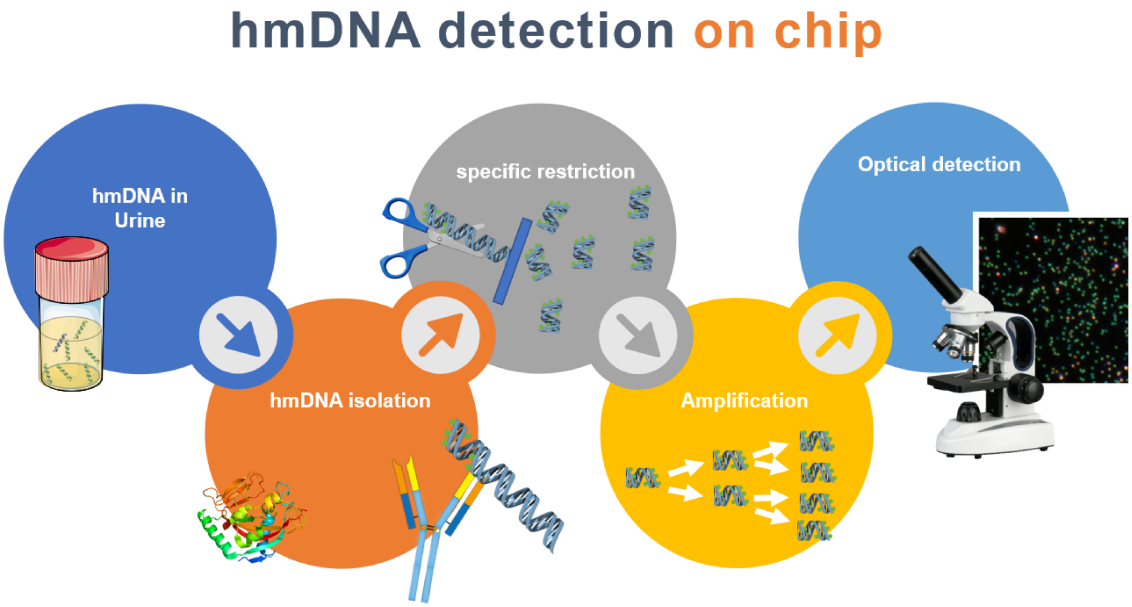

Figure 1: The different steps that are taken for detection on the microfluidic chip.

BIOS lap-on-a-chip group works on designing a microfluidic chip that implements all different parts that are shown in figure 1. A microfluidic chip is a chip that has a pattern of channels which direct the fluid, urine in this case, throughout the chip. At first the hmDNA must be isolated from the excess of the urine. Secondly specific restriction is needed to make sure the correct DNA sequences are amplified. This directly brings us to the amplification stage which is there to make sure there is enough hmDNA to be detected. Lastly the optical detection is required to identify whether the specific hmDNA is found in the sample.

1.2 Gold nanoparticles for biosensing

The use of noble metal nanoparticles in medical applications is increasing since they allow for faster and less invasive testing. In the category of noble metal nanoparticles, gold nanoparticles are most popular for biosensing applications. This is due to their biocompatibility, optical and electronic properties and their comparatively simple production and modification. The optical behavior of gold surfaces, where irradiation with light of one specific wavelength, causes an oscillation of the electrons in the conduction band is specifically important. This concept is called resonant surface plasmons which is explained in section 2.1[5].

1.3 Problem description

The focus of this thesis will be on the last step, namely, the optical detection. Figure 2 is a schematic description of what happens when the hmDNA gets in contact with an array of GNPs. First there is an island array filled with GNP's oscillating in the green range, 520 nm to 560 nm. Next a target sequence can partly complement with the desired DNA. Lastly a GNP functionalized with a gold nano sphere can complement with the target DNA which result in an optical redshift of the gold nanoparticle. However as described in section 2.1 the sensitivity of the GNPs is substantially dependent on the shape and size of the GNP. Therefore, simulations will be carried out with the MNPBEM toolbox in MATLAB. The corresponding fields of these shapes and sizes will be simulated, in addition to their spectra upon coupling with a range of sizes of DNA functionalized spherical gold nanoparticles (GNP's). This toolbox is explained in further detail in section 4.1. The GNPs will be placed on top of a substrate of SiO_2. Lastly a short overview of widely used fabrication methods can be found in appendix C. To sum things up, the aim of this study is to simulate different shapes and sizes of GNPs and also their spectra after coupling in order to find out which shape-size combination is optimal.

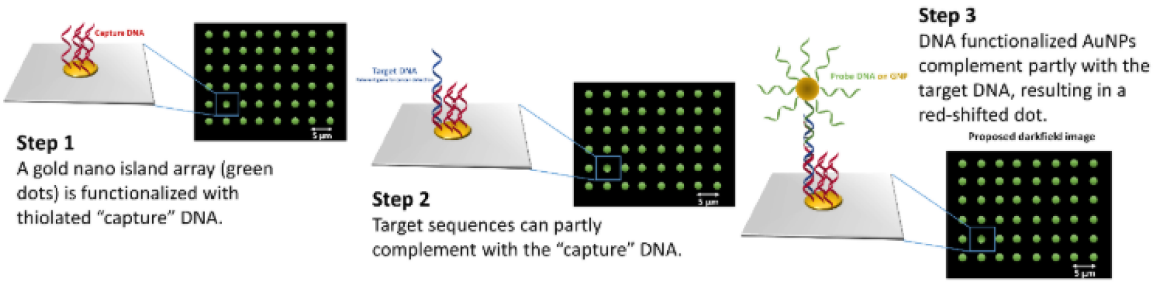

Figure 2: Schematic overview of DNA sensing by the use of gold nanoparticle arrays[6].

2 Theoretical background

2.1 Optical detection

Surface plasmon resonance (SPR) is a favored method for quantitative and real-time analysis. SPR can take place when p-polarized light, light with an electric field parallel to the plane of incidence, contacts

a thin metal film of approximately 50 nm thickness under total internal reflection (TIR). TIR is the phenomenon where specific surfaces, such as water, reflect like a mirror. For example when one looks at a lake one can see itself if looking with the right angle. Under TIR conditions, the free electrons of the metal film interact with the photons which results in a consistent oscillation of conduction electrons on both sides of the film. This concept is called surface plasmon resonance. Usually measurements are carried out by changing angles of incidence of the light beam. On the angle where minimal of reflectance occurs, surface plasmons are excited. This angle is called the resonance angle. The binding of biomolecules to the surface of this film causes the reflective index to change. Therefore, the SPR conditions change causing the resonance angle to shift. This shift is proportional to the quantity of the material that is bound to the sensor surface[7] .

2.1.1 LSPR

Localized SPR (LSPR)is a specific case of SPR where the light interacts with noble metallic nanoparticles. For noble metals, such as gold and silver, the resonant frequencies lie in the visible range of the electromagnetic spectrum. LSPR results in a strong enhancement of the scattering and absorption spectra and a strong local enhancement of the applied electric field as can be seen in figure 3[8].

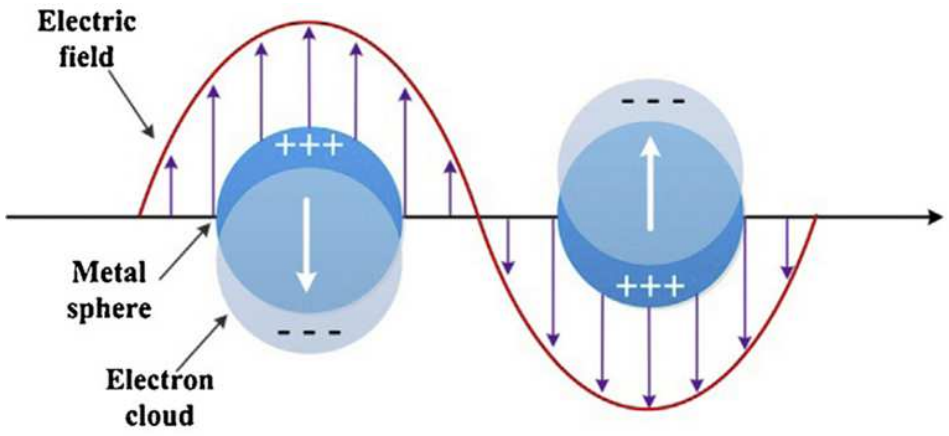

Figure 3: representation of the excitation of LSPR [9].

Noble metal nanoparticles are universally used for amplification of well accepted detection methods. Therefore, the LSPR of gold nanoparticles (GNPs) can also be taken advantage of to analyze certain concentrations. The difference between SPR and LSPR is the noble metal surface. Where SPR uses a continuous gold film, LSPR makes use of noble metal nanoparticles[10].

The sensitivity of the LSPR depends on the size and shape of the GNPs. GNP's with a larger size are likely to show higher peaks in the scattering cross section but also a higher peak wavelength. Furthermore sharp corners yield more resonance[7]. However, it was found that one GNP as an individual sensor does not show sufficient sensitivity, the addition of a second GNP results in a substantial improvement in sensitivity. This is because the particles are now likely to couple with each other which yields stronger resonance [7]. Gold and silver are most widely used for SPR sensing since their resonance peak is at a convenient location in the visible region, namely 400 nm to 700 nm. Gold is more stable in comparison to silver since silver is more sensitive to refractive index changes and more likely to react with ions from a buffer[11]. In the project an array of GNPs is used, therefore significant sensitivity will be assumed since, as stated before, the nanoparticles are likely to couple which enlarges the resonance.

2.1.2 Near-field enhancement

Near-field enhancement is a cornerstone aspect of optical interaction of nanoparticles. A system is in resonance when the eigen frequency of the collective electron oscillation, alternatively the plasma

frequency, matches the frequency of the electromagnetic wave. This resonance consequentially enhances the absorption of the light energy which in turn gives a preeminent near-field enhancement[12][13].The enhancement is at a maximum at the surface of the particle and decays both inside the particle and in a dielectric environment. In the case that two or more nanoparticles are in close proximity they will couple via their near-fields. This means that their LSPR modes couple. The resonance frequency is dependent on multiple aspects such as the distance between the particles, the size and the shape of the particles. Generally a red-shift can be observed when particles are coupled[14]. Furthermore, coupling is more likely to happen when the near-field enhancement is larger. Therefore, it is desired to have strong near-field enhancements. Moreover, when particles are in an array the behavior of the particles changes. One crucial effect is that the particle resonance frequency shifts because of the interference of particles. This can either be a red or blue shift depending on the polarization of the light. In the case of this project a red-shift will be observed for coupling in an array[15]. The near-field enhancement can be calculated numerical by following the following steps. Let start with assuming a perfect dipole. [16]

$$E_{in} = \nabla \phi_{in} \tag{1}$$

$$E_0 = \nabla \phi_0 \tag{2}$$

Where E_{in} and E_0 are the electromagnetic field inside and outside the particle. ϕ_{in} and ϕ_0 are the potentials which are given by the following equations which are Laplace equations

$$\nabla^2 \phi_{in} = 0 \tag{3}$$

$$\nabla^2 \phi_0 = 0 \tag{4}$$

At the particle boundary V_{in} is equal to V_0 which yield the following equation[8]:

$$\epsilon_{in} \frac{\delta \phi_{in}}{\delta r} = \epsilon_{out} \frac{\delta \phi_0}{\delta r} \tag{5}$$

Where ϵ_{in} and ϵ_{out} are the dielectric functions in and outside the particle and r is the distance to the particle center. The potential outside of the particle is given by the dipole potential which is given by Feynman as follows [17]:

$$\phi_{out} = -E_0 r cos\theta + \frac{\mathbf{p} \cdot \mathbf{r}}{4\pi\epsilon_0\epsilon_{out} r^3} \tag{6}$$

Where $\mathbf{P}$ is given by

$$\mathbf{p} = 4\pi\epsilon_0\epsilon_{out} R^3 \frac{\epsilon_{in} - \epsilon_0}{\epsilon_{in} + 2\epsilon_0} \mathbf{E}_0 \tag{7}$$

Where $2R$ is the distance between the poles of the dipole. θ is the angle between the observation point and the poles and ϵ_0 is the dielectric constant of free space. Next the polarizability is needed which is the ability of instantaneous forming of dipoles and is defined as follows[17]:

$$\alpha = \frac{\mathbf{p}}{\mathbf{E}\epsilon_0\epsilon_{out}} = 4\pi R^3 \frac{\epsilon_{in} - \epsilon_0}{\epsilon_{in} + 2\epsilon_0} \tag{8}$$

Taking into account that the dielectric function of metals is a complex function and depends on the angular frequency ω. The formula entails:

$$\epsilon_{in} = \epsilon_r(\omega) + i\epsilon_i(\omega) \tag{9}$$

Where the real and imaginary part are dependant on κ, which is the extinction coefficient, and n is the refractive index.

$$\epsilon_r(\omega) = n^2 - \kappa^2 \tag{10}$$

$$\epsilon_i(\omega) = 2n\kappa \tag{11}$$

By taking a close look at the polarizability it can be seen that there is a resonant enhancement when $|\epsilon_{in} + 2\epsilon_{out}|$ is minimal. When $Im[\epsilon_{in}]$ is small or slowly varying around the resonance frequency the following condition arises:

$$Re[\epsilon_{in}(\omega)] = -2\epsilon_{out} \tag{12}$$

Now with a lot of rewriting a formula for $\mathbf{E}_{out}$ can be found and is as follows

$$\mathbf{E}_{out} = -\nabla\phi_{out} = \mathbf{E}_0 + \frac{3\mathbf{n}(\mathbf{n}\cdot\mathbf{p}) - \mathbf{p}}{4\pi\epsilon_0\epsilon_{out}r^3} \tag{13}$$

Where the vector $\mathbf{n}$ points from the position of the dipole to the observation point and $\mathbf{p}$ is defined as

$$\mathbf{p} = \epsilon_0\epsilon_{out}\alpha\mathbf{E}_0 \tag{14}$$

It is possible to rewrite the formula for the field $\mathbf{E}_{out}$ into Cartesian coordinates. This is however not included. [17][18][8]

2.2 Boundary Element Method

First the BEM without layer structure will be explained step by step followed by a stepwise description of BEM with layer structure. For both cases the full Maxwell equations are explained and not the quasistatic approximation. The quasistatic approximation can be employed when the particle size is considerably, over a factor 10, smaller than the wavelength of visible light which is 400 nm to 700 nm. In this case the approximation would not be suitable since particle sizes up to 180 nm are considered.

The BEM approach works exclusively for dielectric environments, described through local and isotropic dielectric functions $\varepsilon_j(\omega)$. In addition the particles have to be separated by sharp boundaries. The main elements for the BEM approach are:

- dielectric bodies V
- boundaries between dielectric bodies ∂V
- outer surface normals used to define the in- and outside of a particle $\mathbf{n}$
- dielectric functions for the in- and outside of the particle ε_1 and ε_2

An illustration of these variables can be seen in figure 4.

A good starting point is at the Maxwell equations in frequency space ω, which are valid for sources in dielectric environments, as can be found below[17][19]

$$\nabla\cdot\mathbf{D} = 4\pi\rho \tag{15}$$

$$\nabla\times\mathbf{H} + ik\mathbf{D} = \frac{4\pi}{c}\mathbf{j} \tag{16}$$

$$\nabla\cdot\mathbf{B} = 0 \tag{17}$$

$$\nabla\times\mathbf{E} - ik\mathbf{B} = \nabla\times\mathbf{E} + \frac{\partial\mathbf{B}}{\partial t} = 0 \tag{18}$$

Where $k = \omega/c$ and in this case c is the speed of light in vacuum. $\mathbf{D} = \varepsilon\mathbf{E}$ which gives the electric displacement where ϵ is the permittivity of the dielectric. $\mathbf{B} = \mu\mathbf{H}$ is the magnetic permeability where is assumed $\mu = 1$ and $\mathbf{H}$ is the magnetizing field vector which is in this case equal to the magnetic permeability. $\mathbf{E}$ is the electric field, ρ is electric charge density and $\mathbf{j}$ is the electric current density. The fundamental elements of the BEM approach are the scalar and vector potentials $\Phi(\mathbf{r})$ and $\mathbf{A}(\mathbf{r})$. Equation 21 can be found since equation 17 states that the divergence is always equal to zero and

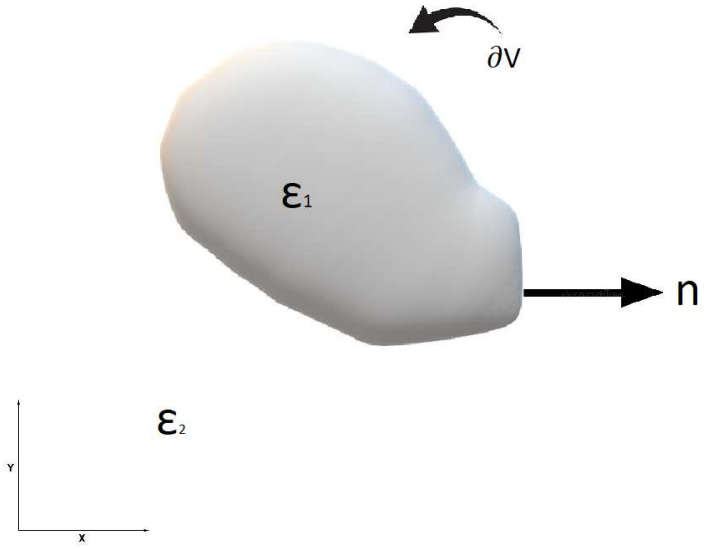

Figure 4: Schematic drawing showing variables needed for the boundary element method.

therefore **B** can be written as the curl of an other vector field, which can be mathematically proven with equation 19[17].

$$\nabla \cdot (\nabla \times \mathbf{A}) = 0 \tag{19}$$

$$\nabla \cdot \mathbf{B} = \nabla \cdot (\nabla \times \mathbf{A}) = 0 \tag{20}$$

$$\mathbf{B} = \nabla \times \mathbf{A} \tag{21}$$

The equation for **E** is derived below. The derivatives of the field of **A** and **B** are very similar since they both describe a vector field. It is important to keep in mind that when the curl is zero there is a gradient, this is a basic vector calculus rule.

$$\nabla \times \mathbf{E} = \frac{\partial}{\partial t} \nabla \times \mathbf{A} \rightarrow \nabla \times (\mathbf{E} + \frac{\partial \mathbf{A}}{\partial t}) = 0 \rightarrow \mathbf{E} + \frac{\partial \mathbf{A}}{\partial t} = -\nabla \Phi \tag{22}$$

$$\mathbf{E} = ik\mathbf{A} - \nabla \cdot \Phi \tag{23}$$

The Lorentz gauge condition, $\nabla \cdot \mathbf{A} = ik\varepsilon\Phi$, connects the potentials. The next step is to introduce the Green function derived from the Helmholtz equation. The following equation describes the Fourier transform of the homogeneous wave equation with the implementation of the Green function.

$$(\nabla^2 + k_j^2) G_j(\mathbf{r} - \mathbf{r}') = -4\pi\delta(\mathbf{r} - \mathbf{r}') \tag{24}$$

The Green function for Poisson is as follows and needed for the next step [20]:

$$\nabla^2 \phi = -\frac{\rho}{\varepsilon_0} \tag{25}$$

which is a solution to

$$\nabla^2 G_j(\mathbf{r} - \mathbf{r}') = \delta(\mathbf{r} - \mathbf{r}') \tag{26}$$

When taking into account the Poisson equation 25 which is the $k \to 0$ limit of equation 24 . This leaves multiple options for G however the following is chosen:

$$G_j(\mathbf{r}-\mathbf{r}') = \frac{e^{ik_j|\mathbf{r}-\mathbf{r}'|}}{\mid \mathbf{r}-\mathbf{r}' \mid} \tag{27}$$

Where k_j is the wave number is medium $\mathbf{r} \epsilon V_j$ and can be described with the formula $k_j = \sqrt{\varepsilon_j}k$.

This is where it gets complicated. Here the solutions of the Maxwell equations in ad-hoc form are introduced, for an inhomogeneous dielectric environment, as described by Hohenester, Waxenegger and Trugler [19], as follows:

$$\Phi_j(\mathbf{r}) = \Phi_j^e(\mathbf{r}) + \oint_{\partial V_j} G_j(\mathbf{r},\mathbf{s})\sigma_j(\mathbf{s})da \tag{28}$$

$$\mathbf{A}_j(\mathbf{r}) = \mathbf{A}_j^e(\mathbf{r}) + \oint_{\partial V_j} G_j(\mathbf{r},\mathbf{s})\mathbf{h}_j(\mathbf{s})da \tag{29}$$

$\Phi_j(\mathbf{r})$ and $\mathbf{A}_j(\mathbf{r})$ are in this case the scalar and vector potentials which characterize the external disruption within a given medium j. $\Phi_j^e(\mathbf{r})$ and $\mathbf{A}_j^e(\mathbf{r})$ are the solutions of the homogeneous wave equation. $\mathbf{A_j}$ is essentially the sum of the homogeneous solution and a rewritten version of equation 16. σ_j is the surface charge and $\mathbf{h}_j$ describes the current distributions, which are chosen such that the Maxwell equations boundary conditions hold at the interfaces between regions of deviating permittivities ε_j.

The next step is to introduce a matrix notation, in the form of $G\sigma$ instead of the integration used in equation 28. This allows for alteration to the BEM approach, where the boundary is divided into elements of finite size suitable for numerical implementation. σ_1 and $\mathbf{h}_1$ denote the surface charge and current inside the particles and σ_2 and $\mathbf{h}_2$ the surface charge and current outside the particle boundary. In accordance the continuity of scalar and vector potentials are obtained at the particle boundaries with the following equations:

$$G_1\sigma_1 - G_2\sigma_2 = \Phi_2^e - \Phi_1^e \tag{30}$$

$$G_1\mathbf{h}_1 - G_2\mathbf{h}_2 = \mathbf{A}_2^e - \mathbf{A}_1^e \tag{31}$$

Taking into account the Lorentz gauge condition and the dielectric displacement at the boundary of the particle, as stated in the beginning of this section, after a lot of rewriting the following equations are obtained:

$$H_1\mathbf{h}_1 - H_2\mathbf{h}_2 - ik\hat{\mathbf{n}}(\varepsilon_1 G_1\sigma_1 - \varepsilon_2 G_2\sigma_2) = \alpha \tag{32}$$

$$\alpha = (\hat{\mathbf{n}}\cdot\nabla)(\mathbf{A}_2^e - \mathbf{A}_1^e) + ik\hat{\mathbf{n}}(\varepsilon_1\Phi_1^e - \varepsilon_2\Phi_2^e) \tag{33}$$

$$\varepsilon_1 H_1\sigma_1 - \varepsilon_2 H_2\sigma_2 - ik\hat{\mathbf{n}}(\varepsilon_1 G_1\mathbf{h}_1 - \varepsilon_2 G_2\mathbf{h}_2) = D^e \tag{34}$$

$$D^e = \hat{\mathbf{n}}\cdot[\varepsilon_1(ik\mathbf{A}_1^e - \nabla\Phi_1^e) - \varepsilon_2(ik\mathbf{A}_2^e - \nabla\Phi_2^e)] \tag{35}$$

Where $\hat{\mathbf{n}}$ is the outer surface normal of the boundary ∂V, and the surface derivative of the green function is $H_{1,2} = (\hat{\mathbf{n}}\cdot\nabla)G_{1,2} \pm 2\pi$. Equations 33, 34 and 35 form a set of coupled equations that can be solved with use of the BEM approach in order to retrieve the surface charges and currents[19] [20].

Now BEM equations with layer structure will be explained. The foundation of the BEM approach using layer structure is as follows. Presume a substrate or layer structure where the outer surface normal point upwards in the z-direction. Analysis of equation 34 and 35 shows that in the first case the parallel component of $\mathbf{h}^{||}$, which lies in the xy-plane, does not couple with σ and $h^{\perp}$, which point in the z-direction. In the second case $h^{\perp}$ and σ couple due to layer interactions. A nanoparticle located in a dielectric environment of a layer structure is considered. Next it is assumed that all boundary elements that are connected to the layer structure are outer elements. The potentials inside the

particles can still be expressed using equation 28 and 29. For the outside elements certain adjustments have to be made. For the first case G has to be replaced by the Green function for layer structures and for the second case there has to be accounted for the fact that $h_2^{\perp}$ and σ_2 become coupled. The following equations described by Hohenester, Waxenegger and Trugler [19] describe the scalar and vector potentials taking the layer structure into account.

$$\Phi_2 = \Phi_2^e + G_2^{\sigma\sigma}\sigma_2 + G_2^{\sigma h}h_2^{\perp} \tag{36}$$

$$A_2^{\perp} = A_2^{e\perp} + G_2^{hh}h_2^{\perp} + G_2^{h\sigma} \tag{37}$$

Now the BEM equations of the case without layer structure are re-derived for layer structures.

$$\phi = \Phi_2^e - \Phi_1^e \tag{38}$$

$$\mathbf{a} = \mathbf{A}_2^e - \mathbf{A}_1^e \tag{39}$$

$$G_1\sigma_1 = G_2^{\sigma\sigma}\sigma_2 + G_2^{\sigma h}h_2^{\perp} + \phi \tag{40}$$

$$G_1\mathbf{h}_1^{||} = G_2\mathbf{h}_2^{||} + \mathbf{a}^{||} \tag{41}$$

$$G_1h_1^{\perp} = G_2^{hh}h_2^{\perp} + G_2^{h\sigma}\sigma_2 + a^{\perp} \tag{42}$$

The next step is implementing the continuity of the Lorentz Gauge condition. Which after a great deal of rewriting yields the following equations:

$$H_1\mathbf{h}_1^{||} - H_2\mathbf{h}_2^{||} - ik\hat{\mathbf{n}}^{||}(\varepsilon_1G_1\sigma_1 - \varepsilon_2G_2^{\sigma\sigma}\sigma_2 - \varepsilon_2G_2^{\sigma h}h_2^{\perp}) = \alpha^{||} \tag{43}$$

$$H_1h_1^{\perp} - H_2^{hh}h_2^{perp} - H^{h\sigma}\sigma_2 - ik\hat{n}^{\perp}(\varepsilon_1G_1\sigma_1 - \varepsilon_2G_2^{\sigma\sigma}\sigma_2 - \varepsilon_2G_2^{\sigma h}h_2^{\perp}) = \alpha^{\perp} \tag{44}$$

The continuity of the dielectric displacement becomes:

$$\begin{aligned}\varepsilon_1H_1\sigma_1 - \varepsilon_2H_2^{\sigma\sigma} - \varepsilon_2H^{\sigma h}h_2^{\perp} - ik\hat{\mathbf{n}}^{||}\cdot(\varepsilon_1G_1{\mathbf{h}^{||}}_1 - \varepsilon_2G_2^{||}{\mathbf{h}^{||}}_2)\\ -ik\hat{n}^{\perp}(\varepsilon_1G_1{h^{\perp}}_1 - \varepsilon_2G_2^{hh}{h^{\perp}}_2 - \varepsilon_2G^{\sigma h}\sigma_2) = D^e\end{aligned} \tag{45}$$

In order to get the surface charges and currents, equation 38, 39, 40, 41, 42, 43, 44 and 45 have to be solved. Consecutively to get the working equations for BEM with layer structure, rearranging is required. This gives the following equations after a lot of rewriting and simplifying:

$$\begin{aligned}(\varepsilon_1\Sigma_1G_2^{\sigma\sigma} - \varepsilon_2H_2^{\sigma\sigma})\sigma_2 + (\varepsilon_1\Sigma_1G_2^{\sigma h} - \varepsilon_2H_2^{\sigma h})h_2^{\perp} - ik\hat{\mathbf{n}}^{||}\cdot\Gamma\hat{\mathbf{n}}^{||}(\varepsilon_1 - \varepsilon_2)\\ (G_2^{\sigma\sigma}\sigma_2 + G_2^{\sigma h}h_2^{\perp}) - ik\hat{n}^{\perp}(\varepsilon_1 - \varepsilon_2)(G_2^{h\sigma}\sigma_2 + G_2^{hh}h_2^{\perp})\\ = D^e - \varepsilon_1\Sigma_1\phi + ik\hat{\mathbf{n}}\cdot\varepsilon_1\mathbf{a} + \hat{\mathbf{n}}^{||}\cdot\Gamma(\alpha^{||} - \Sigma_1\mathbf{a}^{||} + ik\hat{\mathbf{n}}^{||}\varepsilon_1\phi)\end{aligned} \tag{46}$$

$$\begin{aligned}(\Sigma_1G_2^{h\sigma} - H_2^{h\sigma})\sigma_2 + (\Sigma_1G_2^{hh} - H_2^{hh})h_2^{\perp} - ik\hat{n}^{\perp}(\varepsilon_1 - \varepsilon_2)\\ (G_2^{\sigma\sigma}\sigma_2 + G_2^{\sigma h}h_2^{\perp}) = \alpha^{\perp} - \Sigma_1a^{\perp} + ik\hat{n}^{\perp}\varepsilon_1\phi\end{aligned} \tag{47}$$

Where $\Sigma_1 = H_1G_1^{-1}$, $\Sigma_2^{||} = H_2^{||}G^{||(-1)}$ and $\Gamma = ik(\varepsilon_1 - \varepsilon_2)(\Sigma_1 - \Sigma_2^{||})^{-1}$. Equations 46 and 47 can be interpreted as a matrix equation for $(\sigma_2, h_2^{\perp})$ and can be solved through matrix inversion. Once σ_2 and $h_2^{\perp}$ are gathered, $\mathbf{h}_2^{||}$ can be obtained through the solution of:

$$(\Sigma_1 - \Sigma_2^{||})G_2^{||}\mathbf{h}_2^{||} = ik\hat{\mathbf{n}}^{||}(\varepsilon_2 - \varepsilon_1)(G_2^{\sigma}\sigma_2 + G_2^{h}h_2^{\perp}) + \alpha^{||} - \Sigma_1\mathbf{a}^{||} + ik\hat{\mathbf{n}}^{||}\varepsilon_1\phi \tag{48}$$

Additionally σ_1 and $\mathbf{h}_1$ can be obtained through the solutions of equations 38, 39, 40, 41 and 42. Solving equations 46 and 47 is more challenging however still possible using a numerical approach. However in this case the equations will be solved using the MNPBEM toolbox in MATLAB [19] [20] [17][18] [21] [22]].

2.2.1 Green functions

The Green functions ($G_2^{||}$, $G_2^{\sigma\sigma}$, $G_2^{\sigma h}$, $G_2^{h\sigma}$ and G_2^{hh}) are crucial functions for the BEM approach for layer structures. In this section their computation will be discussed shortly. Take for example a boundary element with surface charges σ and currents $\mathbf{h}$ in a layer structure. σ and $\mathbf{h}$ lead to potentials $\Phi^e = g\sigma$ and $\mathbf{A}^e = g\mathbf{h}$ affecting the interfaces of the layer structure. Calculation of the reflected Green functions is a process of three steps: First, the position of a set of sources in space has to be defined; Secondly, the surface charges and currents, at a substrate or a layer structure, for each source are calculated; Lastly, the scalar and vector potentials generated by the point sources and influenced by the substrate or layer structure are computed[19].

2.2.2 Required results

In order to get appropriate results it is essential to know which values must be compared. A doublet of results is needed for each separate shape and size combination. The required information consists of the near-field enhancement of the particle. As stated in section 2.1.2 a stronger field enhancement increases the chance at coupling. In addition, the scattering cross section is required. This information is needed to find out the peak wavelength and the intensity of the peak. It is desired to have a size, shape combination with a steep peak at the desired wavelengths and a strong field enhancement. For each shape the optimal size will be determined and for this size the scattering cross section upon coupling with spheres of 20 nm, 40 nm and 60 nm. The angle the sphere will have with respect to the particle will be determined with help of the near-field enhancement plots.

3 Hypothesis

When simulations are performed on different sizes and shapes of GNPs, different scattering spectra will be gathered. When these spectra are compared to the spectra for coupling with different sizes DNA functionalized GNP's it is expected to find that some shapes are more useful than others, for the purpose of this project. Useful being shapes with a strong near-field enhancement and a clear peak in the green light range for uncoupled particles and in the red light range for coupled particles. The shapes that are expected to be useful are non-spherical particles. This is the expectation since it was stated that sharp corners yield strong near-field enhancements. When two particles with near-field enhancements are significantly close, maximum 40 nm distance, their electric field couples which leads to a red-shift in the scattering cross section and a large coupled field[23]. The second aspect that can influence the optical shift in the spectrum is the size of GNPs. The expectation is that larger GNPs will lead to a larger optical shift if being coupled. This is based upon the experiment explained by Verdoold (p95-p100) [7]. Furthermore, when the size of a GNP increases the peak wavelength will red-shift [24]. Because of this the size is expected to be neither small nor large thus in the area ranging from 60 nm to 140 nm since this will likely yield the highest peak wavelength in the green light range.

4 Method

4.1 MNPBEM toolbox in MATLAB

The MNPBEM toolbox allows simulations of metallic nanoparticles (MNP) with the use of the boundary element method (BEM). The toolbox solves Maxwell equations for metallic nanoparticles in a dielectric environment. It theoretically works for arbitrary dielectric bodies which show dielectric properties and are separated by abrupt surfaces. However, the toolbox is designed and tested for particles with diameters of a few to a few hundred nanometers and for frequencies in the optical and near infrared range[25].
The toolbox is less general in comparison to other tool kits that can be used to solve Maxwell equations. Other tool kits use for example the finite difference time domain (FDTD) approach or the dyadic Green function technique[25]. This toolbox assumes a dielectric environment where bodies with isotropic and homogeneous dielectric functions are parted by abrupt interfaces. This mostly differs since the other

tool kits assume a general inhomogeneous dielectric environment. This also leads to the advantage that only the boundaries between different dielectrics have to be discretized and not the entire volume. This results in faster simulations which also takes up less memory[25]. The units that are used in the toolbox are Gauss units, that means that for example, that lengths are measured in nanometers. Furthermore, the light wavelength λ (in vacuum) is also in nanometers[25].

4.1.1 BEM in the toolbox

There are three kinds of BEM solvers implemented in the MATLAB toolbox. These are categorized in Quasistatic solvers and a full solver. The quasisatic solvers are based upon the quasistatic approximation. Instead of solving the Helmholtz equation for the vector and scalar potentials the Poisson or Laplace equation is used. This approximation holds for particles that are significantly smaller than the light wavelength. This is a simpler process and is therefore faster. The quasistatic solvers bemstat and bemstateig are used to give a fair approximation of the results. Especially for particles with sizes significantly smaller than the light wavelength they work properly. The full BEM solver uses the full Maxwell equations as elaborated upon in section 2.2 and is therefore considerably slower. For a particle with N faces there are N^3 matrix inversions needed. The results, however, are very precise[25].

For this purpose the full BEM solvers are operated since particle sizes up to 180 nm are considered which is not considerably smaller than the light wavelength which ranges from 400 nm to 900 nm.

4.2 Simulation details

The particles will be all simulated on a substrate of SiO_2 and in air. The near-field will be scaled with the particle size in order to be able to compare them properly. The scale is from minus the particles size to plus the particle size horizontally and the same vertically only then there is an offset because of the substrate. The shape size combinations that are found to be favorable are coupled with spheres of 20 nm, 40 nm and 60 nm. The spheres are distanced between 5 nm and 40 nm from the particles to have a valid chance of coupling. This was a set condition to make sure coupling will be possibly. Below three tables can be found with the parameters of the simulations or the various shapes. The diameter will be the exact diameter since this MATLAB provides a theoretical approach. The incidence angle of 90 degrees is chosen since this is commonly used in all papers that were used for validation and other purposes[8][11][19][25][26]. The wavelength of 540 nm is chosen since it is in the middle of the green range. Lastly, the 1 nm distance to the substrate is chosen since to particle is on the substrate but not merged with the substrate.

Shape	Sphere	Cube
Size [nm]	Diameter: 20, 40 , 60, 80, 100, 120, 140, 160, 180	Sides: 20, 40, 60, 80, 100, 120, 140, 160, 180
Distance to substrate [nm]	1	
Angle of incidence [degree]	90	
Wavelength used for near-field [nm]	540	

Table 1: Table displaying the simulation properties of the sphere and the cube.

Shape	Rod	Triangle
Size [nm]	Diameter: 20, 40 , 60, 80, 100, 120, 140, 160, 180 Height: 10, 50, 75, 100	Sides: 20, 40 , 60, 80, 100, 120, 140, 160, 180 Height: 10, 50, 75, 100
Distance to substrate [nm]	1	1
Angle of incidence [degree]	90	90
Wavelength used for near-field [nm]	540	540

Table 2: Table displaying the simulation properties of the rod and the triangle.

Shape	Torus
Size [nm]	Outside diameter: 20, 40 , 60, 80, 100, 120, 140, 160, 180 Inside diameter: 10, 20, 30, 40, 50, 60, 70, 80, 90, 100, 110, 120, 130, 140, 150, 160, 170
Distance to substrate [nm]	1
Angle of incidence [degree]	90
Wavelength used for near-field [nm]	540

Table 3: Table displaying the simulation properties of the torus.

5 Experiments

5.1 Validation

It is important to validate the code before using it. Otherwise the results are not trustworthy. In this case more than one validation is needed to examine whether the code is accurate. This is since separate parts of the code are validated with different papers. The separate parts are: scattering cross sections for uncoupled particles, near-field enhancements for uncoupled particles and scattering cross sections for coupled particles.

5.1.1 Validation for single GNP's

The code for separate GNP's is validated using the paper of Waxenegger, Trugler and Hohenester [19]. In order to validate the code the dielectric environments are set to air and glass, 1 and 2.25, respectively. Figure 5a is from the aforementioned paper and is used to validate the code that will be used for single GNP's above a substrate. The plane wave excitation will be with a 90 degree angle to the substrate. The diameter of the spheres in figure 5a and 5b is 20 nm, the distance between substrate and sphere is 5 nm and 144 vertices for the discretization of the sphere boundary are used. As can be seen in figure 5 the plots in 5a and 5b are nearly identical. The left most data point of the figure from to paper is approximately 0.51 and the left most data point of the figure generated by MATLAB is 0.447. The code that was used for the generation of the plot can be found in the appendix A.

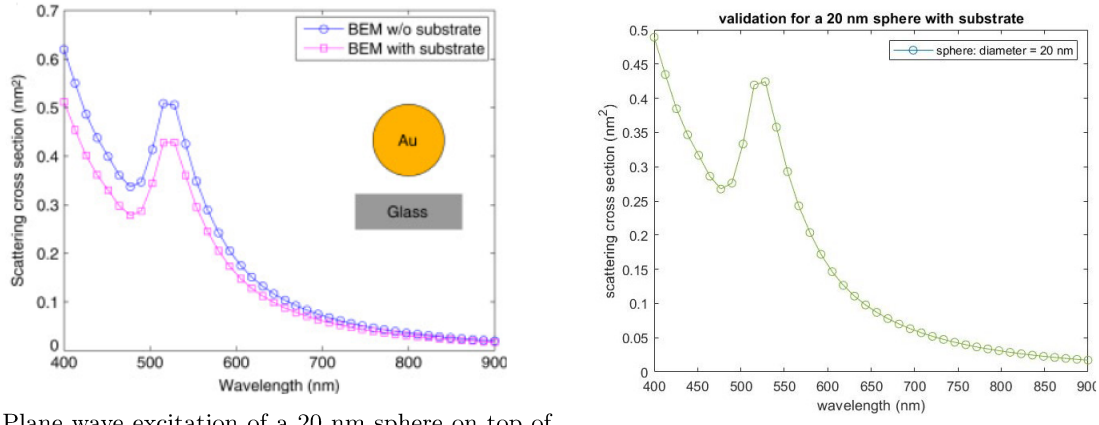

(a) Plane wave excitation of a 20 nm sphere on top of a substrate. The figure is obtained from Waxenegger, Trugler and hohenester[19].

(b) Scattering cross section of a 20 nm sphere obtained from MATLAB.

Figure 5: Planewave excitation of a 20 nm gold nanosphere with layer structure, on top of a substrate.

The next step is to validate the code for the near-field enhancement plots. This is done using the paper of Lalisse, Tessier, Plain and Baffou [26]. They gather near-field enhancements of spheres made

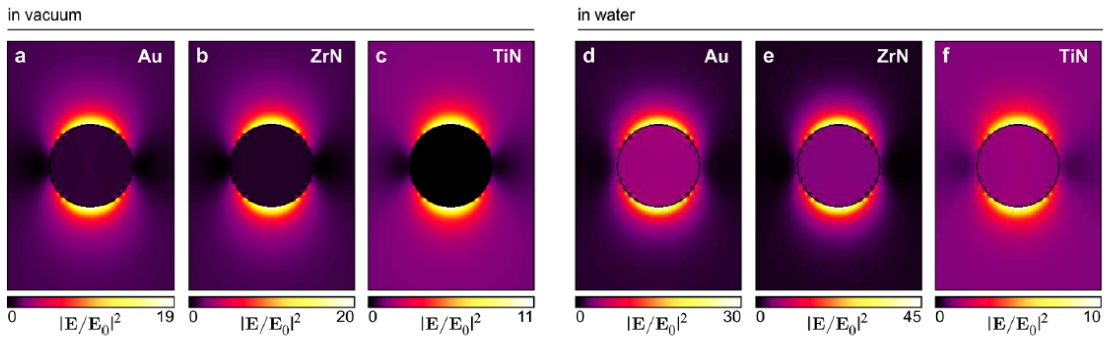

g

	BEM simulations		Figures of merit		
	$P\ (\mu W)$	$\lvert E_{max}/E_0\rvert^2$	Jo	Fa	$-\varepsilon'/\varepsilon''$
Au	1.12	19.0	5.15	19.3	1.58
ZrN	0.695	20.0	3.15	20.2	2.63
TiN	1.08	11.1	4.96	11.2	0.497

h

	BEM simulations		Figures of merit		
	$P\ (\mu W)$	$\lvert E_{max}/E_0\rvert^2$	Jo	Fa	$-\varepsilon'/\varepsilon''$
Au	4.13	30.1	19.1	30.4	1.58
ZrN	3.63	45.7	16.1	43.9	2.63
TiN	2.28	10.1	10.5	10.2	0.497

Figure 6: Figure obtained from the paper of Lalisse, Tessier, Plain and Baffou [26] showing the near-field enhancements of spherical particles of different materials(a-f) and tables with properties of the near-field enhancements(g,h).

out of gold, titanium nitride and zirconium nitride with use of the MNPBEM toolbox in MATLAB. The spheres are simulated both in a vacuum and in water. The near-field enhancements they gathered can be seen in figure 6. In figure 6 a-c contain near-field enhancements of spherical particles with a diameter of 20 nm in a vacuum. In the same figure d-f contain near-field enhancements of the same spherical particles with a diameter of 20 nm but now in water. For all simulations a light wavelength of 522 nm is used. Lastly, g and h contain tables listing the heat power and near-field enhancement obtained by BEM simulations, along with the calculated figures of merit. For the purpose of validation only sub-figures a and d will be used along with the maximum values for $\mid E/E_0 \mid^2$ which can be found in table g and h. The circumstances described in the aforementioned paper were recreated in the MNPBEM toolbox in MATLAB. As can be seen in figure 7 subfigure a and b are similar except that

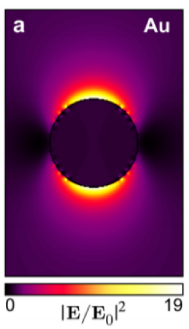

(a) Magnified version of figure 6a which displayes a 20 nm sphere in a vacuum with planewave excitation along the x-axis [26].

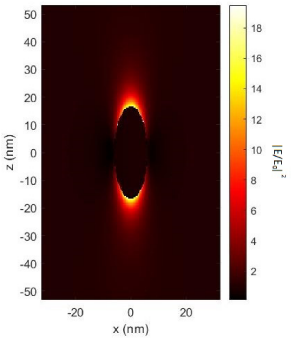

(b) Near-field enhancement of a 20 nm sphere in a vacuum with plane wave excitation along the x-axis obtained from MATLAB.

Figure 7: Near-field enhancement of sphere with a diameter of 20 nm in a vacuum.

b looks a bit stretched out, however, the same boundaries for the near-field enhancement are used. This is non-crucial since the order of magnitude and the shape of the field are comparable. In figure 6 g can be seen that the maximum field enhancement is found to be 19.0. The maximum value of the near-field enhancement obtained from MATLAB is 19.51.

Taking figure 8 into account an equivalent observation can be made as for figure 7. The figure

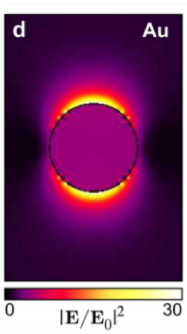

(a) Magnified version of figure 6which displayes a 20 nm sphere in water with planewave excitation along the x-axis [26].

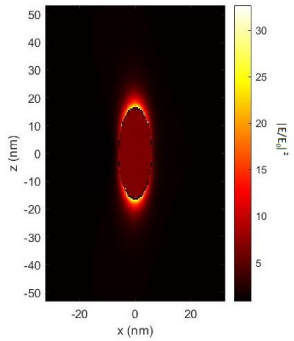

(b) Near-field enhancement of a 20 nm sphere in water with plane wave excitation along the x-axis obtained from MATLAB.

Figure 8: Near-field enhancement of sphere with a diameter of 20 nm in water.

from MATLAB seems stretched out again, in figure 6 h is 30.1, the maximum value collected from MATLAB is 32.6.

In conclusion the near-field enhancement code written in MATLAB is validated. The code that was used can be found in appendix A.

5.1.2 Validation for coupled GNP's

For this validation a figure from the paper of Goeken is used. In this figure the scattering cross sections of gold spheres of 60 nm, 80 nm, 100 nm and 125 nm with and without coupling with a 40 nm sphere are displayed[11]. The 40 nm sphere is positioned left of the sphere it is coupled with. As can be seen in figure 9, figure 9a and 9b are not a perfect match. The peak wavelength, from Goeken, for the 125 nm sphere coupled with the 40 nm sphere is approximately at $8.05 \times 10^{-14} m^2$. The peak wavelength for the same coupled spheres yielded from MATLAB is $7.25 \times 10^4 nm$. However, the peak wavelengths are an exact match. The peak height is slightly higher in the figure taken from Goeken [11]. This can be caused by multiple aspects such as a deviation in the exact BEM solver, the exact distance between the particles and several other aspects. However since the exact peak height is not important only the order of magnitude and the peak wavelength the code can be considered useful and validated. The exact code that was used can be found in appendix A Furthermore the coupling in this case is in the x-direction and in this paper the coupling will be in the z-direction. This can influence the coupling rate since the field in the x-direction is not necessarily the same as the field in the z-direction. This is because the plane wave excitation is from above which yields a field symmetry in the z direction. The code that was used can be found in appendix A.

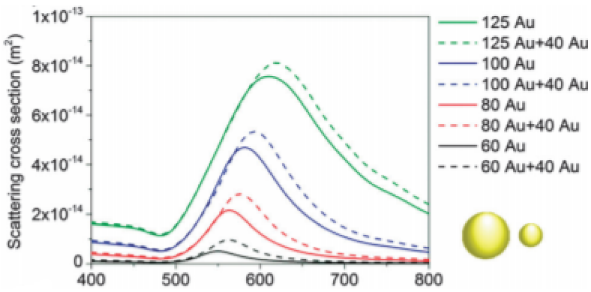

(a) Graph of spheres of various sizes of GNP's coupled with and without coupling with a 40 nm sphere in the x direction. This figure is obtained from Goeken [11].

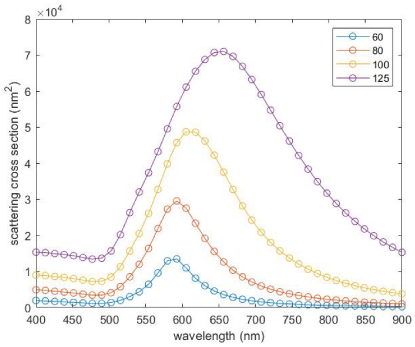

(b) Graph of spheres of various sizes of GNP's coupled with a 40 nm sphere in the x-direction.

Figure 9: Both figures show spheres coupled in the x-direction. One taken from a paper and one generated from MATLAB.

5.1.3 Accuracy

In the table below the accuracy for all the validations can be found. It can be seen that all validations are well over 85% and therefore all codes are considered validated.

Validation	Accuracy
Scattering cross section of uncoupled particles	88.0%
Near-field enhancement of uncoupled particles	Vacuum: 97.4% Water: 92.1%
Scattering cross section of coupled particles	90.1%

Table 4: Table displaying the accuracies of the performed validations.

5.2 Shapes

The aim is to simulate different shapes and sizes of nanoparticles. For each shape the code is slightly adjusted. The different codes for all the shapes can be found in the appendix B. In figure 10 a preview of all simulated shapes can be seen with arbitrary sizes.

5.3 Red shift of the wavelength

It is crucial that the distinction between coupled and uncoupled nanoparticles can be observed. Therefore it is most convenient if the shift in wavelength corresponds with a perceptible change in color. Considering the common wavelengths of coupled and uncoupled particles it is most convenient to aim at a shift from green to red light. The wavelength of green light is 520 nm to 560 nm and the wavelength of red light is 635 nm to 700 nm as can be seen in figure 11. Therefore, the field enhancement for uncoupled nanoparticles is gathered at a wavelength of 540 which is in the middle of the green range.

6 Results and discussion

For the uncoupled particles the scattering cross section and the near-field enhancement are gathered. In the scattering cross section plots vertical lines are added showing the range of green light which is 520 nm to 560 nm as indicated in figure 11. The peak wavelength should be in this range and as large as possible. The near-field plots show the maximum field enhancement for a 540 nm light wave

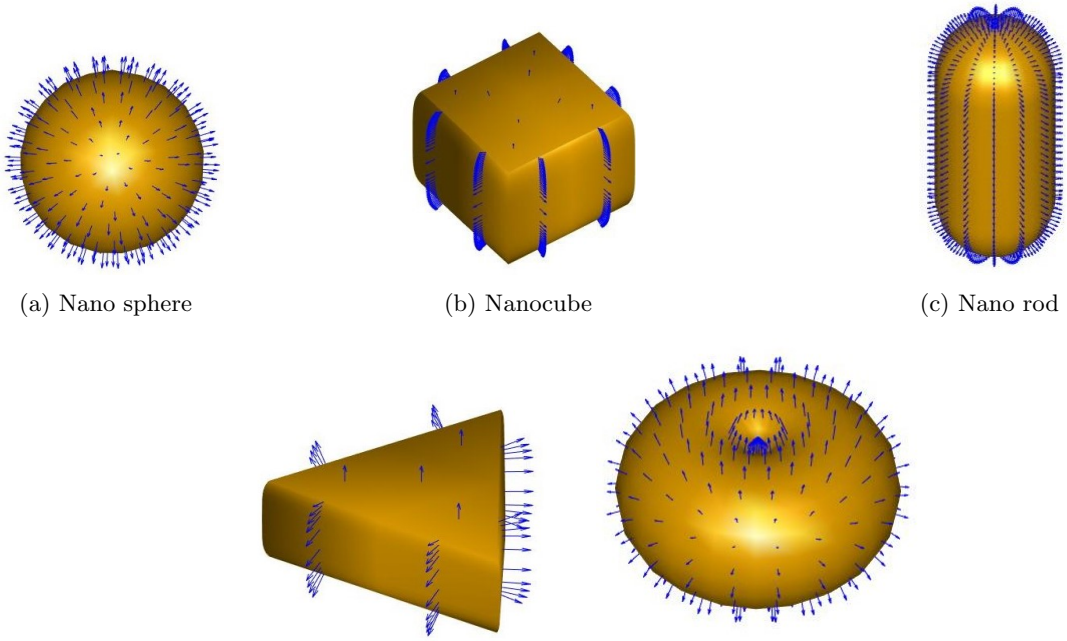

(a) Nano sphere (b) Nanocube (c) Nano rod

(d) Nano triangle (e) Nano torus

Figure 10: A with MATLAB created preview of the shapes that will be simulated with help of the MNPBEM toolbox. These shapes are of arbitrary size and the arrows indicate the direction of the field around each shape.

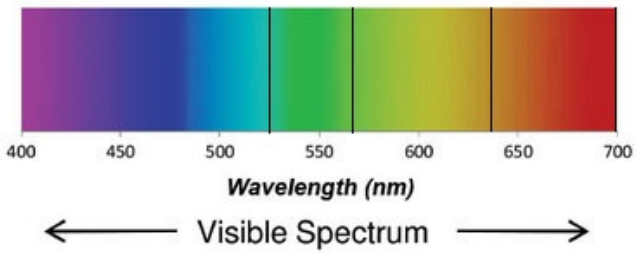

Figure 11: Spectrum of visible light. The lines indicate the green and red range. Figure adapted from[27].

gathered from the separate near-field plots. The enhancement should be as large as possible since this leads to easier electromagnetic coupling with other particles. For the coupled particles only the scattering cross section is relevant and gathered for coupling with spheres of 20 nm, 40 nm and 60 nm. For these aforementioned scattering cross sections the range of red light, 635 nm to 700 nm, is indicated by vertical lines, and the peak wavelength is desired to be in this range. For every shape one near-field enhancement plot is displayed which shows the shape of the field most clear. The remainder of the near-field enhancement plots van be found in appendix D.

6.1 Sphere

As can be seen in figure 12a when the diameter of the sphere increases the scattering cross section increases aswell. This is desired since this leads to clear results. However an unwanted effect of the increasing diameters is that the peak wavelength also increases. The peak wavelength is required to be in the range of green light, which is indicated by the vertical lines.

In figure 12b can be seen that the field enhancement increases with size aswell. Therefore, the optimum size for spheres lies around 140 nm which gives the highest peak for the scattering cross section in the green range and has the largest field enhancement.

In figure 13 the scattering cross section of spheres, sizes ranging between 130 nm and 150 nm, are displayed, also vertical lines are added to indicate the range of green light. In this figure can be seen that a sphere with a diameter of 146 nm is optimal since it has the highest peak wavelength that is in the green range however the maximum field enhancement is not optimal for this size. The near-field enhancement of a particle of 130 nm is more than twice as big and therefore, the coupling of a sphere of 130 nm and 146 nm is computed in order to find out whether the coupling of both is convenient.

The coupling will be with a 45 degree angle with respect to the z-axis which will be taken into account by placing the second sphere. This angle is chosen since the near-field enhancement plot shows that this is most convenient. A 90 degree angle with respect to the z-axis shows the strongest field, however, on the 45 degree angle is binding more likely. All near-field enhancement plots can be found in figure 45 in appendix D. As can be seen for both spheres the coupling is in the red range. Therefore, they both meet the set conditions.

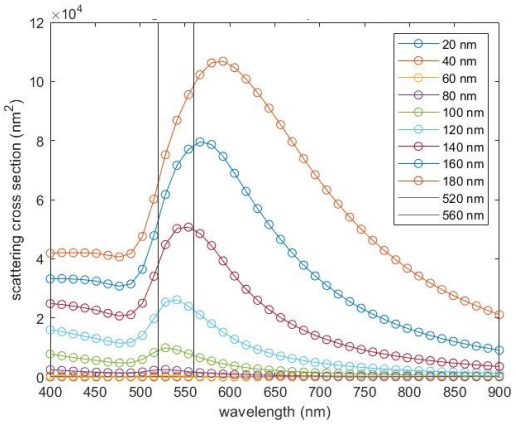

(a) Scattering cross section of a sphere sized between 20 nm and 180 nm. The green range is indicated by vertical lines and indicates where the peaks are desired to be.

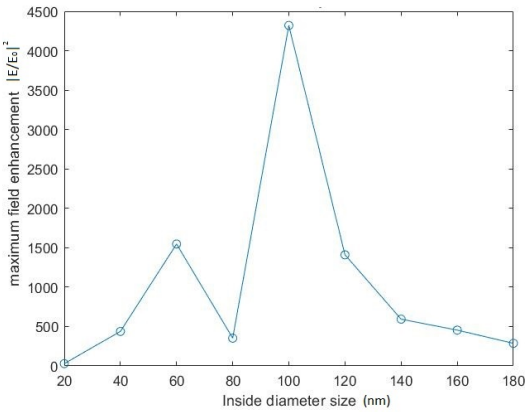

(b) Maximum field enhancement of a sphere sized between 20 nm and 180 nm. This is a graph of the maximum-field enhancement at 540 nm for various diameters.

Figure 12: Plane wave excitation with a 90 degree angle of a sphere of various sizes.

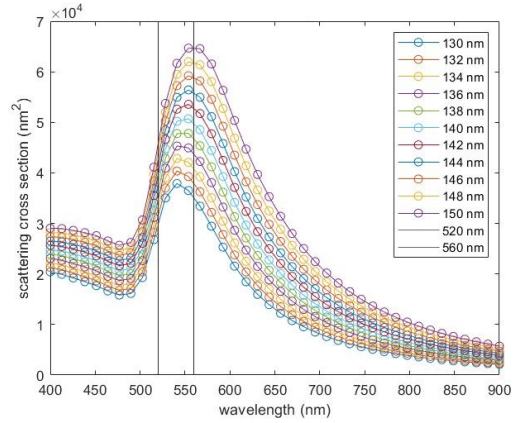

(a) Scattering cross section of a sphere sized between 130 nm and 150 nm. The green range is indicated by the vertical lines and indicates where the peaks are desired to be.

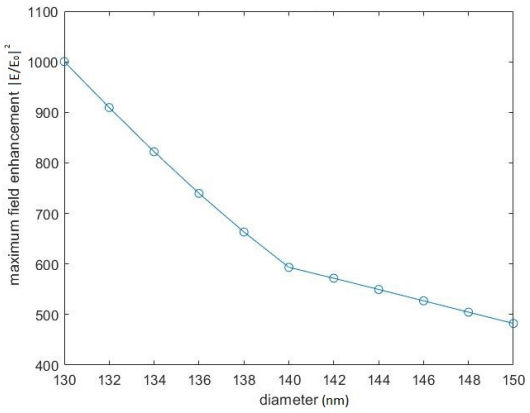

(b) Maximum field enhancement of a sphere sized between 130 nm and 150 nm. This is a graph of the maximum-field enhancement at 540 nm for various diameters.

Figure 13: Simulations of a sphere of various sizes zoomed in on the optimal diameter range.

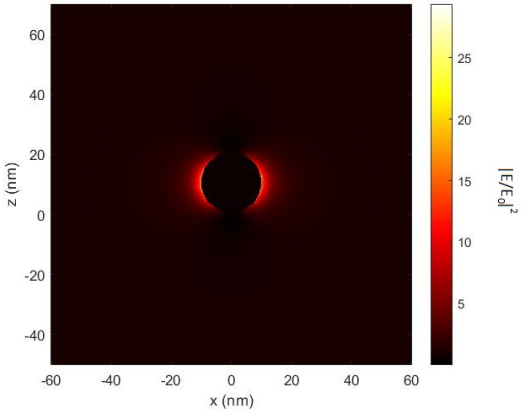

Figure 14: The near-field enhancement plot of a 20 nm sphere. This particular size is displayed here since it best shows the shape of the field.

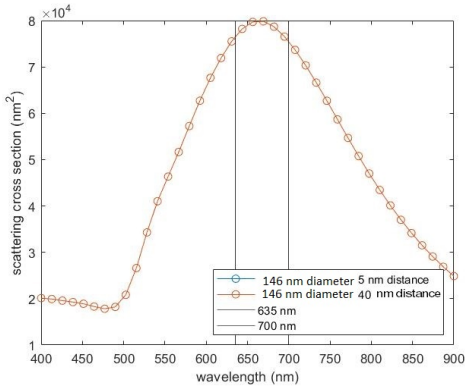

(a) A 146 nm sphere coupled with a 20 nm sphere in the z-direction with a 45 degree angle. The distance between the spheres is 5 nm and 40 nm.

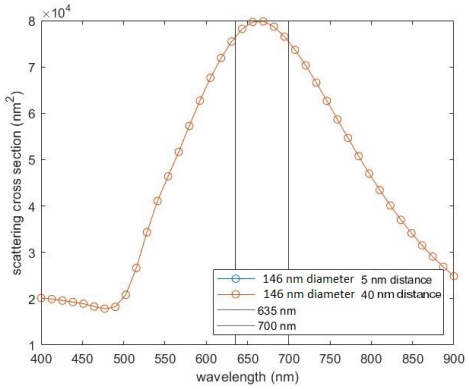

(b) A 146 nm sphere coupled with a 40 nm sphere in the z-direction with a 45 degree angle. The distance between the spheres is 5 nm and 40 nm.

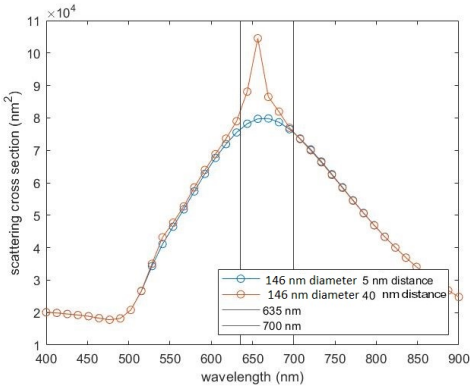

(c) A 146 nm sphere coupled with a 60 nm sphere in the z-direction with a 45 degree angle. The distance between the spheres is 5 nm and 40 nm.

Figure 15: Coupling with spheres of various diameters with a sphere of 146 nm.

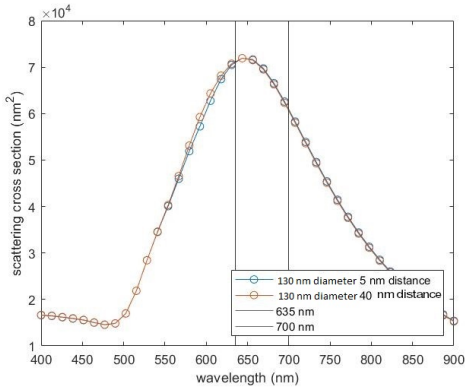

(a) A 130 nm sphere coupled with a 20 nm sphere in the z-direction with a 45 degree angle. The distance between the spheres is 5 nm and 40 nm. The vertical lines indicate the red light range.

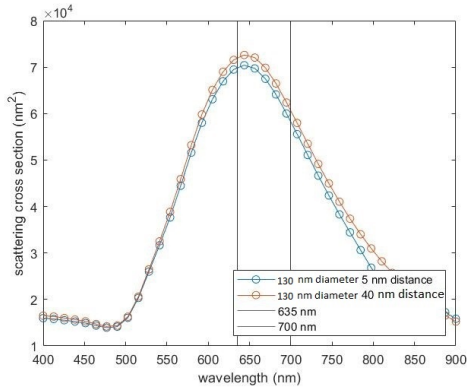

(b) A 130 nm sphere coupled with a 40 nm sphere in the z-direction with a 45 degree angle. The distance between the spheres is 5 nm and 40 nm. The vertical lines indicate the red light range.

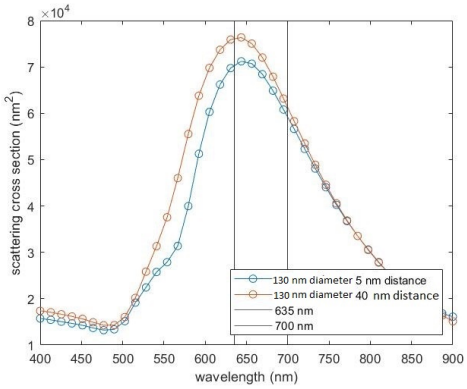

(c) A 130 nm sphere coupled with a 60 nm sphere in the z-direction with a 45 degree angle. The distance between the spheres is 5 nm and 40 nm. The vertical lines indicate the red light range.

Figure 16: Coupling with spheres of various diameters with a sphere of 130 nm.

6.2 Cube

In figure 17 the scattering cross section and near-field enhancement of cubes of various sizes can be found. It can be seen in figure 17a that the peak wavelength is in the green range for cubes of 100 nm and smaller. The near-field enhancement does not show a clear distinction between particles except for a 120 nm cube which is not in the green range and therefore not convenient. The near-field enhancements of other particles are not zero, they however are in a different order of magnitude. In figure 18 the scattering cross section (18a) and near-field enhancement (18b), zoomed in on the area of interest, are shown. It can clearly be seen that a cube of 106 nm is the preferred option since the near-field enhancement shows a large peak and the scattering cross section is in the green range.

Again a 45 degree angle is chosen for coupling with spheres. In this case that is because this shows the largest near-field enhancement. In figure 20 it can be seen that for all coupled particles there are peaks in the red range. However, for the 60 nm sphere there is also a peak at 750 nm which is in the infrared range.

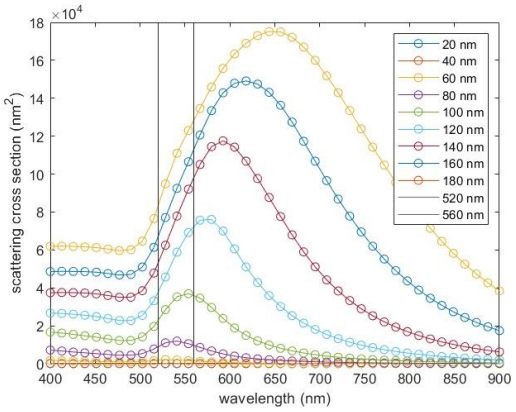

(a) Scattering cross section of a cube sized between 20 nm and 180 nm. The green range is indicated by the vertical lines and indicates where the peaks are desired to be.

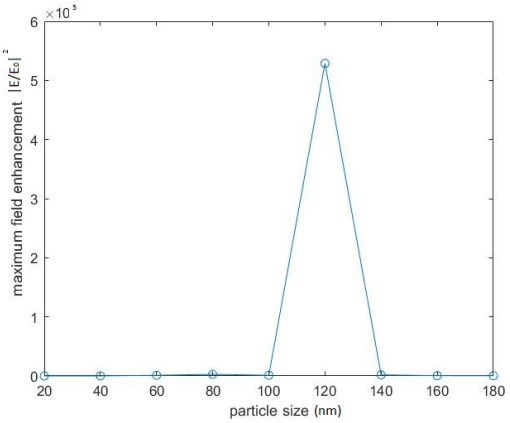

(b) Maximum field enhancement of a cube sized between 20 nm and 180 nm. This is a graph of the maximum-field enhancement at 540 nm for various diameters.

Figure 17: Plane wave excitation of a cube of various sizes.

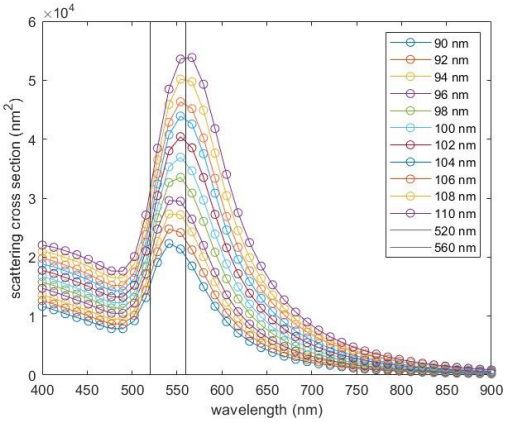

(a) Scattering cross section of a cube sized between 90 nm and 110 nm. The green range is indicated by the vertical lines and indicates where the peaks are desired to be.

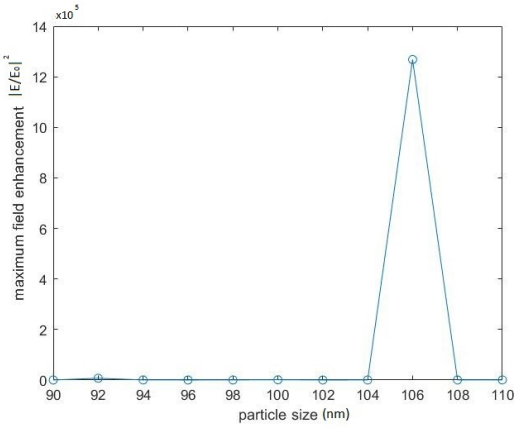

(b) Maximum field enhancement of a sphere sized between 90 nm and 110 nm. This is a graph of the maximum-field enhancement at 540 nm for various diameters.

Figure 18: Plane wave excitation, with a 90 degree angle, of a cube of various sizes.

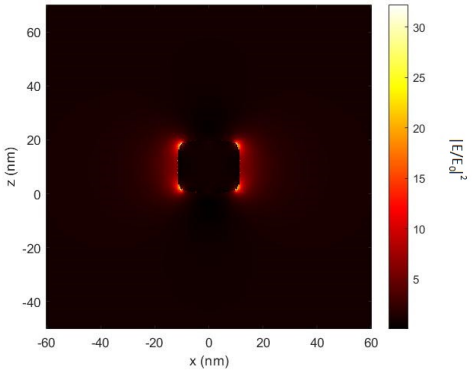

Figure 19: The near-field enhancement plot of a cube with 20 nm sides. This exact size is displayed since it shows the shape of the field most clear. The other near-field enhancements can be found in figure 46 in appendix D.

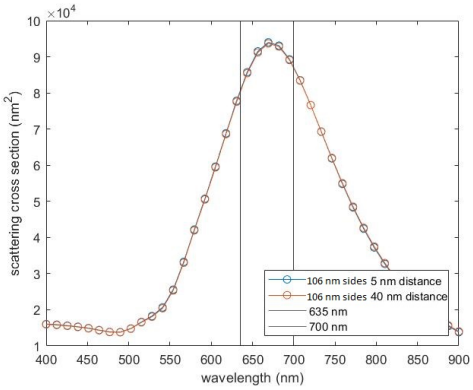

(a) A 106 nm cube coupled with a 20 nm sphere with a 45 degree angle with respect to the z-axis. The distance between the sphere and the cube is 5 nm and 40 nm. The vertical lines indicate the red light range.

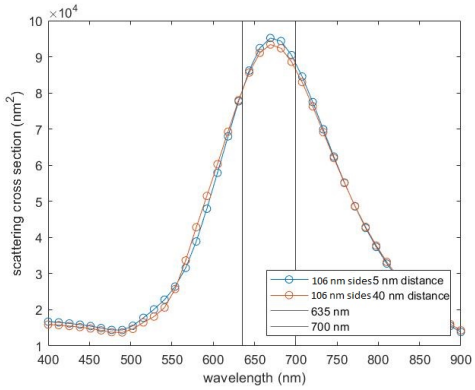

(b) A 106 nm cube coupled with a 40 nm sphere with a 45 degree angle with respect to the z-axis. The distance between the sphere and the cube is 5 nm and 40 nm. The vertical lines indicate the red light range.

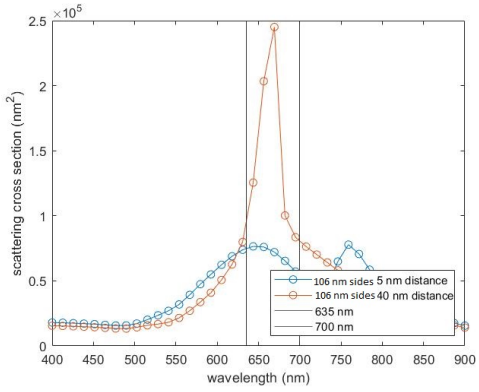

(c) A 106 nm cube coupled with a 60 nm sphere with a 45 degree angle with respect to the z-axis. The distance between the sphere and the cube is 5 nm and 40 nm. The vertical lines indicate the red light range.

Figure 20: Coupling with spheres of various diameters with a cube of 106 nm.

6.3 Rod

For the rod two variables are tuned, namely, the diameter and the height. For the height 4 values, specifically, 10 nm, 50 nm, 75 nm and 100 nm, are used.

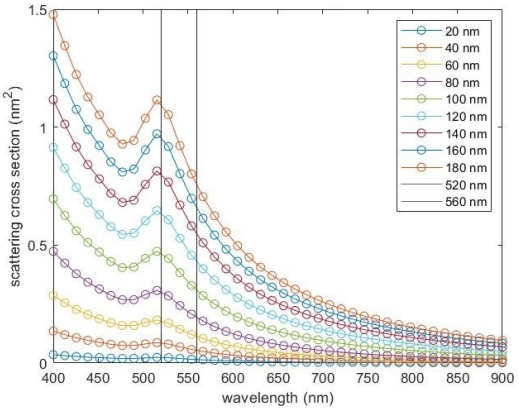

(a) Scattering cross section of a rod sized between 20 nm and 180 nm and 10 nm height. The green range is indicated by the vertical lines and indicates where the peaks are desired to be.

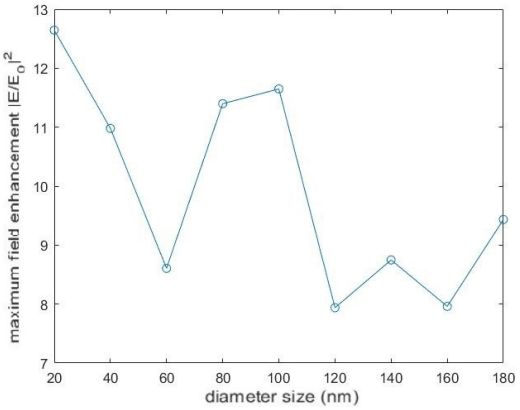

(b) Maximum field enhancement of a rod sized between 20 nm and 180 nm with a height of 10 nm. This is a graph of the maximum-field enhancement at 540 nm.

Figure 21: Plane wave excitation of a rod of various diameters and 10 nm height.

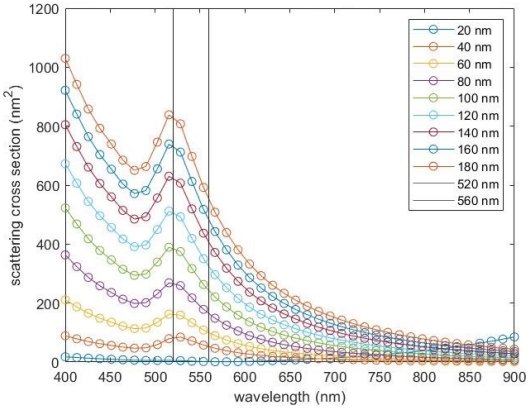

(a) Scattering cross section of a rod sized between 20 nm and 180 nm and 50 nm height. The green range is indicated by the vertical lines and indicates where the peaks are desired to be.

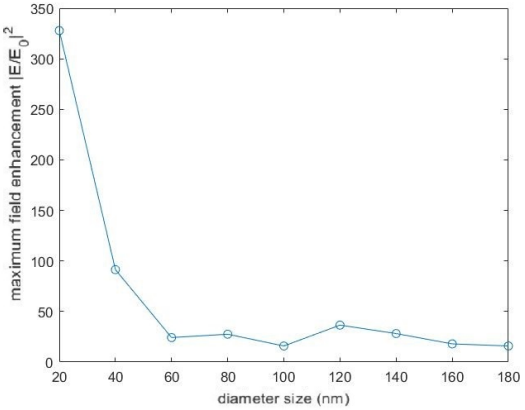

(b) Maximum field enhancement of a rod sized between 20 nm and 180 nm and a height of 50 nm. This is a graph of the maximum-field enhancement at 540 nm.

Figure 22: Plane wave excitation of a rod of various diameters and 50 nm height.

As can be seen in figures 21, 22, 23 and 24 only the rods with a height of 75 nm and 100 nm fall in the green light range. The rod of 60 nm diameter and 100 nm height is most suited since the scattering cross section is comparatively high aswell as the near-field enhancement. Again a 45 degree angle is chosen since this shows the highest field enhancement.

The coupled rod has a peak wavelength that falls in the red range which is desired.

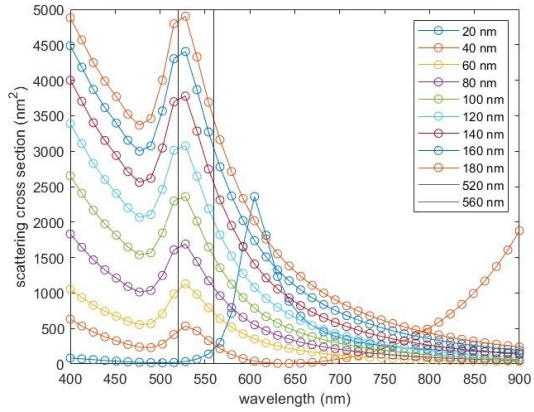

(a) Scattering cross section of a rod sized between 20 nm and 180 nm and 75 nm height. The green range is indicated by the vertical lines and indicates where the peaks are desired to be.

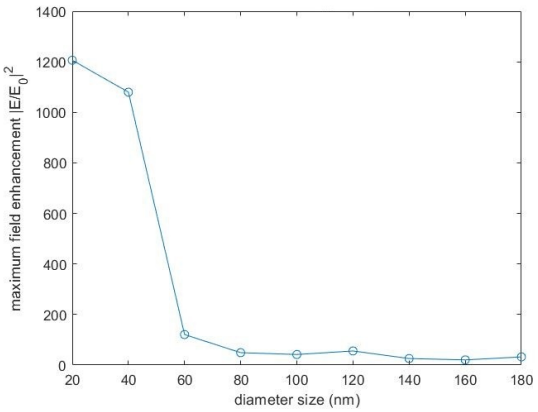

(b) Maximum field enhancement of a rod sized between 20 nm and 180 nm and a height of 75 nm. This is a graph of the maximum-field enhancement at 540 nm.

Figure 23: Plane wave excitation of a rod of various diameters and 75 nm height.

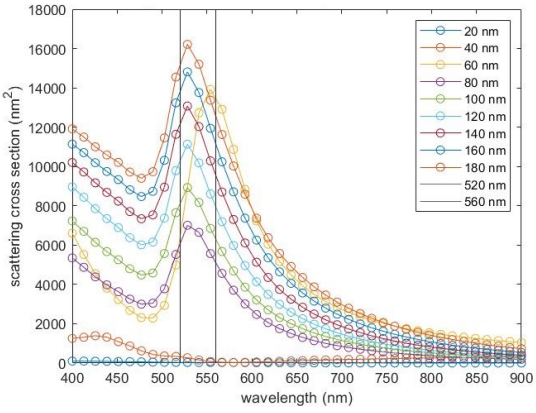

(a) Scattering cross section of a rod sized between 20 nm and 180 nm and 100 nm height. The green range is indicated by the vertical lines and indicates where the peaks are desired to be.

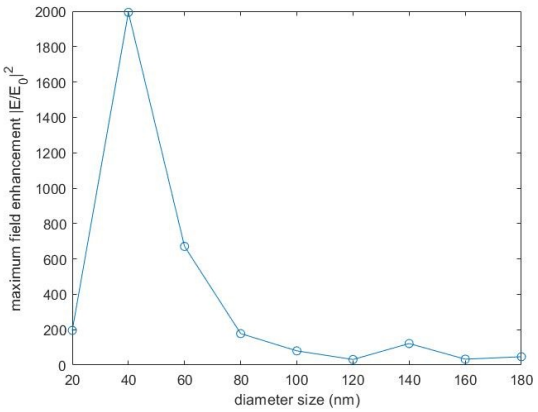

(b) Maximum field enhancement of a rod sized between 20 nm and 180 nm and a height of 100 nm. This is a graph of the maximum-field enhancement at 540 nm.

Figure 24: Plane wave excitation of a rod of various diameters and 100 nm height.

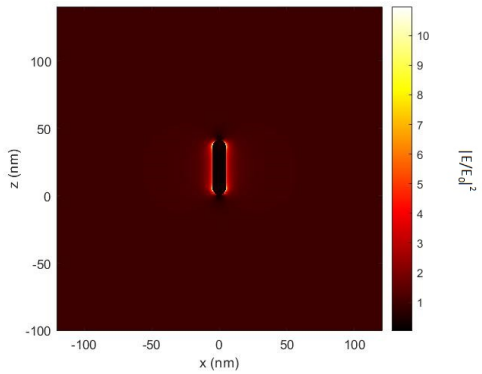

Figure 25: Near-field enhancement of a rod with 10 nm diameter and 50 nm height. This size combination is displayed since it clearly shows the shape of the field around the rod. The near-field enhancements computed for rods of different sizes can be found in appedix D.

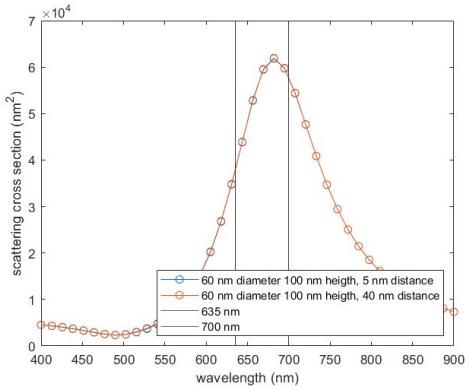

(a) A 60 nm diameter and 100 nm high rod coupled with a 20 nm sphere with a 45 degree angle with respect to the z-axis. The distance between the sphere and the cube is 5 nm and 40 nm. The vertical lines indicate the red light range.

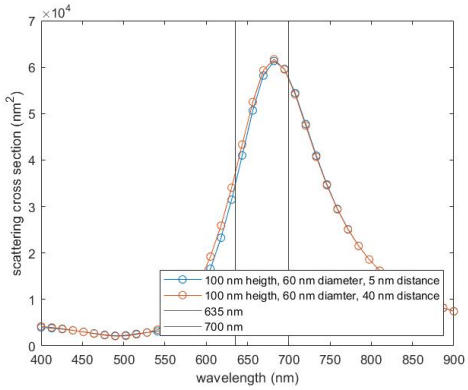

(b) A 60 nm diameter and 100 nm high rod coupled with a 40 nm sphere with a 45 degree angle with respect to the z-axis. The distance between the sphere and the cube is 5 nm and 40 nm. The vertical lines indicate the red light range.

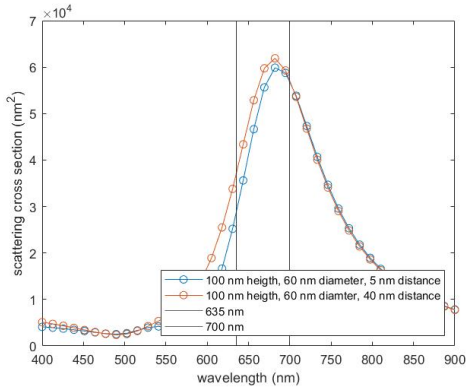

(c) A 60 nm diameter and 100 nm high rod coupled with a 60 nm sphere with a 45 degree angle with respect to the z-axis. The distance between the sphere and the cube is 5 nm and 40 nm. The vertical lines indicate the red light range.

Figure 26: Coupling with spheres of various diameters with a rod of 100 nm height and 60 nm diameter.

6.4 Triangle

For the triangle there are also two variables that can be tuned, the thickness and the sides of the triangle. For the thickness four variables are taken, namely, 10 nm, 50 nm, 75 nm and 100 nm.

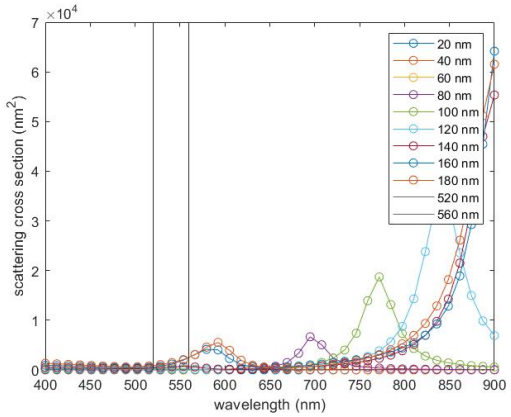

(a) Scattering cross section of triangle sizes between 20 nm and 180 nm with 10 nm thickness. The green range is indicated by the vertical lines which is were the peaks are desired to be.

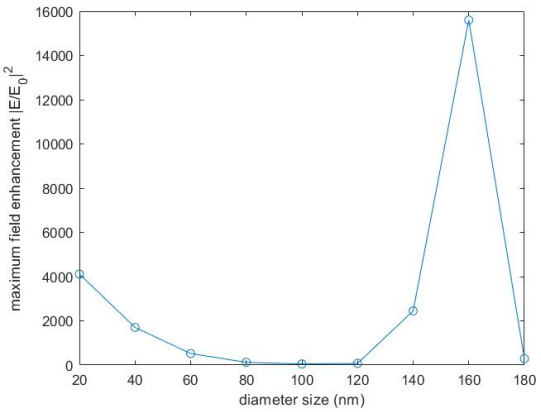

(b) Near-field enhancement of a triangle sized between 20 nm and 180 nm with a height of 10 nm. This is a graph of the maximum field enhancement at 540 nm.

Figure 27: Plane wave excitation of a triangle with various side lengths and 10 nm thickness.

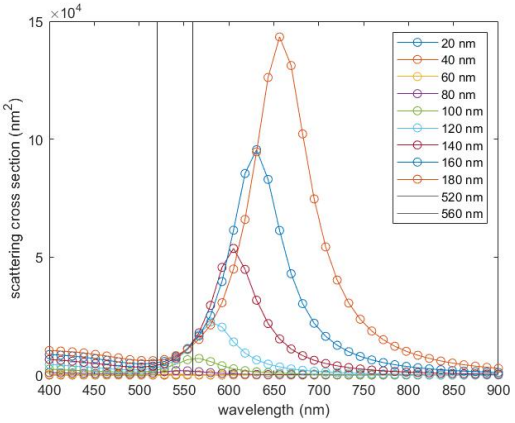

(a) Scattering cross section of triangle sizes between 20 nm and 180 nm with 50 nm thickness. The green range is indicated by the vertical lines which is were the peaks are desired to be.

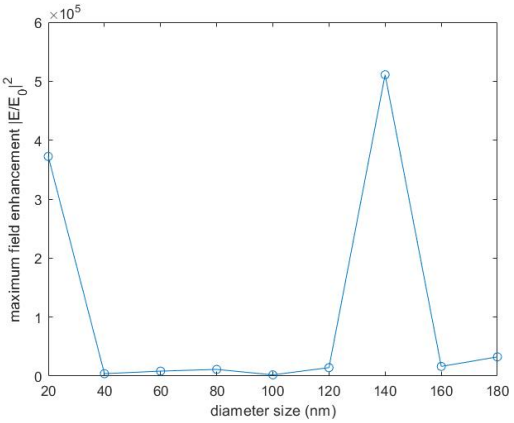

(b) Near-field enhancement of a triangle sized between 20 nm and 180 nm with a height of 50 nm. This is a graph of the maximum field enhancement at 540 nm.

Figure 28: Plane wave excitation of a triangle with various side lengths and 50 nm thickness.

As can be seen in figure 27 and 28 triangles with a low thickness do not meet the set conditions properly. In the plots in figure 29 and 30 certain options do meet the conditions. In this case it is beneficial to compute the scattering cross section of the coupling for a triangle of 100 nm thickness and with sides of 80 nm since this has a high near-field enhancement.

The coupled triangle has peak wavelengths outside the red color range. When the coupling of a triangle sized larger than 80 nm is computed the peak is likely to fall in the red range however the near-field is significantly lower and the scattering cross section of the uncoupled particles might not be in the green range.

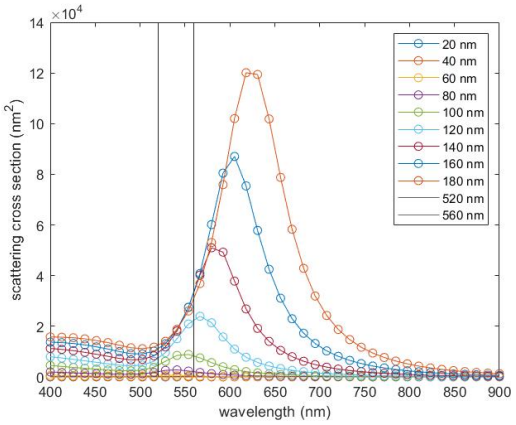

(a) Scattering cross section of triangle sizes between 20 nm and 180 nm with 75 nm thickness. The green range is indicated by the vertical lines which is were the peaks are desired to be.

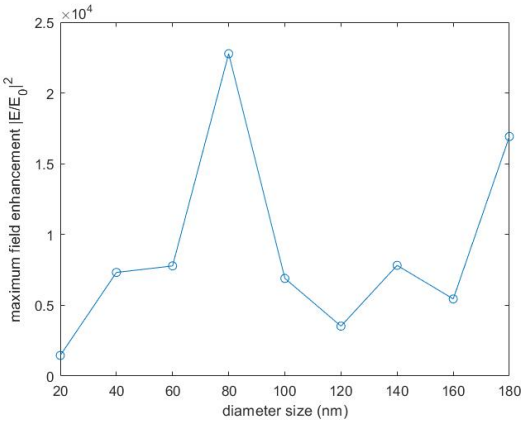

(b) Near-field enhancement of a triangle sized between 20 nm and 180 nm with a height of 75 nm. This is a graph of the maximum field enhancement at 540 nm.

Figure 29: Plane wave excitation of a triangle with various side lengths and 75 nm thickness.

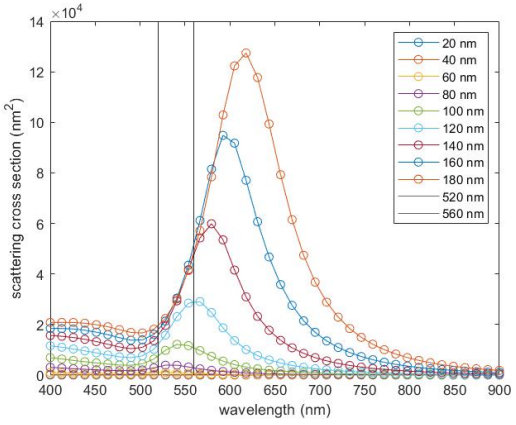

(a) Scattering cross section of triangle sizes between 20 nm and 180 nm with 100 nm thickness. The green range is indicated by the vertical lines which is were the peaks are desired to be.

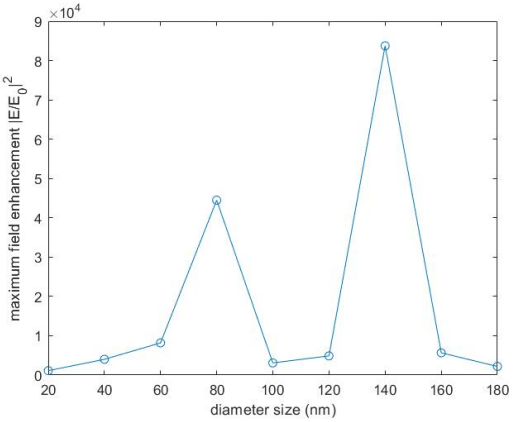

(b) Near-field enhancement of a triangle sized between 20 nm and 180 nm with a height of 100 nm. This is a graph of the maximum field enhancement at 540 nm.

Figure 30: Plane wave excitation of a triangle with various side lengths and 100 nm thickness.

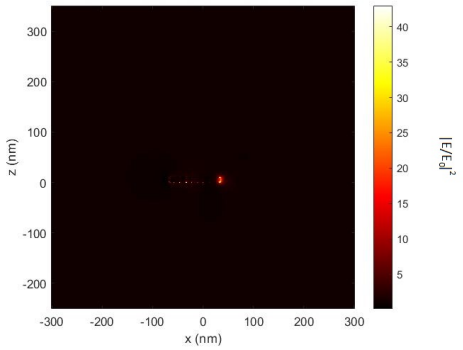

Figure 31: Near-field enhancement of a triangle with sides of 100 nm and 10 nm thickness. The shape of the field is not very clear to see however this is the size combination which yields the most apparent field. The other near-field enhancements can be found in D.

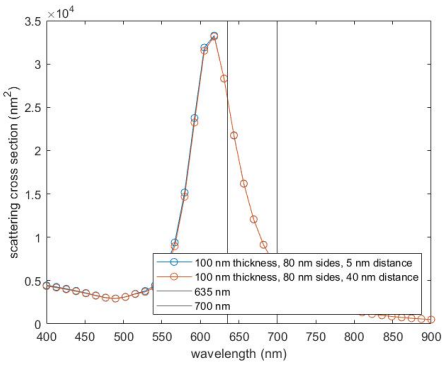

(a) A 80 nm triangle with 100 nm thickness coupled with a 20 nm sphere with a 45 degree angle with respect to the z-axis. The distance between the sphere and the cube is 5 nm and 40 nm. The vertical lines indicate the red light range.

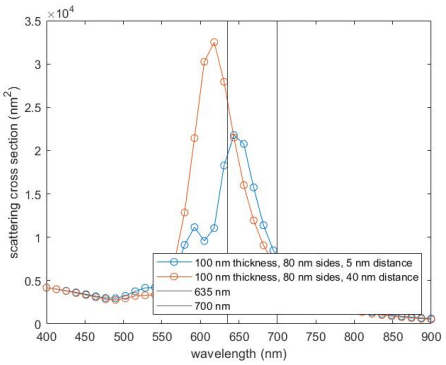

(b) A 80 nm triangle with 100 nm thickness coupled with a 40 nm sphere with a 45 degree angle with respect to the z-axis. The distance between the sphere and the cube is 5 nm and 40 nm. The vertical lines indicate the red light range.

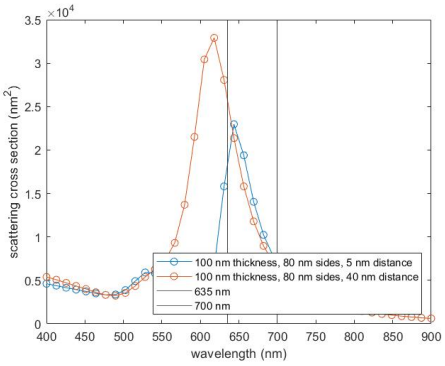

(c) A 80 nm triangle with 100 nm thickness coupled with a 60 nm sphere with a 45 degree angle with respect to the z-axis. The distance between the sphere and the cube is 5 nm and 40 nm. The vertical lines indicate the red light range.

Figure 32: Coupling with spheres of various diameters with a triangle with sides of 80 nm and 100 nm thickness.

6.5 Torus

For the torus also two variables are tuned. These are the inside and outside diameter of the torus. For the inside diameter steps of 10 nm are taken instead of steps of 20 nm. This is because a preview showed significant change within these smaller steps.

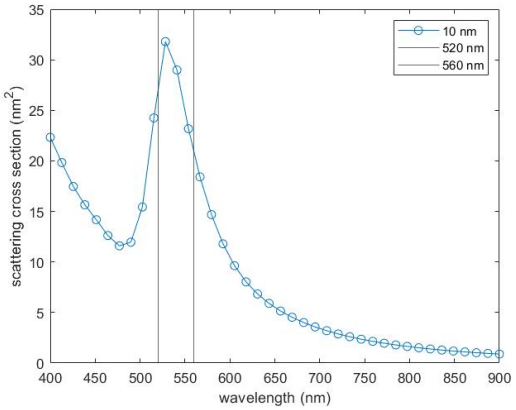

(a) Scattering cross section of a torus of 20 nm outside diameter and 10 nm inside diameter. The green range is indicated by vertical lines which is where the peaks are desired to be.

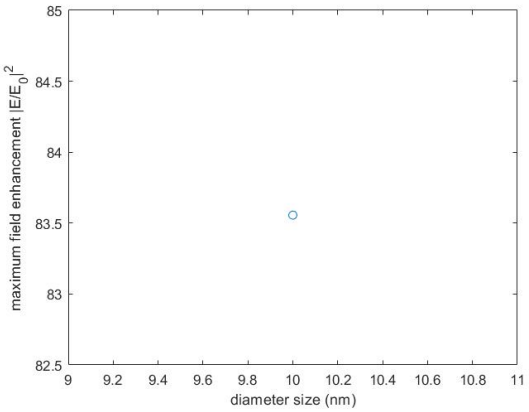

(b) Near-field enhancement of a torus of 20 nm outside diameter and 10 nm inside diameter. The light wavelength used for this simulation is 540 nm.

Figure 33: Plane wave excitation of a torus of 20 nm and 10 nm inside diameter.

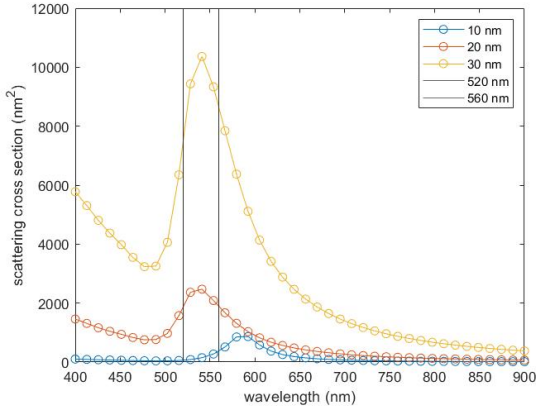

(a) Scattering cross section of a torus of 40 nm outside diameter and various inside diameters. The green range is indicated by vertical lines which is where the peaks are desired to be.

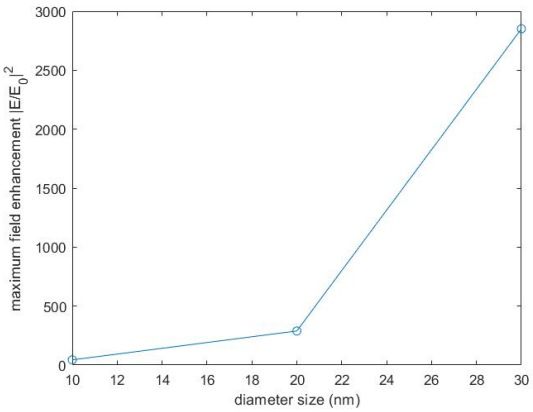

(b) Near-field enhancement of a torus of 40 nm outside diameter and various inside diameters. The light wavelength used for this simulation is 540 nm.

Figure 34: Plane wave excitation of a torus of 40 nm and varying inside diameters.

The torus that is most suited for coupling is the torus with 60 nm outside diameter and 30 nm inside diameter. The angle that is chosen is zero degrees with respect to the z-axis which means the sphere will be right above the hole of the torus. For the coupled torus it seems that all requirements are met.

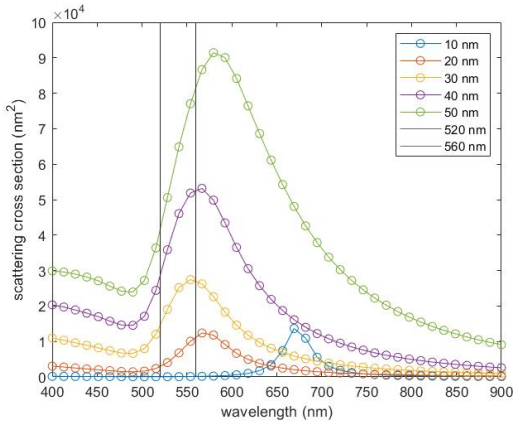

(a) Scattering cross section of a torus of 60 nm outside diameter and various inside diameters. The green range is indicated by vertical lines which is where the peaks are desired to be.

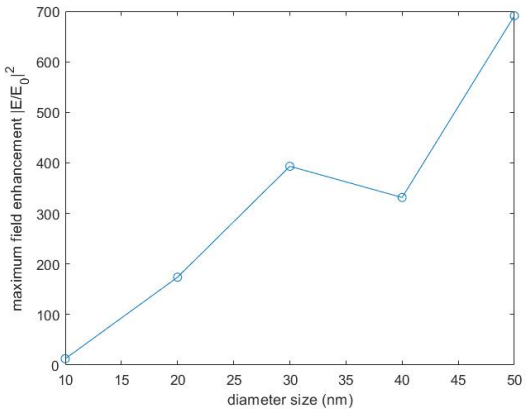

(b) Near-field enhancement of a torus of 60 nm outside diameter and various inside diameters. The light wavelength used for this simulation is 540 nm.

Figure 35: Plane wave excitation of a torus of 60 nm and varying inside diameters.

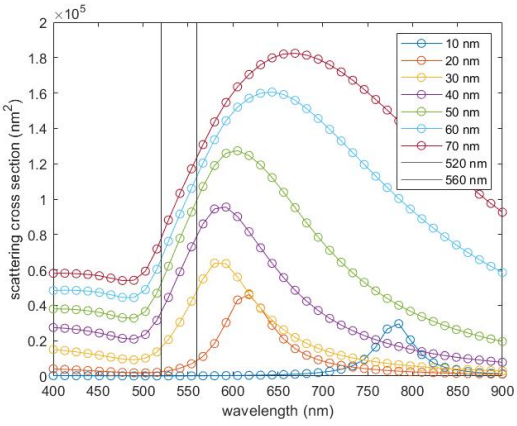

(a) Scattering cross section of a torus of 80 nm outside diameter and various inside diameters. The green range is indicated by vertical lines which is where the peaks are desired to be.

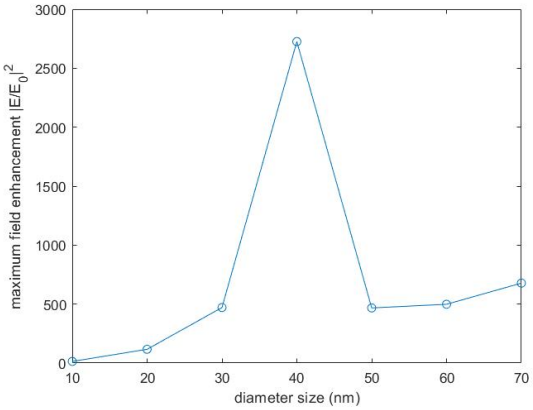

(b) Near-field enhancement of a torus of 80 nm outside diameter and various inside diameters. The light wavelength used for this simulation is 540 nm.

Figure 36: Plane wave excitation of a torus of 80 nm and varying inside diameters.

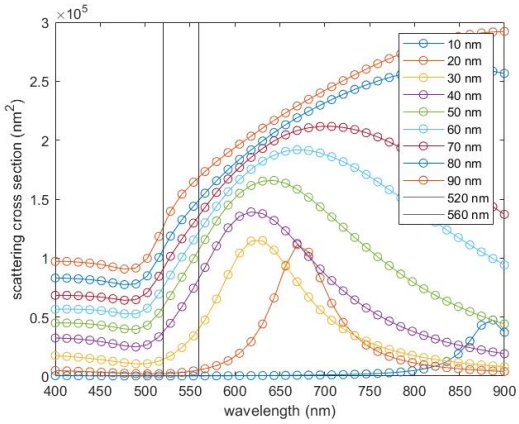

(a) Scattering cross section of a torus of 100 nm outside diameter and various inside diameters. The green range is indicated by vertical lines which is where the peaks are desired to be.

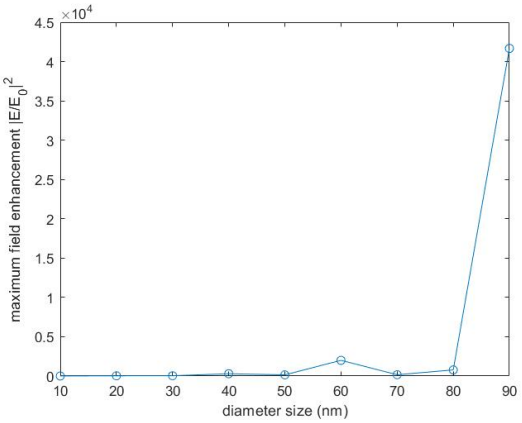

(b) Near-field enhancement of a torus of 100 nm outside diameter and various inside diameters. The light wavelength used for this simulation is 540 nm.

Figure 37: Plane wave excitation of a torus of 100 nm and varying inside diameters.

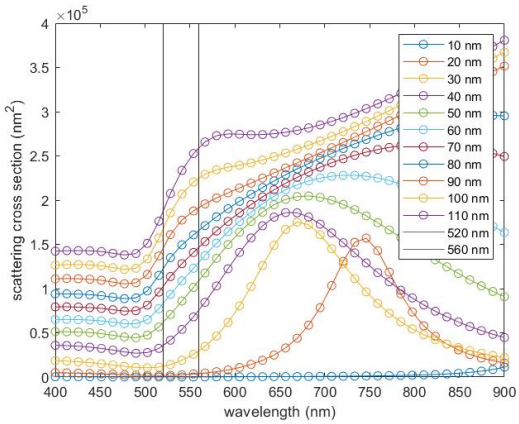

(a) Scattering cross section of a torus of 120 nm outside diameter and various inside diameters. The green range is indicated by vertical lines which is where the peaks are desired to be.

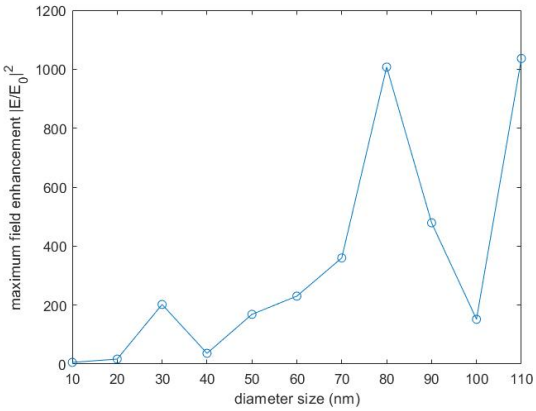

(b) Near-field enhancement of a torus of 120 nm outside diameter and various inside diameters. The light wavelength used for this simulation is 540 nm.

Figure 38: Near-field enhancement of a torus of 120 nm outside diameter and various inside diameters. The light wavelength used for this simulation is 540 nm.

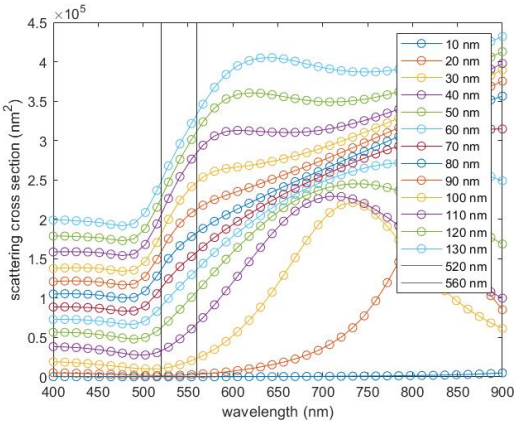

(a) Scattering cross section of a torus of 140 nm outside diameter and various inside diameters. The green range is indicated by vertical lines which is where the peaks are desired to be.

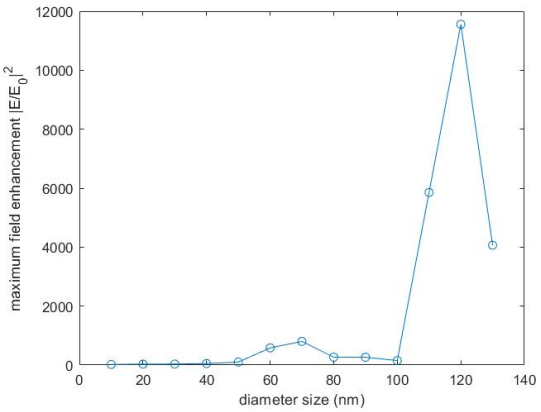

(b) Near-field enhancement of a torus of 140 nm outside diameter and various inside diameters. The light wavelength used for this simulation is 540 nm.

Figure 39: Plane wave excitation of a torus of 140 nm and varying inside diameters.

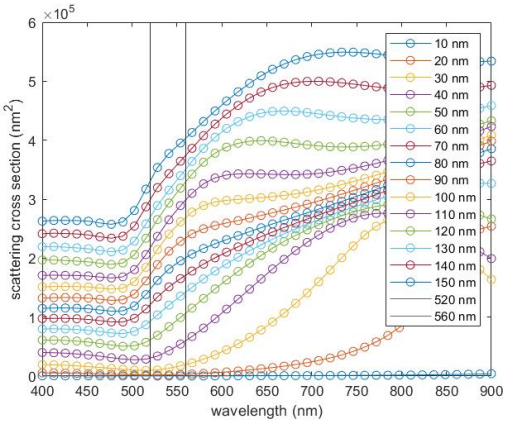

(a) Scattering cross section of a torus of 160 nm outside diameter and various inside diameters. The green range is indicated by vertical lines which is where the peaks are desired to be.

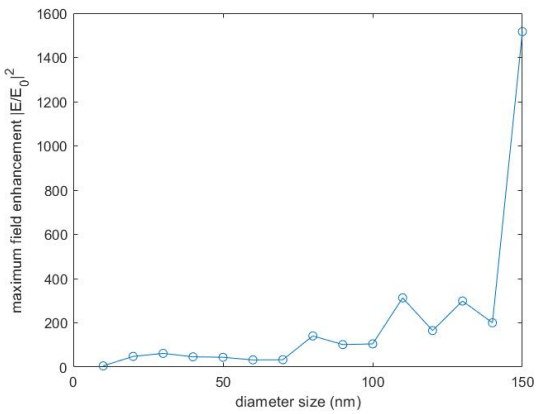

(b) Near-field enhancement of a torus of 160 nm outside diameter and various inside diameters. The light wavelength used for this simulation is 540 nm.

Figure 40: Plane wave excitation of a torus of 160 nm and varying inside diameters.

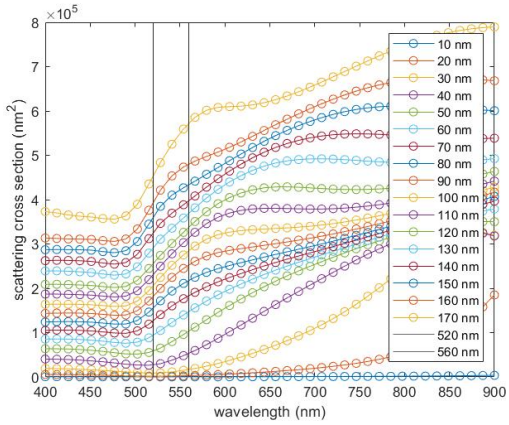

(a) Scattering cross section of a torus of 180 nm outside diameter and various inside diameters. The green range is indicated by vertical lines which is where the peaks are desired to be.

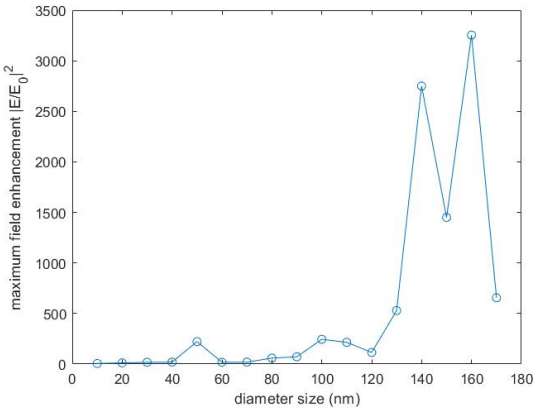

(b) Near-field enhancement of a torus of 180 nm outside diameter and various inside diameters. The light wavelength used for this simulation is 540 nm.

Figure 41: Plane wave excitation of a torus of 180 nm and varying inside diameters.

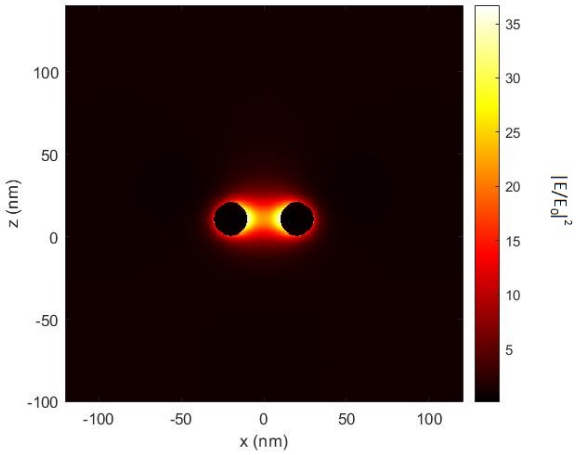

Figure 42: Near-field enhancement of a torus with an outside diameter of 40 nm and an inside diameter of 10 nm. This specific size combination is displayed since the shape of the field is clearly visible. Additionally it can be seen that both sides of the torus couple with each other in the middle. The scattering cross sections for torussen of different sizes can be found in D.

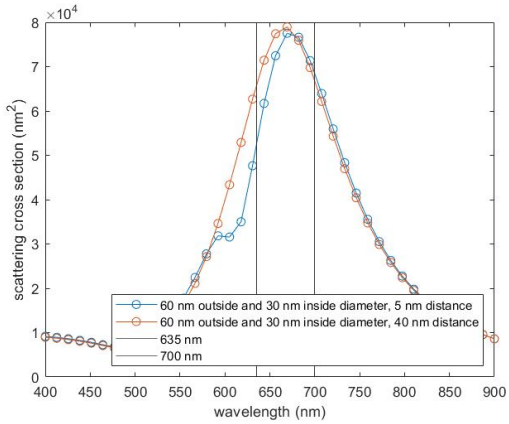

(a) A torus with 60 nm outside diameter and 30 nm inside diameter coupled with a 20 nm sphere with a 45 degree angle with respect to the z-axis. The distance between the sphere and the cube is 5 nm and 40 nm. The vertical lines indicate the red light range.

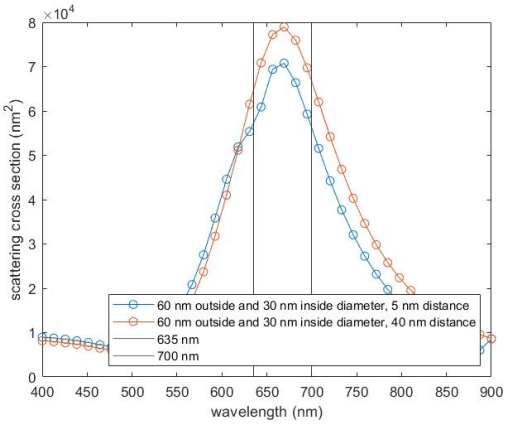

(b) A torus with 60 nm outside diameter and 30 nm inside diameter coupled with a 40 nm sphere with a 45 degree angle with respect to the z-axis. The distance between the sphere and the cube is 5 nm and 40 nm. The vertical lines indicate the red light range.

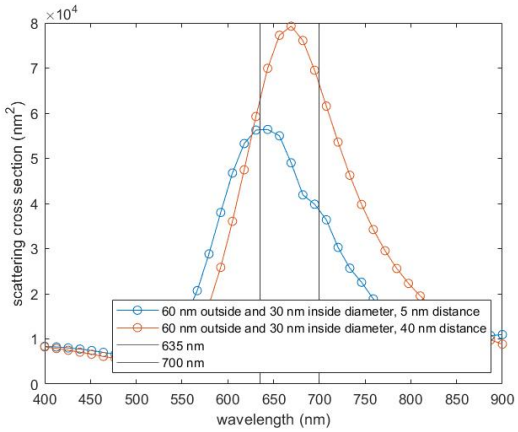

(c) A torus with 60 nm outside diameter and 30 nm inside diamteer coupled with a 60 nm sphere with a 45 degree angle with respect to the z-axis. The distance between the sphere and the cube is 5 nm and 40 nm. The vertical lines indicate the red light range.

Figure 43: Coupling with spheres of various diameters with a torus with an outside diameter of 60 nm and an inside diameter of 30 nm.

7 Conclusion and recommendations

For multiple shapes, in various sizes, the scattering cross section and near-field enhancement were computed. For each shape the optimal size was determined by looking at the peak wavelengths and the maximum field enhancement. For this chosen size the coupling with spheres of 20 nm, 40 nm and 60 nm was gathered. By looking at these graphs the best shape size combination can be determined.

For the shape size combinations of which the coupling was completed, the focus was on the peak wavelength. The peak wavelength of the coupled triangle was not in the red range as desired, therefore, the triangle was found not to be a valid option. This leaves the sphere, cube, rod and torus. All of these coupled shapes have peak wavelengths in the red range and will therefore be suitable. The cube, however, has a second peak which is at 750 nm and therefore just in the infrared range. This is sub-optimal, consequently this option is also considered invalid.

This leaves three shapes that all meet the requirements. Out of these shapes the rod of 60 nm diameter and 100 nm height would be the most obvious choice since the near-field enhancement is the highest, and thus gives the largest chance at coupling. Additionally the peaks of the scattering cross section were relatively high. Furthermore the field distribution allows coupling at multiple angles. The scattering cross section peaks of the 146 nm sphere are higher but coupling is prioritized in this case.

The shape size combination is not in compliance with the hypothesis where it was stated that non-spherical particles are more likely to couple. This deviation from the hypothesis can be because of the sizes that were considered. An advantage of spherical particles is that they have a more distributed field which increases the chance of coupling. The size of the most valid option is in compliance with the hypothesis where it was stated that larger particles yield larger peaks. They however also yield a higher peak wavelength. That the optimum is 60 nm diameter and 100 nm height in this case is, therefore, coherent.

The limiting factor in this thesis was the simulation time of the toolbox. Since the full Maxwell equations had to be solved the elapsed time could reach up to 6 hours for one simulation. That is the most important reason that the amount of simulated shapes was limited. For future researches and simulations mirror symmetry could be implemented. The advantage is that only half or even a quarter of the field of the particle is computed and with the help of symmetry this is expanded to the complete field. For this thesis implementation of mirror symmetry was tried out but did only yield errors or results that deviated from the validation. Something else that could be looked into is the use of the quasistatic approximation and how much the results would deviate. The quasistatic approximation is shortly explained in section 4.1.1. In short it approximates certain values instead of performing full Maxwell equations. The approximation is mostly valid for particles that are significantly, more than a factor 10, smaller than the light wavelength. This makes this method faster and less precise.

References

[1] KWF. kanker in cijfers.

[2] Cancer research UK. world wide cancer statistics.

[3] Willem F. Rurup, Loes I. Segerink, Herbert M. Kraaijenhagen, Roderik A.and Pinedo, Albert Van den Berg, Renske D. M. Steenberg, Idris Nieuwenhuijzen, Jacobus A.and Bache, and Geert Kazemier. Detection of cancer in urine, International Patent WO 2017/171548 Al, Oct. 2017.

[4] Judith Bosschieter, Catrin Lutz, Loes I. Segerink, André N. Vis, Ellen C. Zwarthoff, R. Jeroen A. Van Moorselaar, Bas Wg Van Rhijn, Martijn W. Heymans, Elizabeth P. Jansma, Renske Dm Steenbergen, and Jakko A. Nieuwenhuijzen. The diagnostic accuracy of methylation markers in urine for the detection of bladder cancer: A systematic review. *Epigenomics*, 10(5):673–687, 5 2018.

[5] Michael Holzinger, Alan Le Goff, and Serge Cosnier. Nanomaterials for biosensing applications: a review. *Frontiers in Chemistry*, 2:63, 2014.

[6] J.E. van Dongen. Assignment description, March 2020.

[7] R. Verdoold. *Scattering gold nanoparticles: strategies for ultra sensitive DNA detection.* Universiteit Twente, 9 2012.

[8] Thijs van Eeden. The near-field of gold plasmonic nanoparticles.

[9] Lu Sun, Ping Chen, and Lie Lin. Enhanced molecular spectroscopy via localized surface plasmon resonance. In Mark T. Stauffer, editor, *Applications of Molecular Spectroscopy to Current Research in the Chemical and Biological Sciences*, chapter 18. IntechOpen, Rijeka, 2016.

[10] Eleonora Petryayeva and Ulrich J. Krull. Localized surface plasmon resonance: Nanostructures, bioassays and biosensing—a review. *Analytica Chimica Acta*, 706(1):8 – 24, 2011.

[11] Kristian Göeken, Vinod Subramaniam, and Ron Gill. Enhancing spectral shifts of plasmon-coupled noble metal nanoparticles for sensing applications. *Physical chemistry chemical physics*, 17(1):422–427, 2015. Open access.

[12] T. Gric. *Plasmonics.* IntechOpen, 2018.

[13] Lutz Langguth. Plasmon assisted fluorescence emission: far-field observables and their fluctuations. 2015.

[14] Eduardo Coronado, Ezequiel Encina, and Fernando Stefani. Optical properties of metallic nanoparticles: Manipulating light, heat and forces at the nanoscale. *Nanoscale*, 3:4042–59, 09 2011.

[15] Amitabh Ghoshal. Plasmon enhanced near-field interactions in surface coupled nanoparticle arrays for integrated nanophotonic devices.

[16] I.S. Grant and W.R. Phillips. *Electromagnetism.* Manchester Physics Series. Wiley, 2013.

[17] Richard Phillips Feynman, Robert Benjamin Leighton, and Matthew Sands. *The Feynman lectures on physics; New millennium ed.* Basic Books, New York, NY, 2010. Originally published 1963-1965.

[18] David J Griffiths. *Introduction to electrodynamics; 4th ed.* Pearson, Boston, MA, 2013. Re-published by Cambridge University Press in 2017.

[19] Jürgen Waxenegger, Andreas Trügler, and Ulrich Hohenester. Plasmonics simulations with the mnpbem toolbox: Consideration of substrates and layer structures. *Computer Physics Communications*, 193:138 – 150, 2015.

[20] Ulrich Hohenester. Bem theory.

[21] R.A. Adams and C. Essex. *Calculus: A Complete Course*. Pearson, 2013.

[22] Robert G. Brown. online lectures in physics.

[23] Adam B. Taylor and Peter Zijlstra. Single-molecule plasmon sensing: current status and future prospects. pages 1103–1112, August 2017.

[24] Richard K. Harrison. Mechanisms and applications of near-field and far-field enhancement using plasmonic nanoparticles.

[25] Ulrich Hohenester and Andreas Trügler. Mnpbem – a matlab toolbox for the simulation of plasmonic nanoparticles. *Computer Physics Communications*, 183(2):370–381, Feb 2012.

[26] Adrien Lalisse, Gilles Tessier, Jérome Plain, and Guillaume Baffou. Quantifying the efficiency of plasmonic materials for near-field enhancement and photothermal conversion. *The Journal of Physical Chemistry C*, 119(45):25518–25528, 2015.

[27] The spectrum of visible light.

[28] Ping Chen Lu Sun and Lie Lin. Enhanced molecular spectroscopy via localized surface plasmon resonance.

A Validation code

Below the code that was used for the validation of the scattering cross section of separate GNP's is shown

```
clear all;
close all;
%%
% creating table of dielectric functions (air = 1,
glass = 2.25) epstab = { epsconst( 1 ),
epstable('gold.dat'),  epsconst(2.25)};
% default options for layer structure
op = layerstructure.options;
% set up layer structure
layer = layerstructure( epstab, [ 1, 3 ], 0, op);
% options for BEM simulations
op = bemoptions( 'sim', 'ret', 'layer', layer);
% location of interface of substrate
ztab = 0;
% for loop te loop over different sizes of spheres
(20 nm is used for the validation)
for g = [20]
%%
% create a sphere with 144 vertices
% a diameter of g nm
p = trisphere(144, g);
% set environment of sphere
p = comparticle( epstab, { p }, [ 2, 1], 1, op);
% shift nanosphere above substrate
p = shift(p, [ 0, 0, - min(p.pos(:, 3)) + 1 + ztab])
% light wavelength in a vacuum
 enei = linspace( 400, 900, 40);
 %planewave excitation
 exc = planewave( [ 1, 0, 0], [ 0, 0, -1], op);
 %allocate scattering cross section
 sca = zeros(size(enei));
%%  tabulated Green functions
%  For the retarded simulation first  a table for the
% calculation of the reflected Green function has to be
% set-up. Since this is a slow process and we thus the
% GREENTAB is computed only if it has not been computed
% before.

% For setting up the table for the reflected Green
% function, all points for which it will be computed need
% to be provided. Since the near-field enhancement will
% be computed above and below the layer interfaces using
% the MESHFIELD class, a COMPOINT object is set-up.
% This is not necessary for this part of the validation
% but will be used at a later point
[ x, z ] = meshgrid( linspace( - 200, 200, 401 ),
linspace( - 200, 200, 401 ) );
%  make COMPOINT object
 pt = compoint( p, [ x( : ), 0 * x( : ),
 z( : ) + 1e-3 ], op );
```

```
if ~exist( 'greentab', 'var' ) ||
~greentab.ismember( layer, enei, p, pt )
  %  automatic grid for tabulation
  %  a rather small number NZ is used for tabulation to
  % speed up the simulations
   tab = tabspace( layer, p, pt, 'nz', 10 );
  %  Green function table
   greentab = compgreentablayer( layer, tab );
  %  precompute Green function table
   greentab = set( greentab, enei, op );
end
op.greentab = greentab;

 %%
 %set up BEM solver
bem = bemsolver( p, op );
%for loop to loop over the wavelengths
    for ien = 1 : length( enei )
     %  surface charge
     sig = bem \ exc( p, enei( ien ) );
     %  scattering cross sections
     sca( ien, : ) = exc.sca( sig );
    end
%% plot
figure(1)
plot(enei, sca, 'o-');
legend( sprintf('sphere: diameter = %i nm', g));
xlabel( 'wavelength (nm)');
ylabel( 'scattering cross section (nm^2)' );
title( 'validation for a 20 nm sphere with substrate')

end
```

Below the code can be found for the near-field enhancement. These codes are added together into one code for the gathering of results

```
clear all;
close all;
tic
% table of dielectric functions (air = 1)  SiO2= 2.12314
epstab = { epsconst( 1 ), epstable( 'gold.dat' )};
% options voor BEM simulation
%  default options for layer structure
op = layerstructure.options;
%  set up layer structure
layer = layerstructure( epstab, [ 1, 2 ], 0, op);
%  options for BEM simulations
op = bemoptions( 'sim', 'ret')
%  location of interface of substrate
ztab = 0;
enhancement = zeros(1,1);
k=1
for g = [20]
%%
```

```
%  wavelength of light
for enei = [522];
%%
p = trisphere(144, g);
p = comparticle( epstab, { p }, [2, 1], 1, op );

%
%% tabulated Green functions
%  For the retarded simulation we first have to set up a table for the
%  calculation of the reflected Green function.  This part is usually slow
%  and we thus compute GREENTAB only if it has not been computed before.

%  For setting up the table for the reflected Green function, we need to
%  provide all points for which we will compute it.  As we will compute the
%  near-field enhancement above and below the layer interfaces using the
%  MESHFIELD class, we here set up a COMPOINT object.  Note that the
%  MESHFIELD object must be initialized later because it needs the
%  precomputed Green function table.
[ z, x ] = meshgrid( linspace( - 55, 55, 201 ), linspace( - 35, 35, 201 ) );
%  make COMPOINT object
%    it is important that COMPOINT receives the OP structure because it has
%    to group the points within the layer structure
 pt = compoint( p, [ x( : ), 0 * x( : ), z( : ) + 1e-3 ], op );

if ~exist( 'greentab', 'var' ) || ~greentab.ismember( layer, enei, p, pt )
  %  automatic grid for tabulation
  %    we use a rather small number NZ for tabulation to speed up the
  %    simulations
  tab = tabspace( layer, p, pt, 'nz', 10 );
  %  Green function table
  greentab = compgreentablayer( layer, tab );
  %  precompute Green function table
  greentab = set( greentab, enei, op );
end
op.greentab = greentab;
%%
%  initialize BEM solver
bem = bemsolver( p, op );
exc = planewave( [ 1, 0, 0], [ 0, 0, -1], op);
%  solve BEM equation
sig = bem \ exc( p, enei );

  %% computation of electric field
%  object for electric field
%    MINDIST controls the minimal distance of the field points to the
%    particle boundary
emesh = meshfield( p, x, 0, z + 1e-3, op, 'mindist', 0.15, 'nmax', 5000 );
%  induced and incoming electric field
e_inc = emesh( sig )
e_ind = emesh( exc.field( emesh.pt, enei ) )
e =  e_inc + e_ind;
%  norm of electric field
ee = sqrt( dot( e, e, 3 ) );
```

```
ee_inc = sqrt( dot( e_inc, e_inc, 3 ) );
ee_ind = sqrt( dot( e_ind, e_ind, 3 ) );
ee_div = ee_ind./ee_inc
%% final plot
% plot electric field
figure (k)
imagesc( x( : ), z( : ), abs(ee.^2));
hold on

colorbar; colormap hot( 255 );

xlabel( 'x (nm)' );
ylabel( 'z (nm)' );

title ( 'Field enhancement' );

set( gca, 'YDir', 'norm' );
axis equal tight
hold on
enhancement(k) = max( max(abs(ee.^2)));
k = k+1;

end
end
% figure(5)
% plot(p, 'nvec', true);
% hold on
h = [20];
figure(2);
plot(h, enhancement, 'o-');
xlabel( 'particle size');
ylabel( 'maximum field enhancement' );
title('maximum field enhancement of a sphere of various sizes')
hold on
```

Next the code that will be used for coupling is given

```
clear all;
close all;

% table of dielectric functions glass=2.25
epstab = { epsconst( 2.25 ), epstable( 'gold.dat'),
epstable('gold.dat')};
% default options for layer structure
op = layerstructure.options;
% set up layer structure
layer = layerstructure( epstab, [ 1, 2 ], 1, op);
% options for BEM simulations
op = bemoptions( 'sim', 'ret' );
% location of interface of substrate
ztab = 0;
%Forloop over different sizes of particles
for g = [60 80 100 125]
%%
exc = planewave( [ 1, 0, 0], [ 0, 0, -1], op);
```

```
%  wavelength of red light
enei = 700;
%%
p1 = trisphere(144, g);
%Second sphere the middle of this particle is shift
%right with g nm
p2 = shift(trisphere(144, 40), [g,0, 0]);
%  shift nanosphere above substrate
p = comparticle( epstab, { p1, p2 },
[ 2, 1; 3,1], 1, 2, op);
 p = shift( p, [ 0, 0, - min( p.pos( :, 3 ) )
 + 1 + ztab ])

 tabulated Green functions
%  For the retarded simulation first  a table for the
% calculation of the reflected Green function has to be
% set-up. Since this is a slow process and we thus the
% GREENTAB is computed only if it has not been computed
% before.

% For setting up the table for the reflected Green
% function, all points for which it will be computed need
% to be provided. Since the near-field enhancement will
% be computed above and below the layer interfaces using
% the MESHFIELD class, a COMPOINT object is set-up.
% This is not necessary for this part of the validation
% but will be used at a later point
[ x, z ] = meshgrid( linspace( - 100, 100, 201 ),
linspace( - 100, 100, 201 ) );
% make COMPOINT object
% it is important that COMPOINT receives the OP
% structure because it has to group the points
% within the layer structure
 pt = compoint( p, [ x( : ), 0 * x( : ),
 z( : ) + 1e-3 ], op );
if ~exist( 'greentab', 'var' ) ||
~greentab.ismember( layer, enei, p, pt )
  %  automatic grid for tabulation use a rather
  % small number  NZ for tabulation to speed up the
  % simulations
   tab = tabspace( layer, p, pt, 'nz', 10 );
  %  Green function table
   greentab = compgreentablayer( layer, tab );
  %  precompute Green function table
   greentab = set( greentab, enei, op );
end
op.greentab = greentab;
%%
        %  initialize BEM solver
        bem = bemsolver( p, op );
        exc = planewave( pol, dir, op );
        %  solve BEM equation
        sig = bem \ exc( p, enei );
```

```
  %% computation of electric field
% object for electric field
% MINDIST controls the minimal distance of the
%field points to the particle boundary
emesh = meshfield( p, x, 0, z + 1e-3, op,
'mindist', 0.1, 'nmax', 10000 );
% induced and incoming electric field
e = emesh( sig ) +
emesh( exc.field( emesh.pt, enei ) );
% norm of electric field
ee = sqrt( dot( e, e, 3 ) );

%% final plot
% plot electric field
figure (g)
imagesc( x( : ), z( : ), log10( ee ) );
hold on

colorbar; colormap hot( 255 );

xlabel( 'x (nm)' );
ylabel( 'z (nm)' );

title ( 'Field enhancement' );

set( gca, 'YDir', 'norm' );
axis equal tight
hold on
 %%
 enei = linspace( 400, 900, 40);
 exc = planewave( [ 1, 0, 0], [ 0, 0, -1], op);
 sca = zeros(size(enei));
   for ien = 1 : length( enei )
    % surface charge
    sig = bem \ exc( p, enei( ien ) );
    % scattering cross sections
    sca( ien, : ) = exc.sca( sig );
   end

figure(1)
plot(enei, sca, 'o-');
legend( '60', '80', '100', '125');
xlabel( 'wavelength (nm)');
ylabel( 'scattering cross section (nm^2)' );
hold on
figure(g+1)
plot(p, 'nvec', true);
hold on
end
```

B Shapes

At first the complete code that will be used will be given. Below that the shape specific parts will be given for the separate shapes.

```
clear all;
close all;
tic
% table of dielectric functions (air = 1)  SiO2= 2.12314
epstab = { epsconst( 1 ), epstable( 'gold.dat' )};
% options voor BEM simulation
%  default options for layer structure
op = layerstructure.options;
%  set up layer structure
layer = layerstructure( epstab, [ 1, 2 ], 0, op);
%  options for BEM simulations
op = bemoptions( 'sim', 'ret')
%  location of interface of substrate
ztab = 0;
enhancement = zeros(9,1);
k=1
for g = [20 40 60 80 100 120 140 160 180]
%%
%  wavelength of green light
for enei = [540];
%%shape specific code
%sphere with 144 vertices and a diameter of g nm
p = trisphere(144, g);
p = comparticle( epstab, { p }, [2, 1], 1, op );
%put the particle on the substrate
p = shift( p, [ 0, 0, - min( p.pos( :, 3 ) ) + 1 + ztab ])
f = 3*g
%
tabulated Green functions
%  For the retarded simulation first  a table for the
% calculation of the reflected Green function has to be
% set-up. Since this is a slow process and we thus the
% GREENTAB is computed only if it has not been computed
% before.

% For setting up the table for the reflected Green
% function, all points for which it will be computed need
% to be provided. Since the near-field enhancement will
% be computed above and below the layer interfaces using
% the MESHFIELD class, a COMPOINT object is set-up.
% This is not necessary for this part of the validation
% but will be used at a later point
[ x, z ] = meshgrid( linspace( - f, f, 401 ),
linspace( - f, f, 401 ) );
%  make COMPOINT object
%    it is important that COMPOINT receives the OP
%    structure because it has to group the points
%    within the layer structure
 pt = compoint( p, [ x( : ), 0 * x( : ), z( : ) + 1e-3 ],
 op );
```

```
if ~exist( 'greentab', 'var' ) ||
~greentab.ismember( layer, enei, p, pt )
  %  automatic grid for tabulation
  %    we use a rather small number NZ for tabulation
  %    to speed up the simulations
  tab = tabspace( layer, p, pt, 'nz', 10 );
  %  Green function table
  greentab = compgreentablayer( layer, tab );
  %  precompute Green function table
  greentab = set( greentab, enei, op );
end
op.greentab = greentab;
%%
%  initialize BEM solver
bem = bemsolver( p, op );
exc = planewave( [ 1, 0, 0], [ 0, 0, -1], op);
%  solve BEM equation
sig = bem \ exc( p, enei );

  %%  computation of electric field
%  object for electric field
%    MINDIST controls the minimal distance of the field
%    points to the particle boundary
emesh = meshfield( p, x, 0, z + 1e-3, op,
'mindist', 0.15, 'nmax', 5000 );
%  induced and incoming electric field
e_inc = emesh( sig )
e_ind = emesh( exc.field( emesh.pt, enei ) )
e =  e_inc + e_ind;
%  norm of electric field
ee = sqrt( dot( e, e, 3 ) );

%%  final plot
% plot electric field
figure (k)
imagesc( x( : ), z( : ), abs(ee.^2));
hold on

colorbar;  colormap hot( 255 );

xlabel( 'x (nm)' );
ylabel( 'z (nm)' );

title ( 'Field enhancement' );

set( gca, 'YDir', 'norm' );
axis equal tight
hold on
enhancement(k) = max( max(abs(ee.^2)));
k = k+1;
%%
 enei = linspace( 400, 900, 40);
 exc = planewave( [ 1, 0, 0], [ 0, 0, -1], op);
```

```
 sca = zeros(size(enei));
   for ien = 1 : length( enei )
    %  surface charge
    sig = bem \ exc( p, enei( ien ) );
    %  scattering cross sections
    sca( ien, : ) = exc.sca( sig );
   end

figure(10)
plot(enei, sca, 'o-');
hold on
legend('20 nm', '40 nm', '60 nm', '80 nm',  '100 nm',
'120 nm', '140 nm', '160 nm', '180 nm');
xlabel( 'wavelength (nm)');
ylabel( 'scattering cross section (nm^2)' );
hold on
xline(520);
xline(560);

hold on
title('Scattering cross section of a
sphere of various sizes')
hold on
end
end
figure(5)
plot(p, 'nvec', true);
hold on
h = [20 40 60 80 100 120 140 160 180];
figure(11);
plot(h, enhancement, 'o-');
xlabel( 'particle size');
ylabel( 'maximum field enhancement' );
title('maximum field enhancement of a
sphere of various sizes')
hold on
```

Above the code for uncoupled particles is displayed and below for coupled particles.

```
clear all;
close all;

% table of dielectric functions glass=2.25
epstab = { epsconst( 2.12314 ), epstable( 'gold.dat'), epstable('gold.dat'), epsconst( 1
%  default options for layer structure
op = layerstructure.options;
%  set up layer structure
layer = layerstructure( epstab, [ 4, 1 ], 1, op);
%  options for BEM simulations
op = bemoptions( 'sim', 'ret' );
%  location of interface of substrate
ztab = 0;
%Forloop over different sizes of particles
for g = [130]
% distance from particle taking the particle % size into account
```

```
    for q = [90 130]
%%
exc = planewave( [ 1, 0, 0], [ 0, 0, -1], op);
%  wavelength of red light
enei = 670;
%%
   p1 = trisphere(144, g);
%Second sphere the middle of this particle is shift
%right with g nm
p2 = shift(trisphere(144, 20), [0 ,0, q]);
%  shift nanosphere above substrate
p = comparticle( epstab, { p1, p2 }, [ 2, 1; 3,1], 1, 2, op);
p = shift( p, [ 0, 0, - min( p.pos( :, 3 ) )+ 1 + ztab ])

% tabulated Green functions
%  For the retarded simulation first  a table for the
% calculation of the reflected Green function has to be
% set-up. Since this is a slow process and we thus the
% GREENTAB is computed only if it has not been computed
% before.

% For setting up the table for the reflected Green
% function, all points for which it will be computed need
% to be provided. Since the near-field enhancement will
% be computed above and below the layer interfaces using
% the MESHFIELD class, a COMPOINT object is set-up.
% This is not necessary for this part of the validation
% but will be used at a later point
[ x, z ] = meshgrid( linspace( - g, g, (2*g)+1 ),linspace( - g, g, (2*g)+1 ));
% make COMPOINT object
% it is important that COMPOINT receives the OP
% structure because it has to group the points
% within the layer structure
 pt = compoint( p, [ x( : ), 0 * x( : ),z( : ) + 1e-3 ], op );
if ~exist( 'greentab', 'var' ) ||~greentab.ismember( layer, enei, p, pt )
  %  automatic grid for tabulation use a rather
  % small number  NZ for tabulation to speed up the
  % simulations
  tab = tabspace( layer, p, pt, 'nz', 10 );
  %  Green function table
  greentab = compgreentablayer( layer, tab );
  %  precompute Green function table
  greentab = set( greentab, enei, op );
end
op.greentab = greentab;
%%
        %  initialize BEM solver
        bem = bemsolver( p, op );
    exc = planewave( [ 1, 0, 0], [ 0, 0, -1], op);
        %  solve BEM equation
        sig = bem \ exc( p, enei );

  %%  computation of electric field
%  object for electric field
```

```
% MINDIST controls the minimal distance of the
%field points to the particle boundary
emesh = meshfield( p, x, 0, z + 1e-3, op, 'mindist', 0.1, 'nmax', 10000 );
%  induced and incoming electric field
e = emesh( sig ) + emesh( exc.field( emesh.pt, enei ) );
%  norm of electric field
ee = sqrt( dot( e, e, 3 ) );

%%  final plot
% plot electric field
figure (g)
imagesc( x( : ), z( : ), log10( ee ) );
hold on

colorbar;  colormap hot( 255 );

xlabel( 'x (nm)' );
ylabel( 'z (nm)' );

title ( 'Field enhancement' );

set( gca, 'YDir', 'norm' );
axis equal tight
hold on
 %%
 enei = linspace( 400, 900, 40);
 exc = planewave( [ 1, 0, 0], [ 0, 0, -1], op);
 sca = zeros(size(enei));
   for ien = 1 : length( enei )
    %  surface charge
    sig = bem \ exc( p, enei( ien ) );
    %  scattering cross sections
    sca( ien, : ) = exc.sca( sig );
   end

figure(1)
plot(enei, sca, 'o-');
hold on
legend('20 nm size 5 nm distance', '20 nm size 40 mmm distance')
xlabel( 'wavelength (nm)');
ylabel( 'scattering cross section (nm^2)' );
hold on
xline(635);
xline(700);
hold on
figure(g+1)
plot(p, 'nvec', true);
hold on
    end
end
```

Cube

```
%where g is de length of the sides
   poly = polygon(4,'size',[g,g,])
```

```
edge=edgeprofile(g,11,'min',5)
p = tripolygon(poly,edge);
```

Rod

```
%g is the diameter and q the height
p = trirod(q,g)
```

Triangle

```
%g is the length of the sides and q is
%the thickness
poly = polygon(3,'size',[g,g,])
edge=edgeprofile(1,11,'min',q)
p = tripolygon(poly,edge);
```

Torus

```
% where g is the outside diameter
and q the inside diameter
    p = tritorus(g, q);
```

C Fabrication

Method	Lithography	
Submethod		Electron beam
Process	Employment of a particle beam to directly write nano structures on a surface.	employment of an electron beam
Advantages	Control over the spacing, size and relative orientation	Precise control of the size, shape, and spatial distribution of the nanoparticles synthesized
Disadvantages		Highly time consuming
Shapes	Bow-ties, dimers of gold disks, yagi uda antennas and arrays of gold nano rods	
Method	**Wet chemical synthesis**	**DNA origami**
Submethod		
Process	The metal ions in a solution are reduced until the desired shape is reached.	Thiolated strands of DNA bind immobilized gold particles at an in advance determined location.
Advantages	Can yield large quantities of particles with sizes down to several nano meters	Control over spacing and approximate orientation
Disadvantages		Relatively new method
Shapes	Gold nano-rod with specific aspect ratios and bipyramids	Dimers of gold spheres
Method	**Citrate reduction**	**Seed-mediated grow**
Submethod		
Process	The addition of a calculated amount of citrate solution into boiling metal salt, this solutions contains nano particles	Putting gold in a solution 'grows' the nanoparticle
Advantages	Simplicity	Simplicity, high yield, high quality, convenience of size control and fexibiliy in modifications
Disadvantages		
Shapes	Nano clusters	2D gold rings, core shell nanorods and nanodendrites

Figure 44: Table listing fabrication methods for nanoparticles [23]. [28]

D Near-field enhancements

As can be seen for larger particles the near-field enhancements are less clear. This is because the differences are very large and therefore not clear to see. This can be improved by taking the $10log$ of the values.

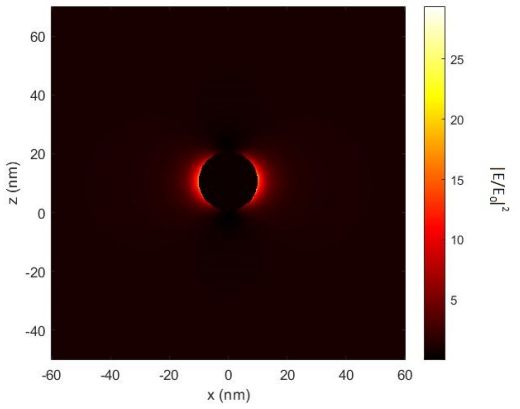

(a) Near-field enhancement of a 20 nm sphere with a light wavelength of 540 nm.

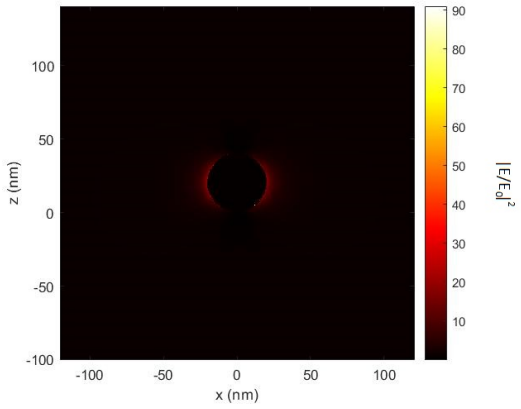

(b) Near-field enhancement of a 40 nm sphere with a light wavelength of 540 nm.

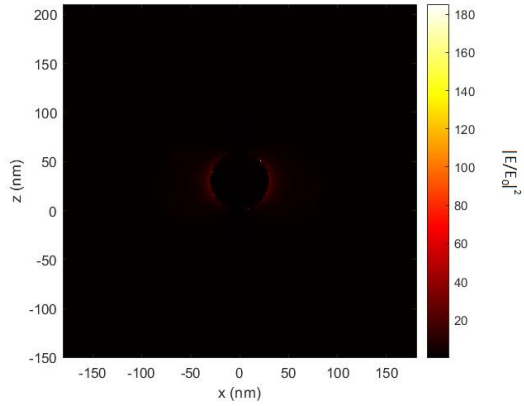

(c) Near-field enhancement of a 60 nm sphere with a light wavelength of 540 nm.

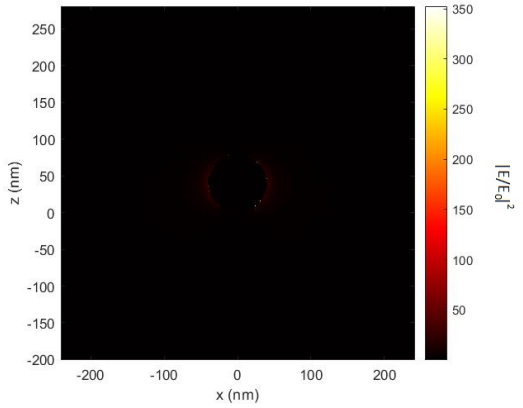

(d) Near-field enhancement of a 80 nm sphere with a light wavelength of 540 nm.

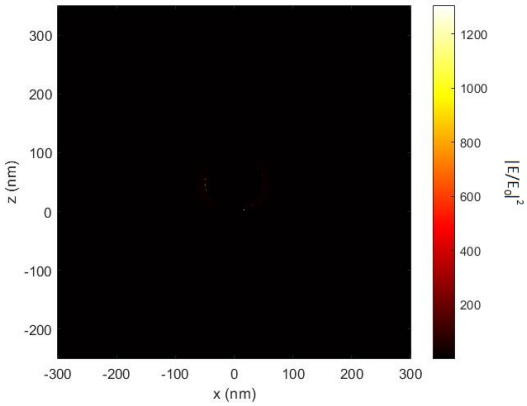

(e) Near-field enhancement of a 100 nm sphere with a light wavelength of 540 nm.

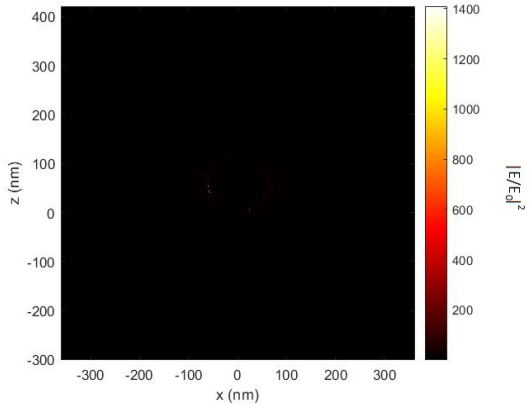

(f) Near-field enhancement of a 120 nm sphere with a light wavelength of 540 nm.

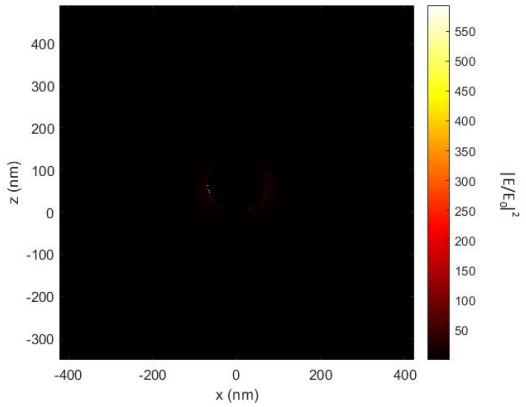

(g) Near-field enhancement of a 140 nm sphere with a light wavelength of 540 nm.

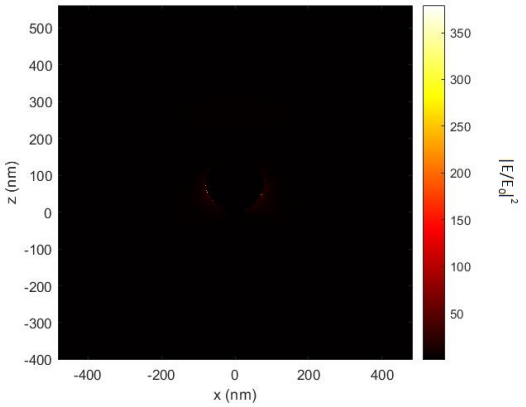

(h) Near-field enhancement of a 160 nm sphere with a light wavelength of 540 nm.

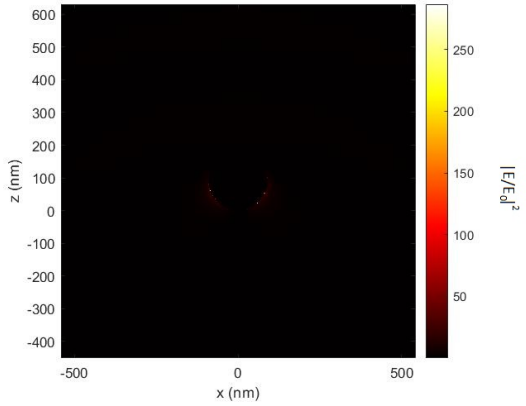

(i) Near-field enhancement of a 180 nm sphere with a light wavelength of 540 nm.

Figure 45: Near-field enhancements of spheres of various diameters.

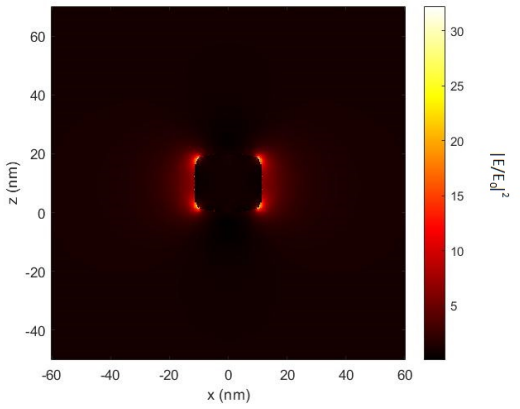

(a) Near-field enhancement of a 20 nm cube with a light wavelength of 540 nm.

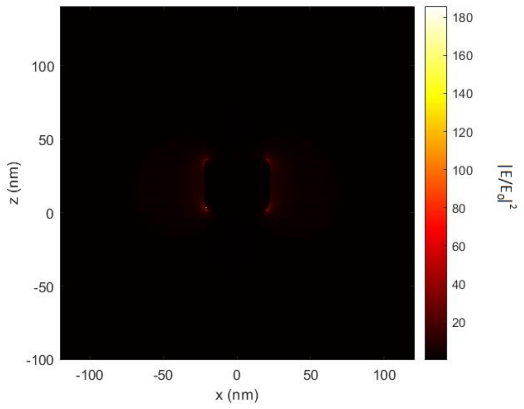

(b) Near-field enhancement of a 40 nm cube with a light wavelength of 540 nm.

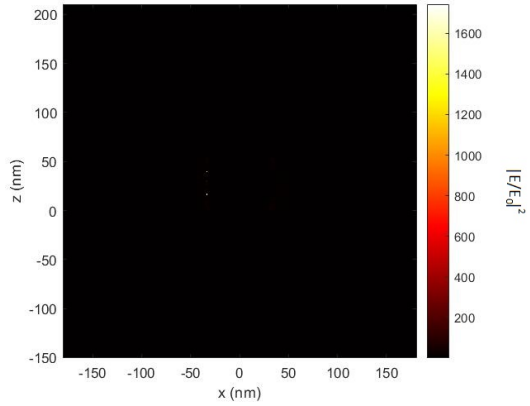

(c) Near-field enhancement of a 60 nm cube with a light wavelength of 540 nm.

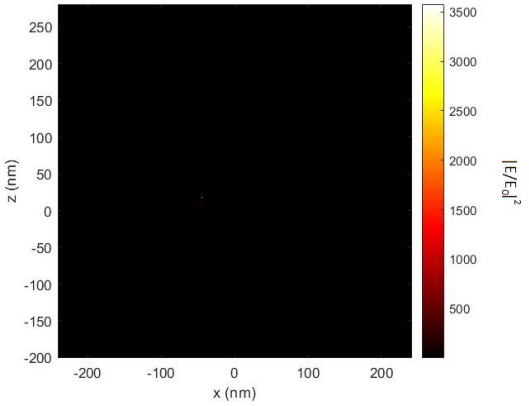

(d) Near-field enhancement of a 80 nm cube with a light wavelength of 540 nm.

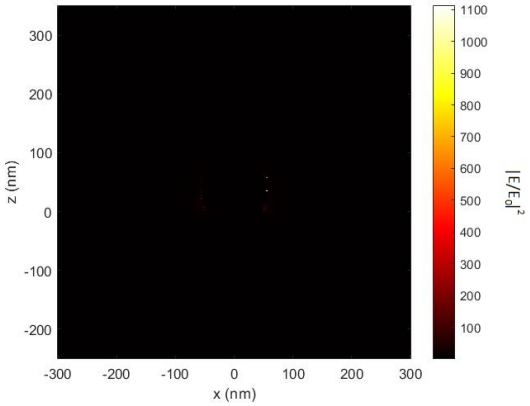

(e) Near-field enhancement of a 100 nm cube with a light wavelength of 540 nm.

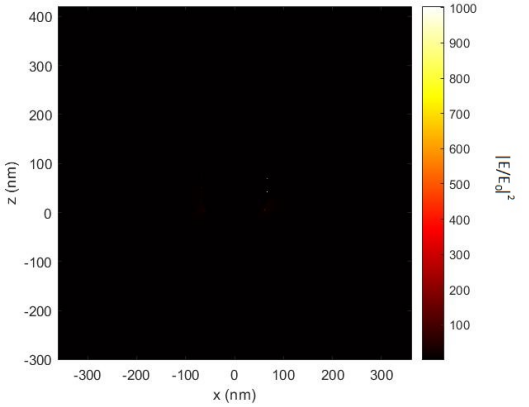

(f) Near-field enhancement of a 120 nm cube with a light wavelength of 540 nm.

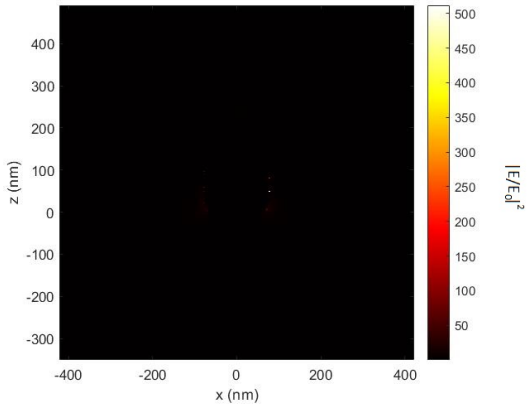

(g) Near-field enhancement of a 140 nm cube with a light wavelength of 540 nm.

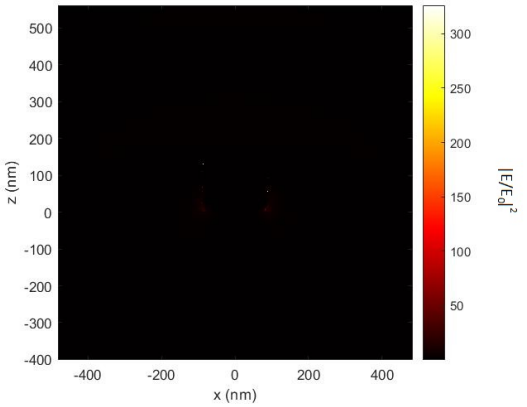

(h) Near-field enhancement of a 160 nm cube with a light wavelength of 540 nm.

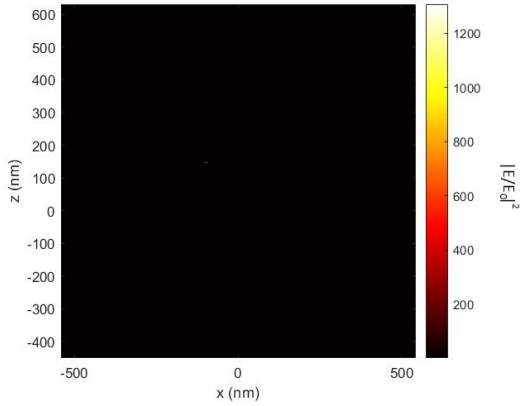

(i) Near-field enhancement of a 180 nm cube with a light wavelength of 540 nm.

Figure 46: Near-field enhancements of cubes of various diameters.

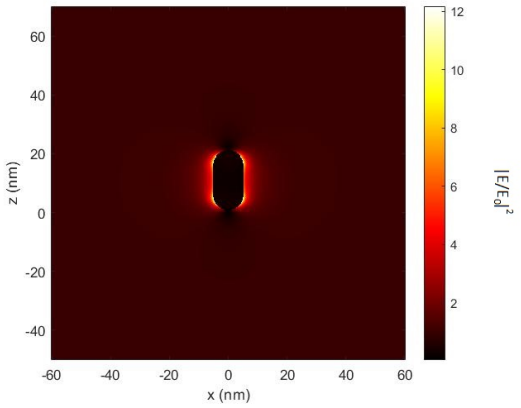

(a) Near-field enhancement of a rod with 20 nm diameter and 10 nm high simulated with a light wavelength of 540 nm.

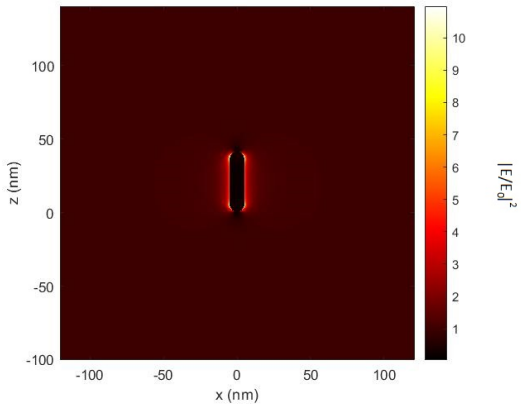

(b) Near-field enhancement of a rod with 40 nm diameter and 10 nm high simulated with a light wavelength of 540 nm.

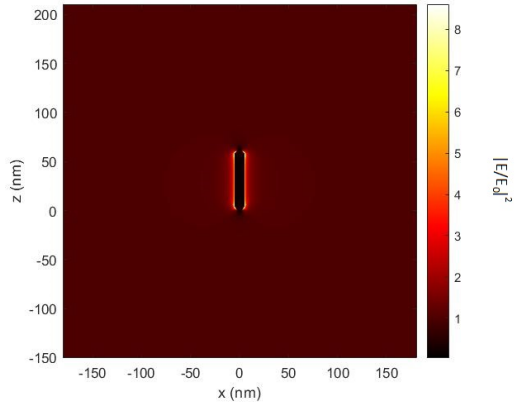

(c) Near-field enhancement of a rod with 60 nm diameter and 10 nm high simulated with a light wavelength of 540 nm.

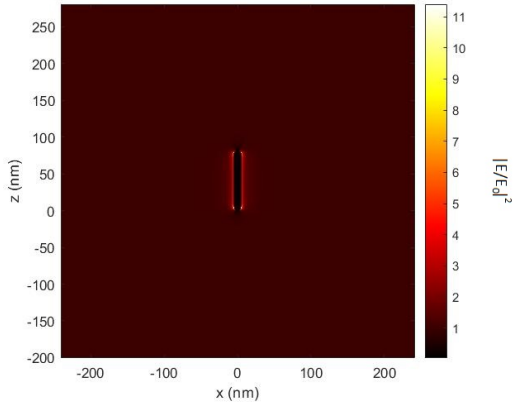

(d) Near-field enhancement of a rod with 80 nm diameter and 10 nm high simulated with a light wavelength of 540 nm.

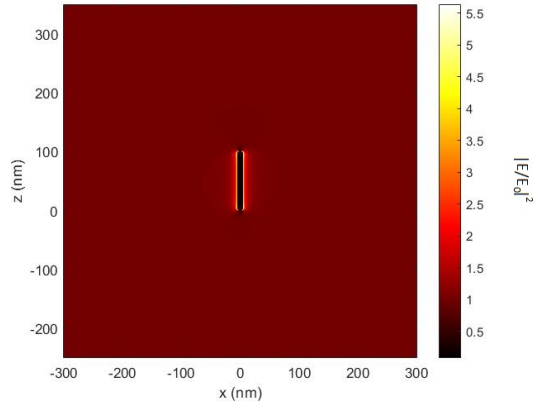

(e) Near-field enhancement of a rod with 100 nm diameter and 10 nm high simulated with a light wavelength of 540 nm.

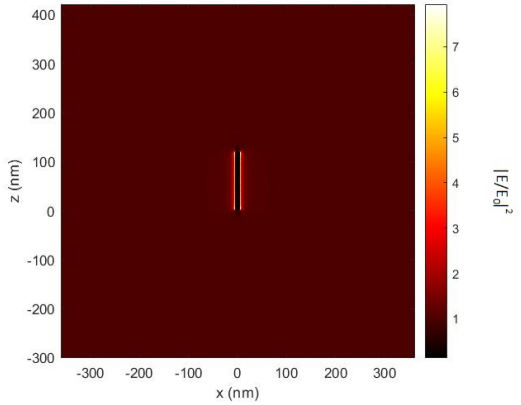

(f) Near-field enhancement of a rod with 120 nm diameter and 10 nm high simulated with a light wavelength of 540 nm.

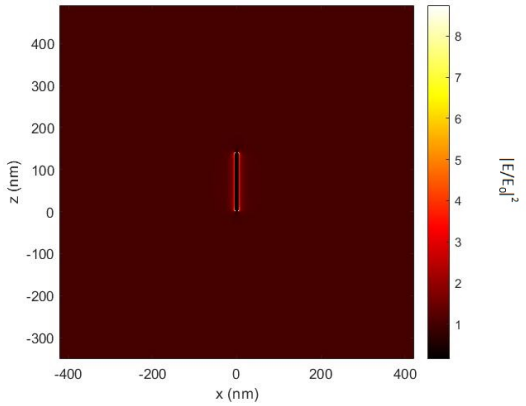

(g) Near-field enhancement of a rod with 140 nm diameter and 10 nm high simulated with a light wavelength of 540 nm.

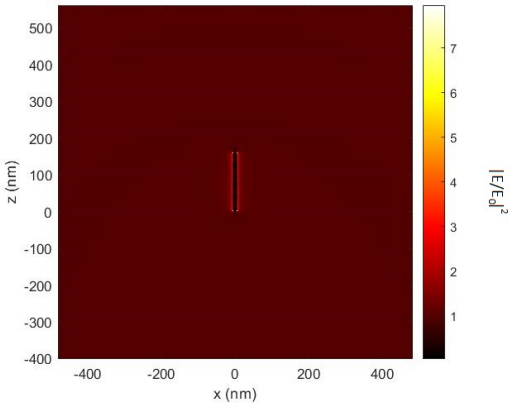

(h) Near-field enhancement of a rod with 160 nm diameter and 10 nm high simulated with a light wavelength of 540 nm.

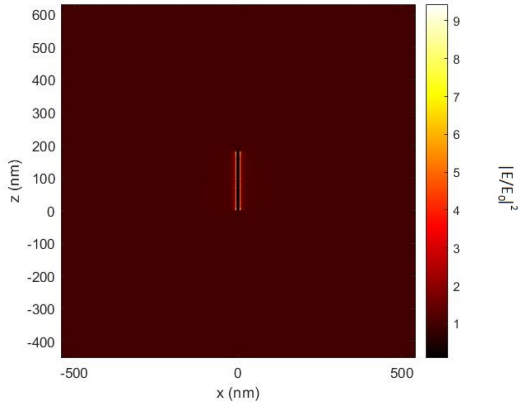

(i) Near-field enhancement of a rod with 180 nm diameter and 10 nm high simulated with a light wavelength of 540 nm.

Figure 47: Near-field enhancements of rods of various diameters and 10 nm height.

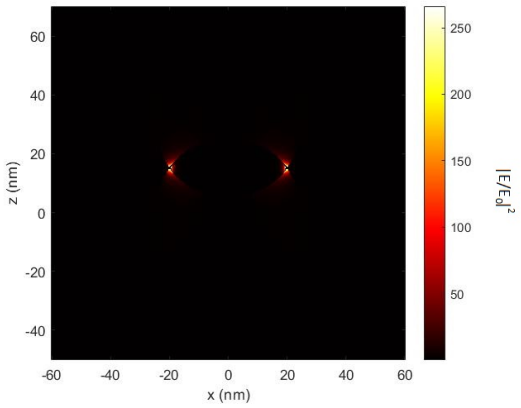

(a) Near-field enhancement of a rod with 20 nm diameter and 50 nm high simulated with a light wavelength of 540 nm.

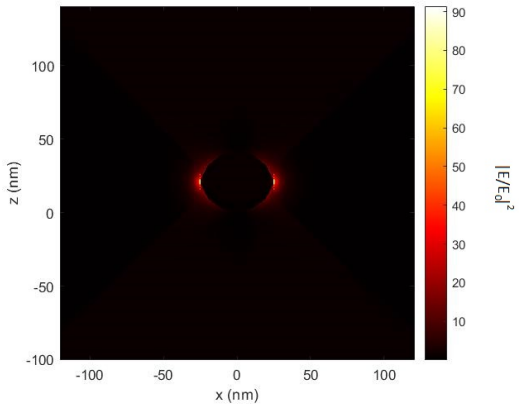

(b) Near-field enhancement of a rod with 40 nm diameter and 50 nm high simulated with a light wavelength of 540 nm.

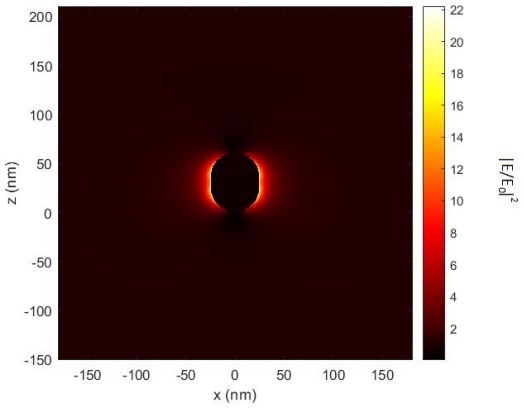

(c) Near-field enhancement of a rod with 60 nm diameter and 50 nm high simulated with a light wavelength of 540 nm.

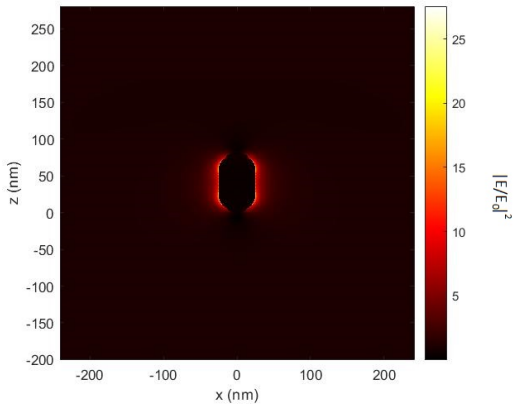

(d) Near-field enhancement of a rod with 80 nm diameter and 50 nm high simulated with a light wavelength of 540 nm.

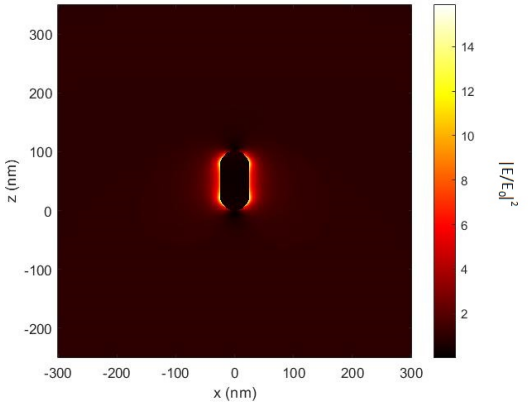

(e) Near-field enhancement of a rod with 100 nm diameter and 50 nm high simulated with a light wavelength of 540 nm.

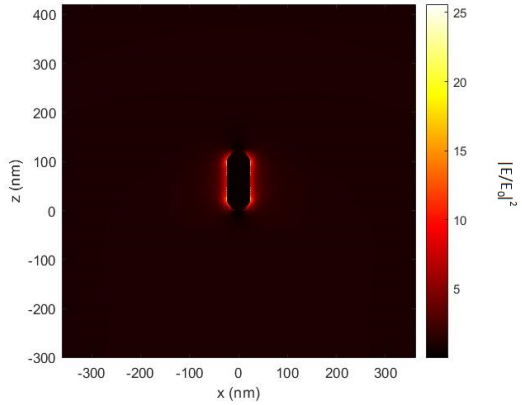

(f) Near-field enhancement of a rod with 120 nm diameter and 50 nm high simulated with a light wavelength of 540 nm.

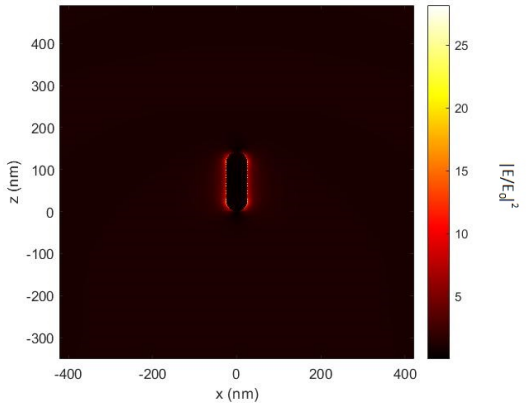

(g) Near-field enhancement of a rod with 140 nm diameter and 50 nm high simulated with a light wavelength of 540 nm.

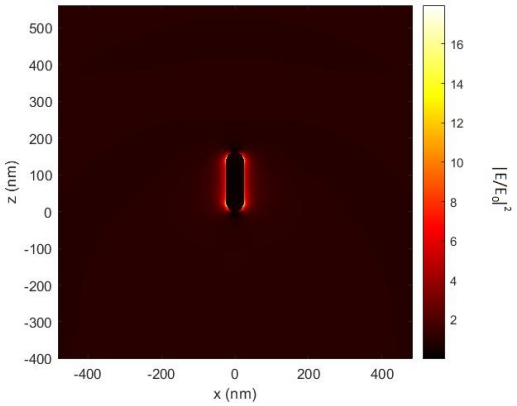

(h) Near-field enhancement of a rod with 160 nm diameter and 50 nm high simulated with a light wavelength of 540 nm.

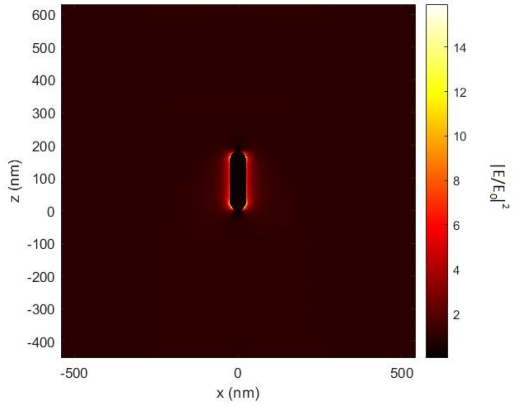

(i) Near-field enhancement of a rod with 180 nm diameter and 50 nm high simulated with a light wavelength of 540 nm.

Figure 48: Near-field enhancements of rods of various diameters and 50 nm height.

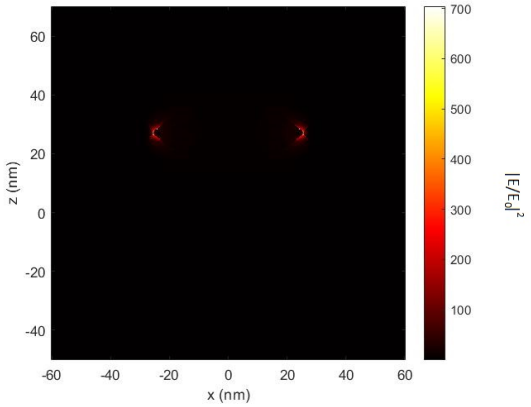

(a) Near-field enhancement of a rod with 20 nm diameter and 75 nm high simulated with a light wavelength of 540 nm.

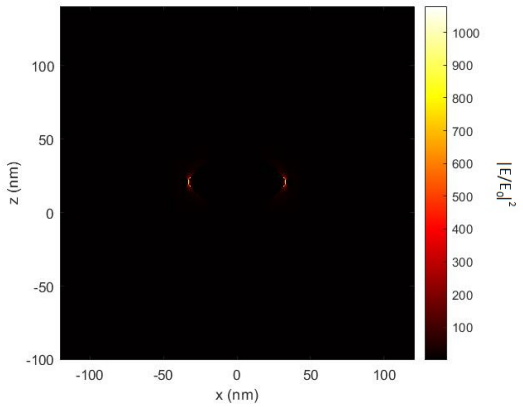

(b) Near-field enhancement of a rod with 40 nm diameter and 75 nm high simulated with a light wavelength of 540 nm.

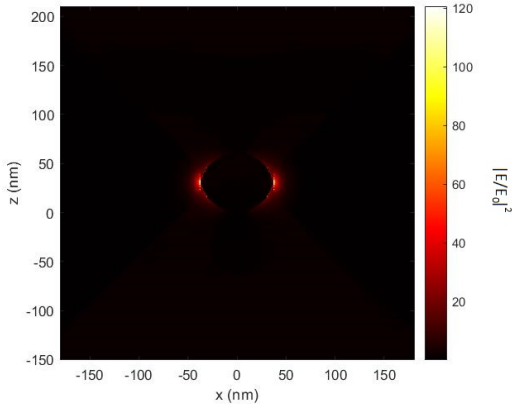

(c) Near-field enhancement of a rod with 60 nm diameter and 75 nm high simulated with a light wavelength of 540 nm.

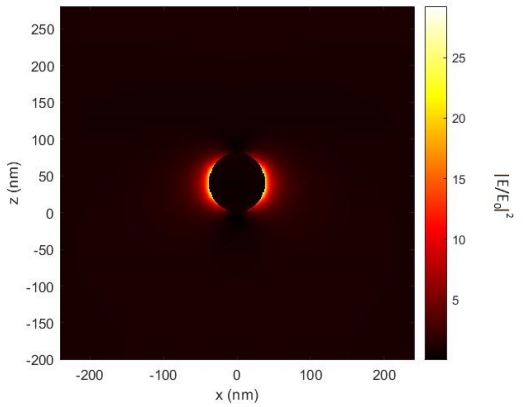

(d) Near-field enhancement of a rod with 80 nm diameter and 75 nm high simulated with a light wavelength of 540 nm.

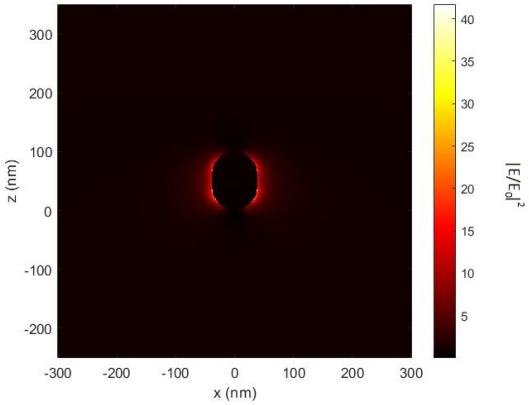

(e) Near-field enhancement of a rod with 100 nm diameter and 75 nm high simulated with a light wavelength of 540 nm.

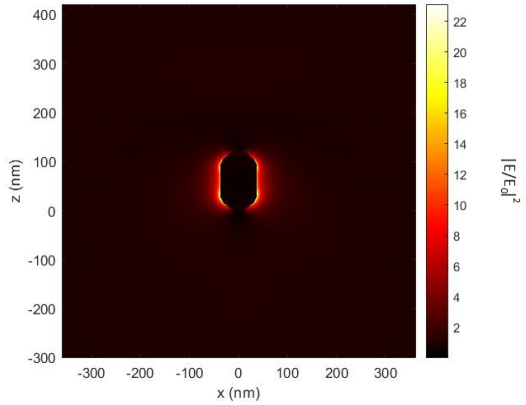

(f) Near-field enhancement of a rod with 120 nm diameter and 75 nm high simulated with a light wavelength of 540 nm.

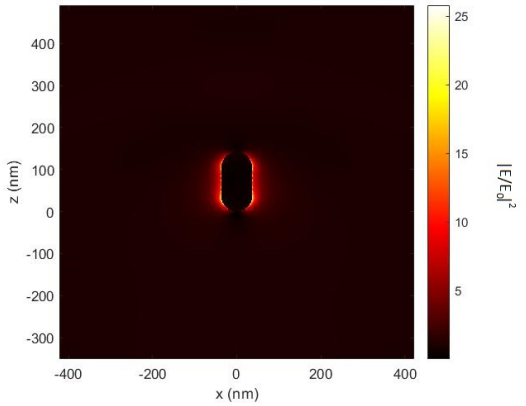

(g) Near-field enhancement of a rod with 140 nm diameter and 75 nm high simulated with a light wavelength of 540 nm.

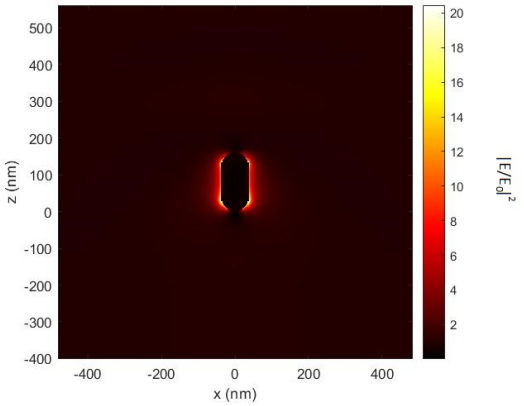

(h) Near-field enhancement of a rod with 160 nm diameter and 75 nm high simulated with a light wavelength of 540 nm.

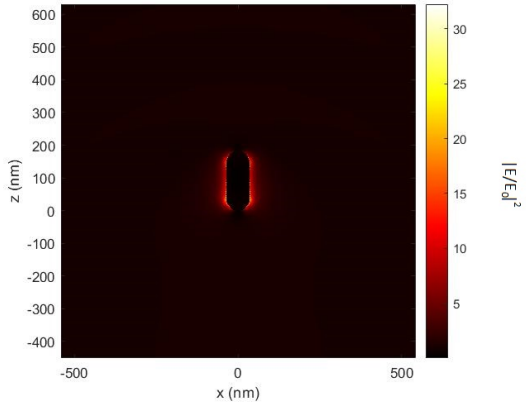

(i) Near-field enhancement of a rod with 180 nm diameter and 75 nm high simulated with a light wavelength of 540 nm.

Figure 49: Near-field enhancements of rods of various diameters and 75 nm height

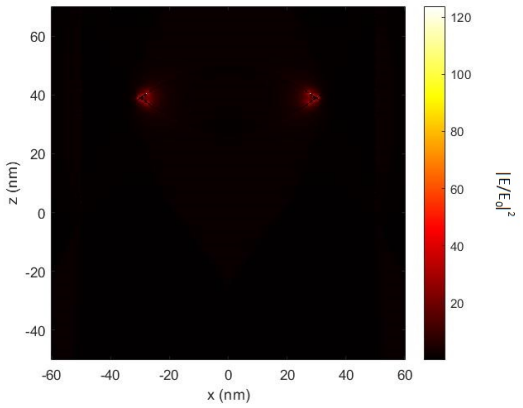

(a) Near-field enhancement of a rod with 20 nm diameter and 100 nm high simulated with a light wavelength of 540 nm.

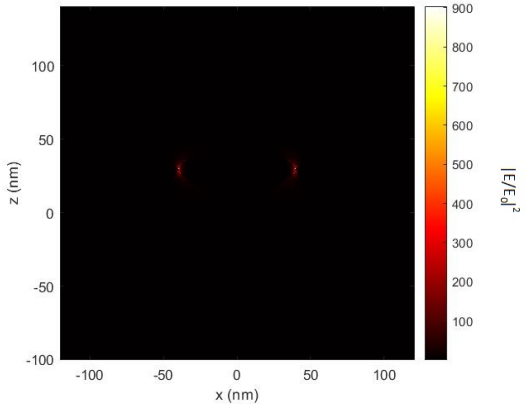

(b) Near-field enhancement of a rod with 40 nm diameter and 100 nm high simulated with a light wavelength of 540 nm.

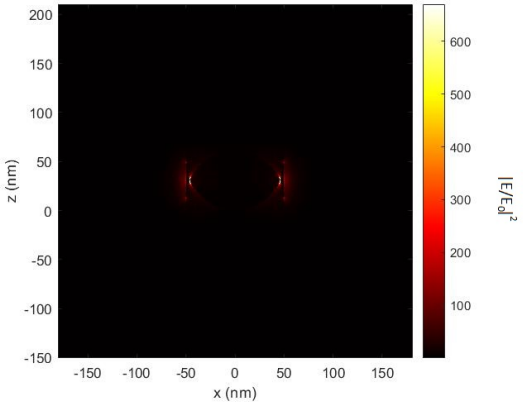

(c) Near-field enhancement of a rod with 60 nm diameter and 100 nm high simulated with a light wavelength of 540 nm.

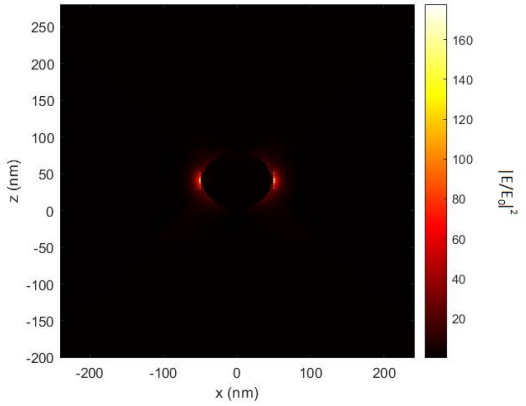

(d) Near-field enhancement of a rod with 80 nm diameter and 100 nm high simulated with a light wavelength of 540 nm.

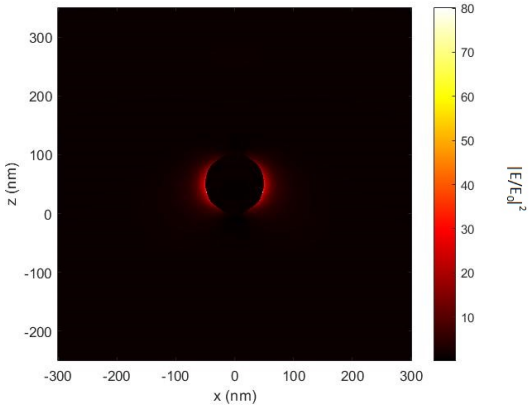

(e) Near-field enhancement of a rod with 100 nm diameter and 100 nm high simulated with a light wavelength of 540 nm.

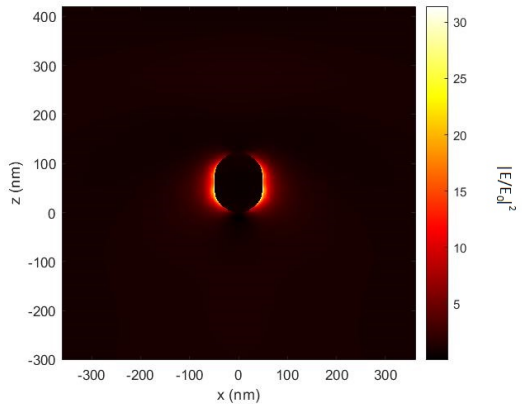

(f) Near-field enhancement of a rod with 120 nm diameter and 100 nm high simulated with a light wavelength of 540 nm.

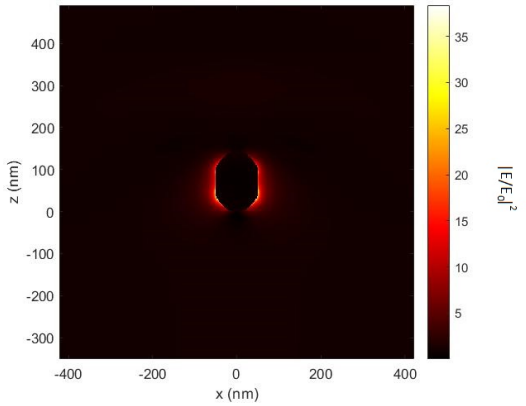

(g) Near-field enhancement of a rod with 140 nm diameter and 100 nm high simulated with a light wavelength of 540 nm.

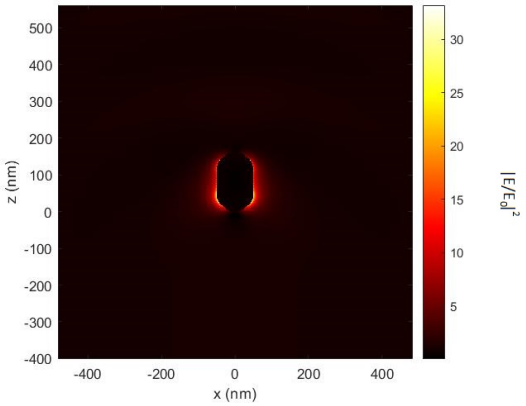

(h) Near-field enhancement of a rod with 160 nm diameter and 100 nm high simulated with a light wavelength of 540 nm.

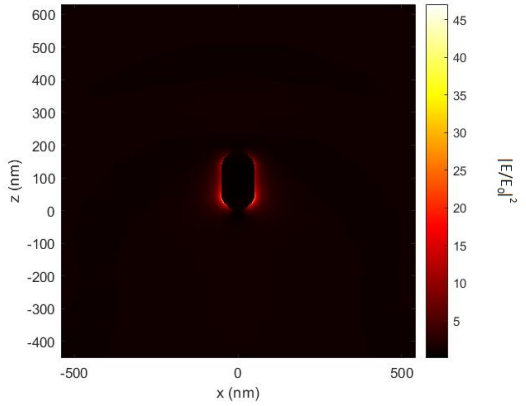

(i) Near-field enhancement of a rod with 180 nm diameter and 100 nm high simulated with a light wavelength of 540 nm.

Figure 50: Near-field enhancements of rods of various diameters and 100 nm height.

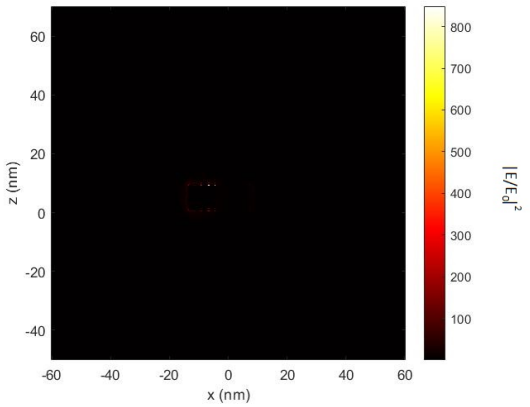

(a) Near-field enhancement of a triangle with 20 nm sides and 10 nm high simulated with a light wavelength of 540 nm.

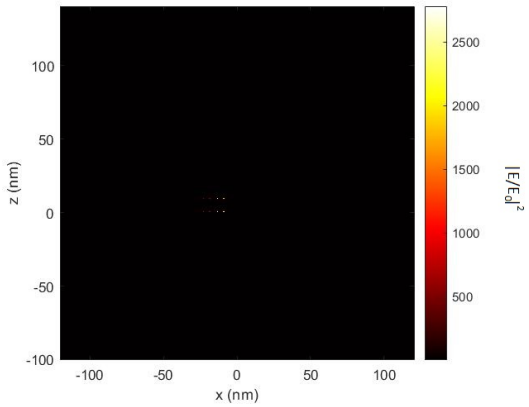

(b) Near-field enhancement of a triangle with 40 nm sides and 10 nm high simulated with a light wavelength of 540 nm.

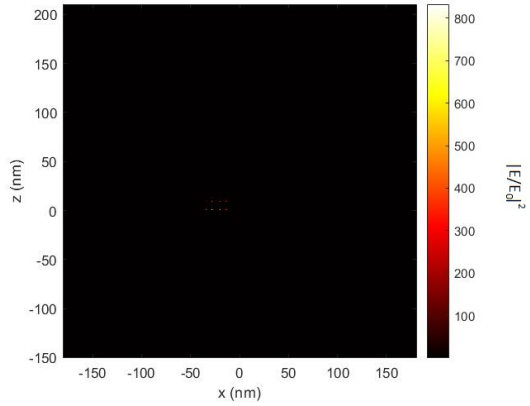

(c) Near-field enhancement of a triangle with 60 nm sides and 10 nm high simulated with a light wavelength of 540 nm.

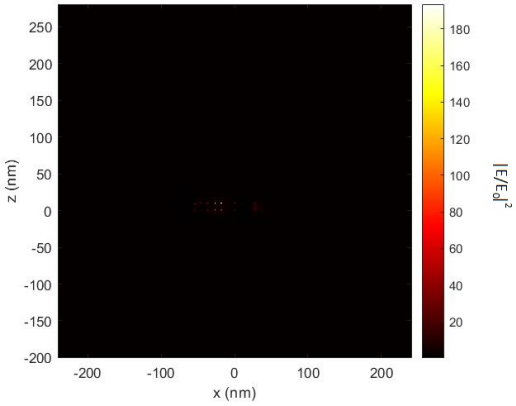

(d) Near-field enhancement of a triangle with 80 nm sides and 10 nm high simulated with a light wavelength of 540 nm.

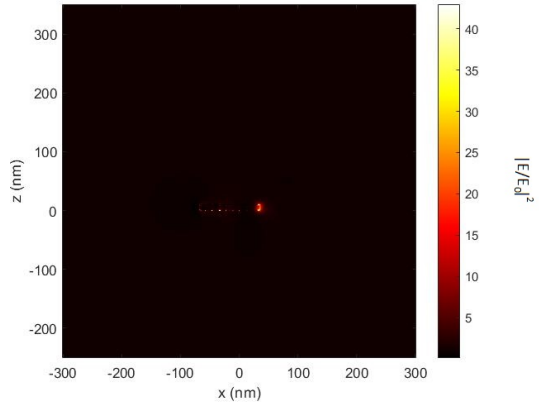

(e) Near-field enhancement of a triangle with 100 nm sides and 10 nm high simulated with a light wavelength of 540 nm.

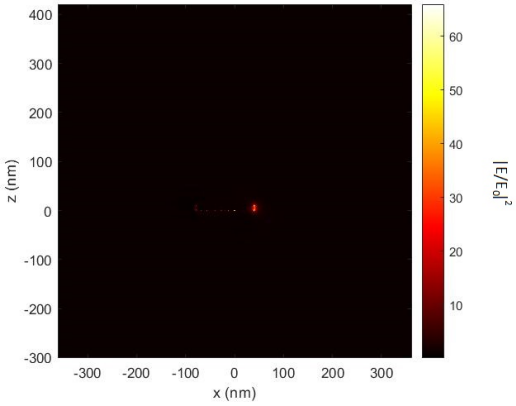

(f) Near-field enhancement of a triangle with 120 nm sides and 10 nm high simulated with a light wavelength of 540 nm.

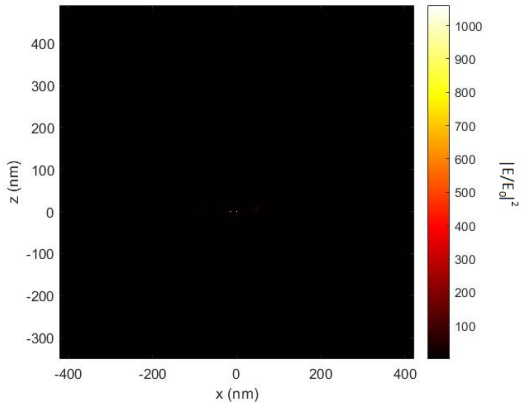

(g) Near-field enhancement of a triangle with 140 nm sides and 10 nm high simulated with a light wavelength of 540 nm.

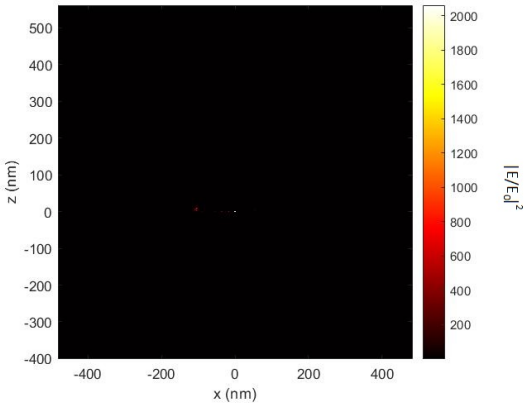

(h) Near-field enhancement of a triangle with 160 nm sides and 10 nm high simulated with a light wavelength of 540 nm.

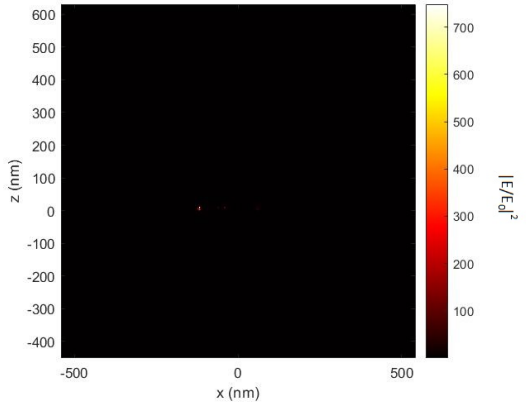

(i) Near-field enhancement of a triangle with 180 nm sides and 10 nm high simulated with a light wavelength of 540 nm.

Figure 51: Near-field enhancements of triangles of various diameters and 10 nm height.

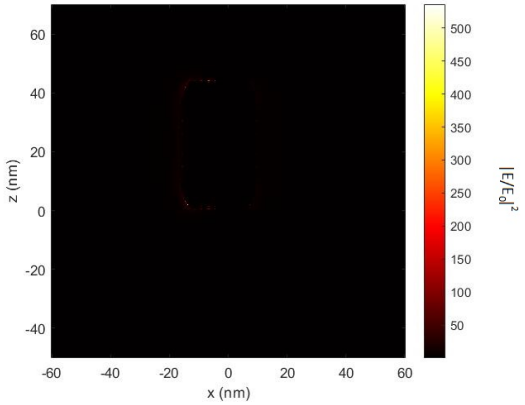

(a) Near-field enhancement of a triangle with 20 nm sides and 50 nm high simulated with a light wavelength of 540 nm.

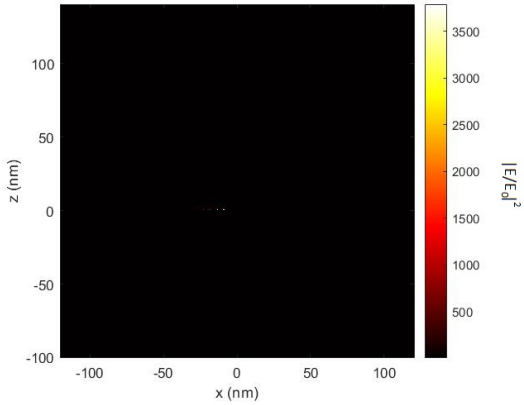

(b) Near-field enhancement of a triangle with 40 nm sides and 50 nm high simulated with a light wavelength of 540 nm.

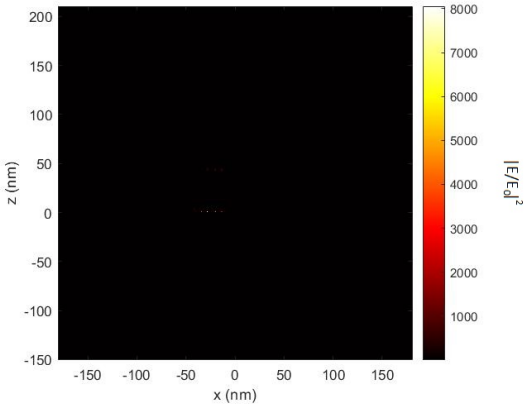

(c) Near-field enhancement of a triangle with 60 nm sides and 50 nm high simulated with a light wavelength of 540 nm.

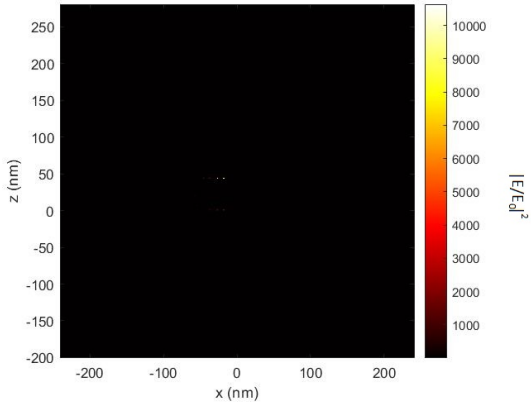

(d) Near-field enhancement of a triangle with 80 nm sides and 50 nm high simulated with a light wavelength of 540 nm.

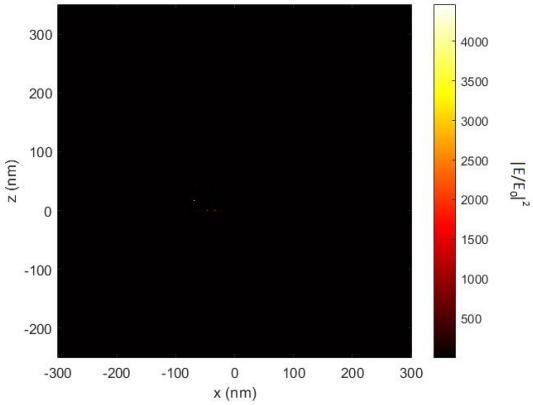

(e) Near-field enhancement of a triangle with 100 nm sides and 50 nm high simulated with a light wavelength of 540 nm.

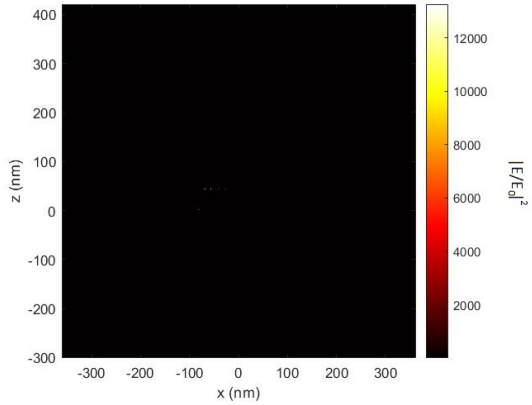

(f) Near-field enhancement of a triangle with 120 nm sides and 50 nm high simulated with a light wavelength of 540 nm.

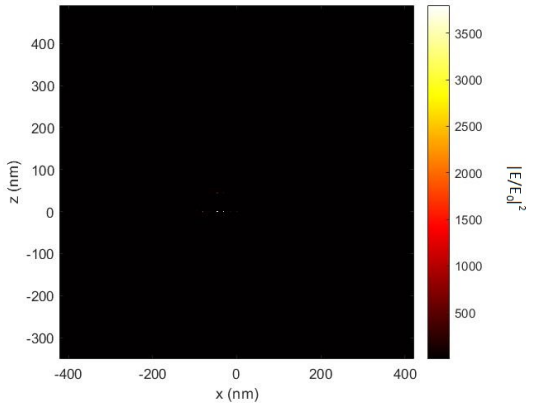

(g) Near-field enhancement of a triangle with 140 nm sides and 50 nm high simulated with a light wavelength of 540 nm.

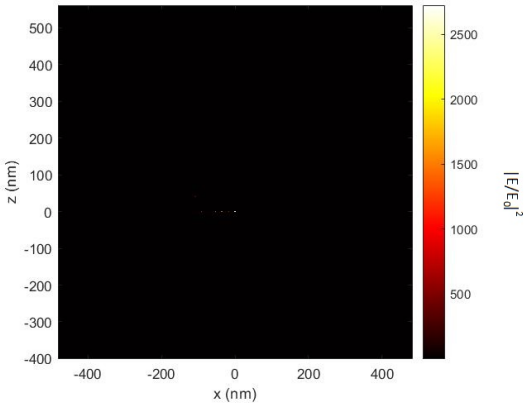

(h) Near-field enhancement of a triangle with 160 nm sides and 50 nm high simulated with a light wavelength of 540 nm.

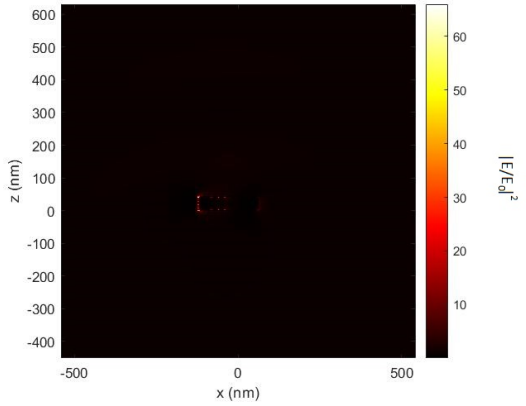

(i) Near-field enhancement of a triangle with 180 nm sides and 50 nm high simulated with a light wavelength of 540 nm.

Figure 52: Near-field enhancements of triangles of various diameters and 50 nm height.

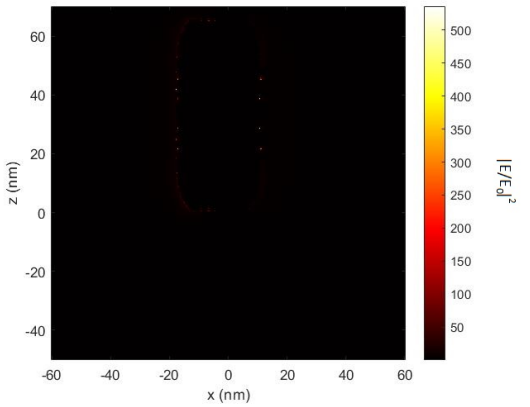

(a) Near-field enhancement of a triangle with 20 nm sides and 75 nm high simulated with a light wavelength of 540 nm.

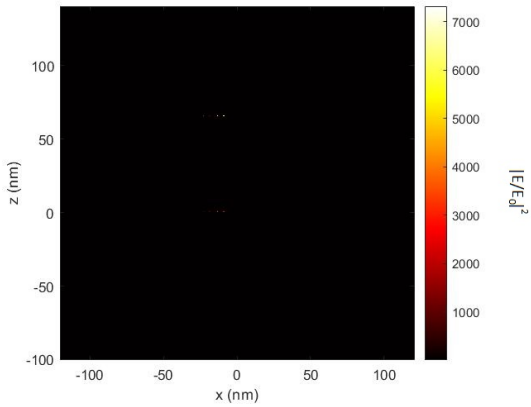

(b) Near-field enhancement of a triangle with 40 nm sides and 75 nm high simulated with a light wavelength of 540 nm.

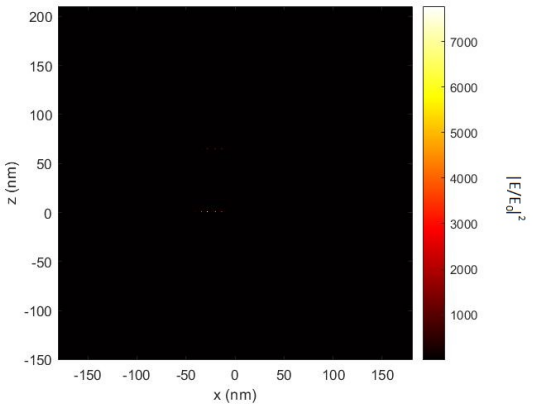

(c) Near-field enhancement of a triangle with 60 nm sides and 75 nm high simulated with a light wavelength of 540 nm.

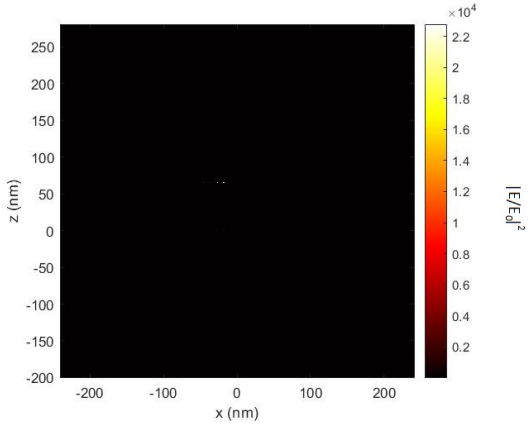

(d) Near-field enhancement of a triangle with 80 nm sides and 75 nm high simulated with a light wavelength of 540 nm.

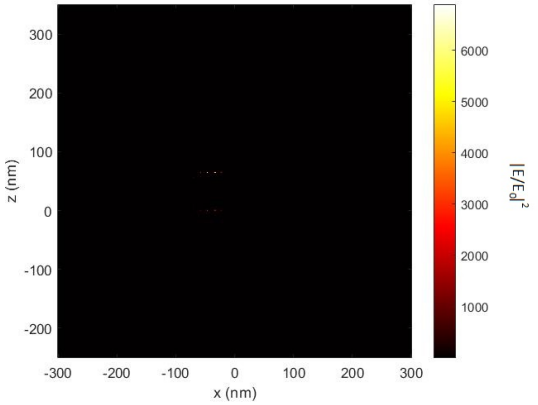

(e) Near-field enhancement of a triangle with 100 nm sides and 75 nm high simulated with a light wavelength of 540 nm.

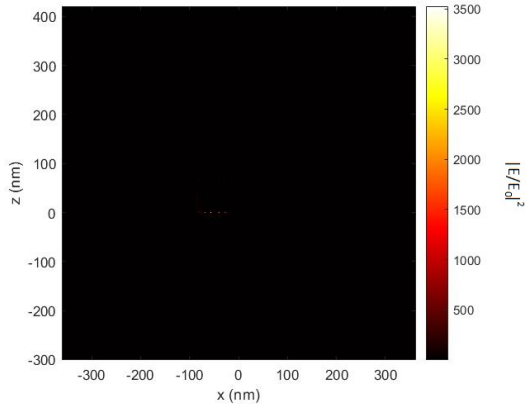

(f) Near-field enhancement of a triangle with 120 nm sides and 75 nm high simulated with a light wavelength of 540 nm.

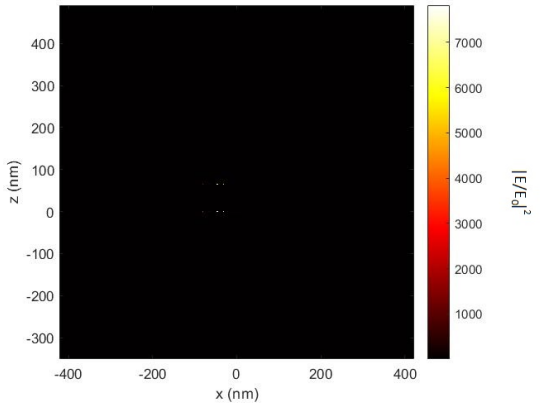

(g) Near-field enhancement of a triangle with 140 nm sides and 75 nm high simulated with a light wavelength of 540 nm.

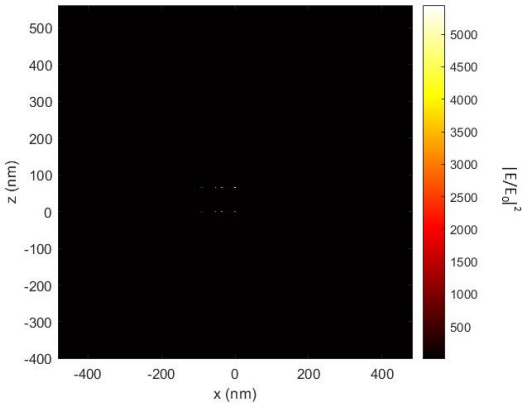

(h) Near-field enhancement of a triangle with 160 nm sides and 75 nm high simulated with a light wavelength of 540 nm.

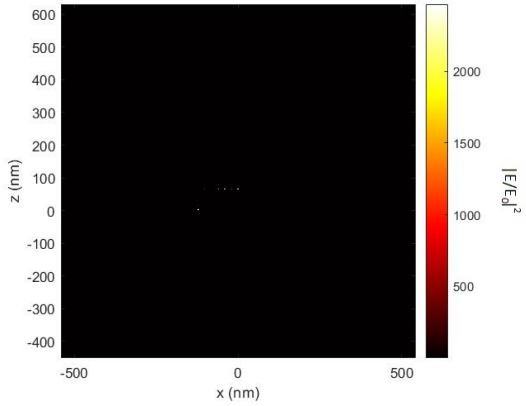

(i) Near-field enhancement of a triangle with 180 nm sides and 75 nm high simulated with a light wavelength of 540 nm.

Figure 53: Near-field enhancements of triangles of various sizes and 75 nm height.

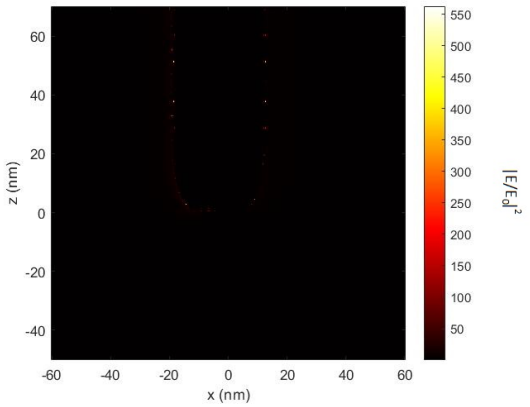

(a) Near-field enhancement of a triangle with 20 nm sides and 100 nm high simulated with a light wavelength of 540 nm.

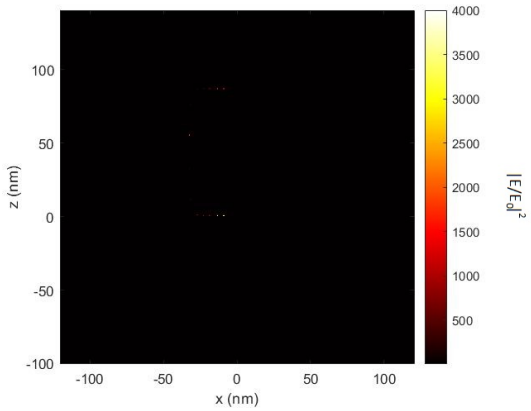

(b) Near-field enhancement of a triangle with 40 nm sides and 100 nm high simulated with a light wavelength of 540 nm.

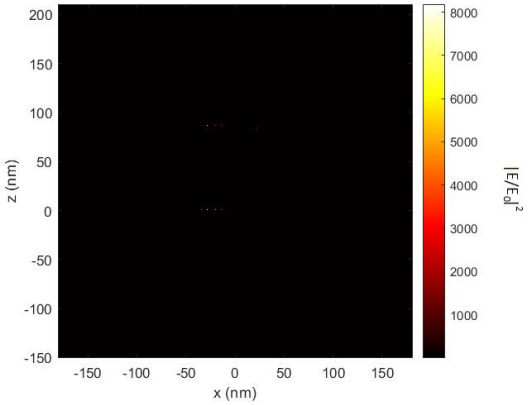

(c) Near-field enhancement of a triangle with 60 nm sides and 100 nm high simulated with a light wavelength of 540 nm.

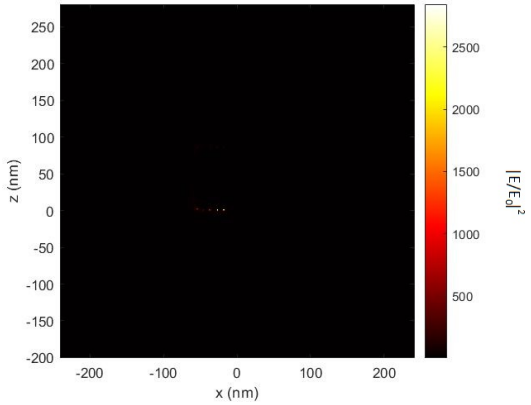

(d) Near-field enhancement of a triangle with 80 nm sides and 100 nm high simulated with a light wavelength of 540 nm.

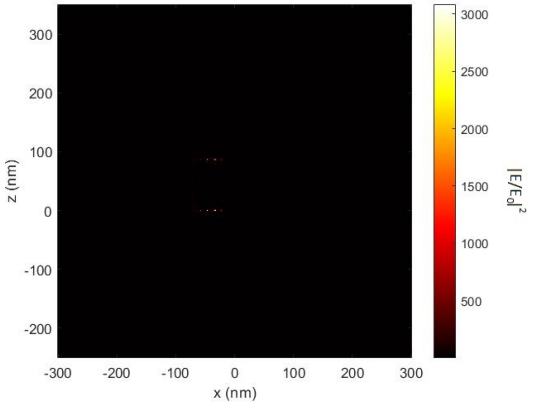

(e) Near-field enhancement of a triangle with 100 nm sides and 100 nm high simulated with a light wavelength of 540 nm.

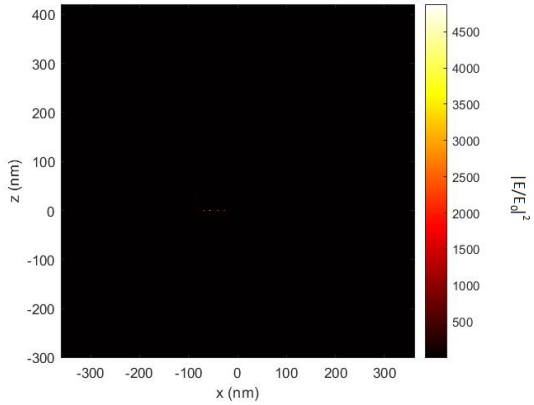

(f) Near-field enhancement of a triangle with 120 nm sides and 100 nm high simulated with a light wavelength of 540 nm.

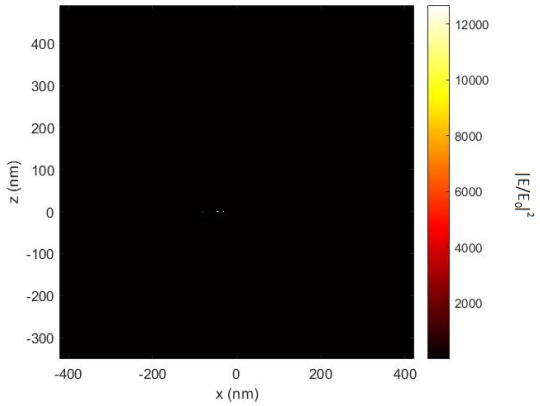

(g) Near-field enhancement of a triangle with 140 nm sides and 100 nm high simulated with a light wavelength of 540 nm.

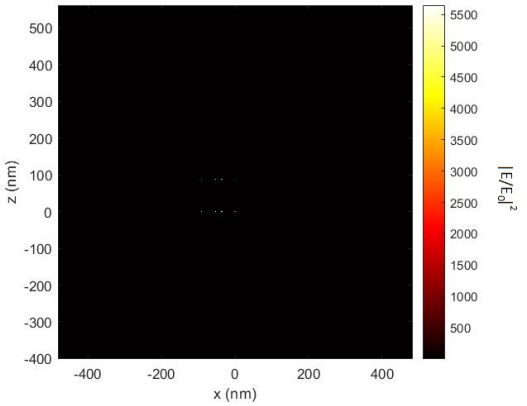

(h) Near-field enhancement of a triangle with 160 nm sides and 100 nm high simulated with a light wavelength of 540 nm.

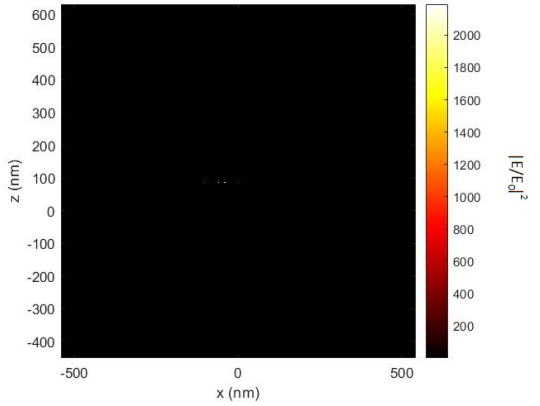

(i) Near-field enhancement of a triangle with 180 nm sides and 100 nm high simulated with a light wavelength of 540 nm.

Figure 54: Near-field enhancements of triangles of various sizes and 100 nm height.

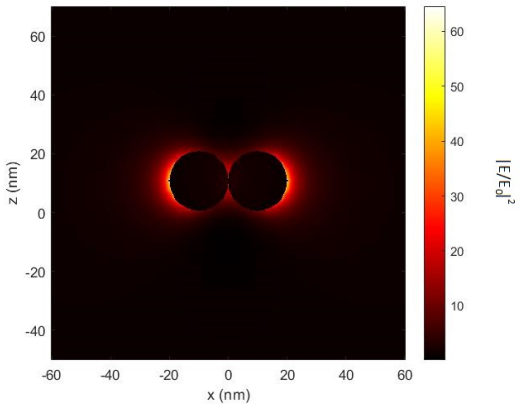

(a) Near-field enhancement of a torus with 20 nm outside diameter and 10 nm inside diameter simulated with a light wavelength of 540 nm.

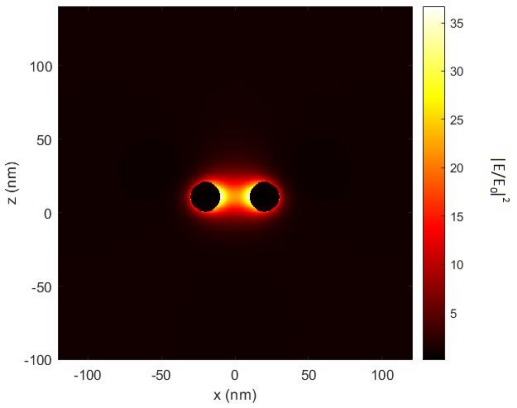

(b) Near-field enhancement of a torus with 40 nm outside diameter and 10 nm inside diameter simulated with a light wavelength of 540 nm.

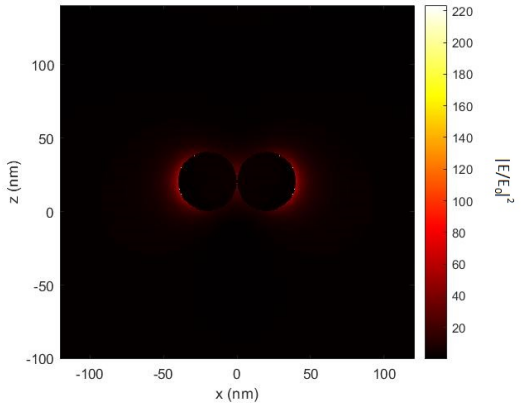

(c) Near-field enhancement of a torus with 40 nm outside diameter and 20 nm inside diameter simulated with a light wavelength of 540 nm.

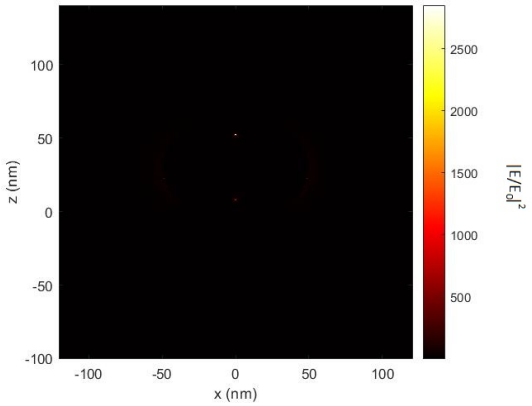

(d) Near-field enhancement of a torus with 40 nm outside diameter and 30 nm inside diameter simulated with a light wavelength of 540 nm.

Figure 55: Near-field enhancement of a torus with 20 nm or 40 nm outside diameter and various inside diameters.

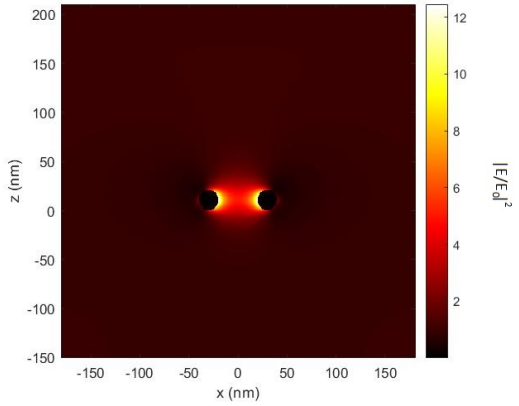

(a) Near-field enhancement of a torus with 60 nm outside diameter and 10 nm inside diameter simulated with a light wavelength of 540 nm.

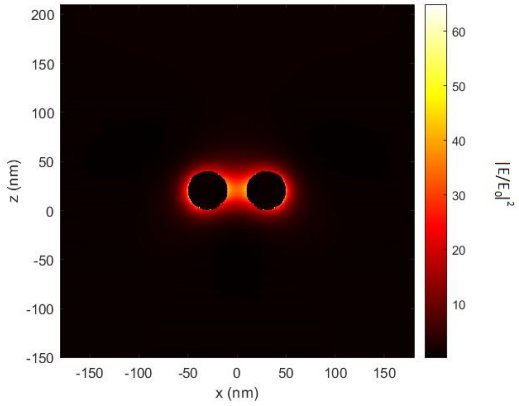

(b) Near-field enhancement of a torus with 60 nm outside diameter and 20 nm inside diameter simulated with a light wavelength of 540 nm.

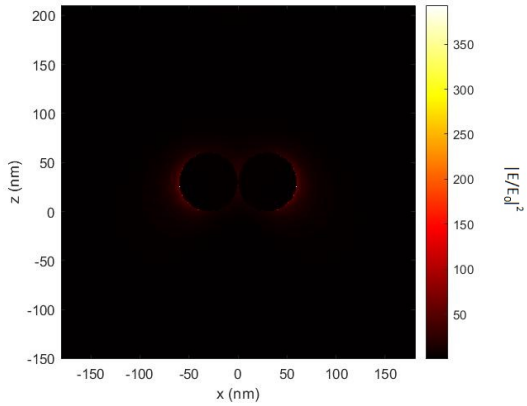

(c) Near-field enhancement of a torus with 60 nm outside diameter and 30 nm inside diameter simulated with a light wavelength of 540 nm.

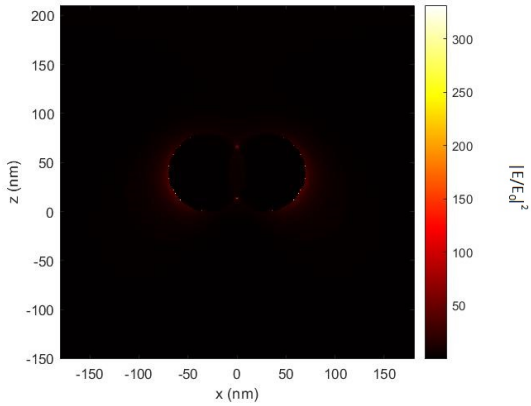

(d) Near-field enhancement of a torus with 60 nm outside diameter and 40 nm inside diameter simulated with a light wavelength of 540 nm.

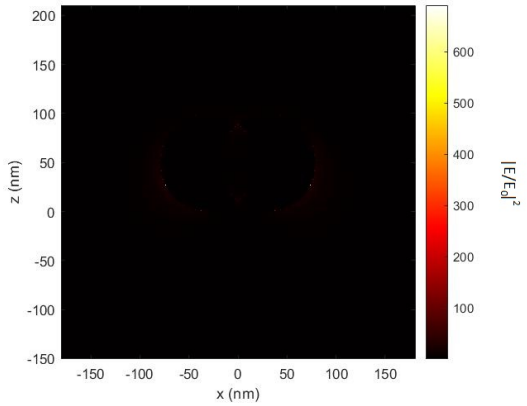

(e) Near-field enhancement of a torus with 60 nm outside diameter and 50 nm inside diameter simulated with a light wavelength of 540 nm.

Figure 56: Near-field enhancement of a torus with 60 nm outside diameter and various inside diameters.

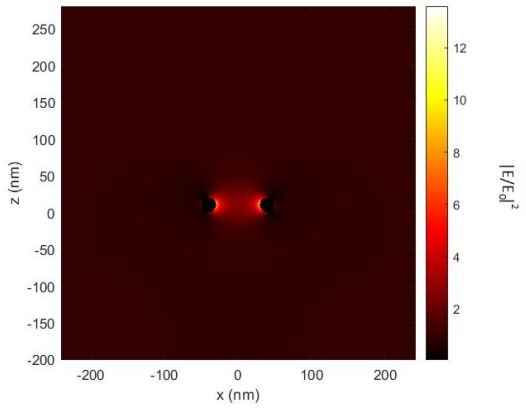

(a) Near-field enhancement of a torus with 80 nm outside diameter and 10 nm inside diameter simulated with a light wavelength of 540 nm.

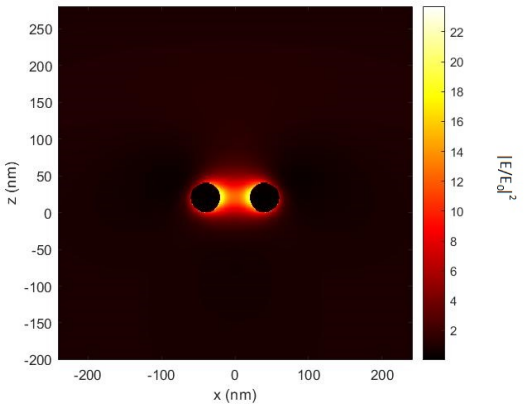

(b) Near-field enhancement of a torus with 80 nm outside diameter and 20 nm inside diameter simulated with a light wavelength of 540 nm.

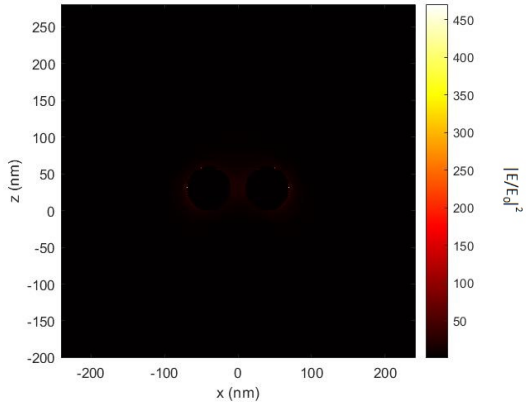

(c) Near-field enhancement of a torus with 80 nm outside diameter and 30 nm inside diameter simulated with a light wavelength of 540 nm.

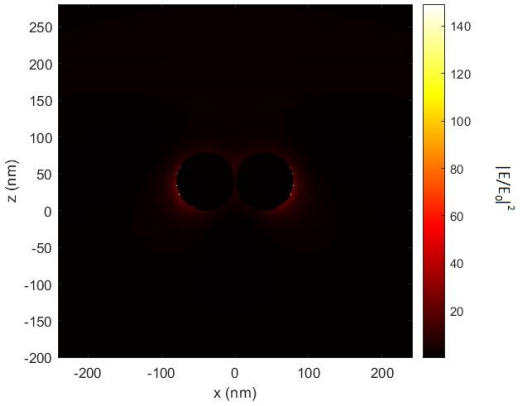

(d) Near-field enhancement of a torus with 80 nm outside diameter and 40 nm inside diameter simulated with a light wavelength of 540 nm.

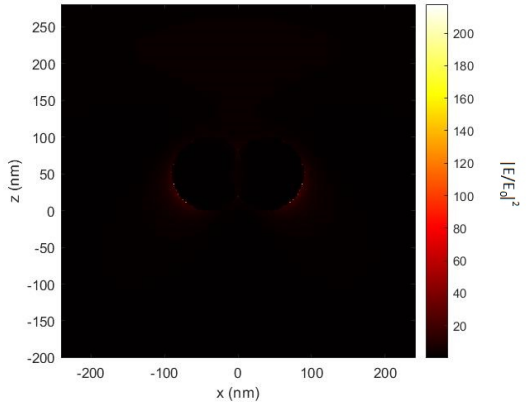

(e) Near-field enhancement of a torus with 80 nm outside diameter and 50 nm inside diameter simulated with a light wavelength of 540 nm.

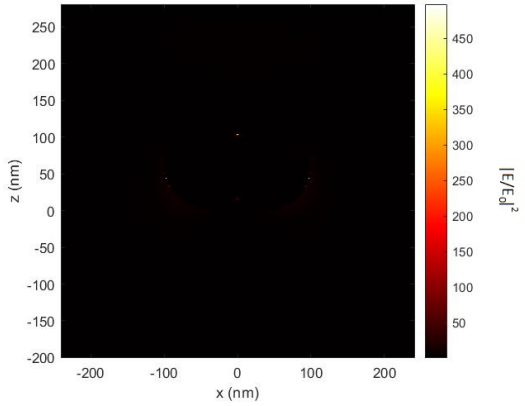

(f) Near-field enhancement of a torus with 80 nm outside diameter and 60 nm inside diameter simulated with a light wavelength of 540 nm.

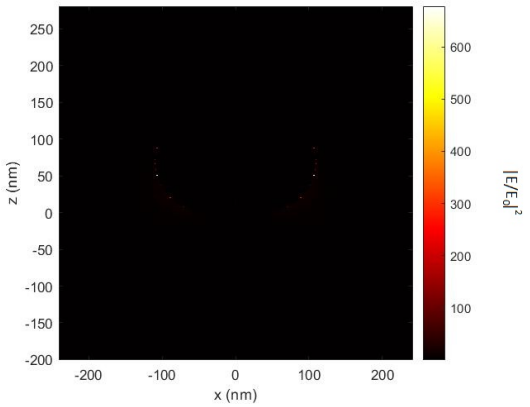

(g) Near-field enhancement of a torus with 80 nm outside diameter and 70 nm inside diameter simulated with a light wavelength of 540 nm.

Figure 57: Near-field enhancement of a torus with 80 nm outside diameter and various inside diameters.

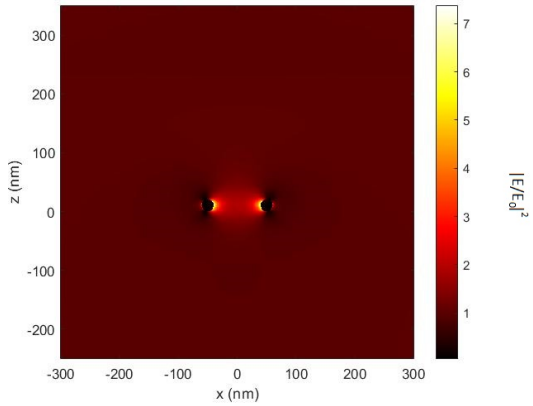

(a) Near-field enhancement of a torus with 100 nm outside diameter and 10 nm inside diameter simulated with a light wavelength of 540 nm.

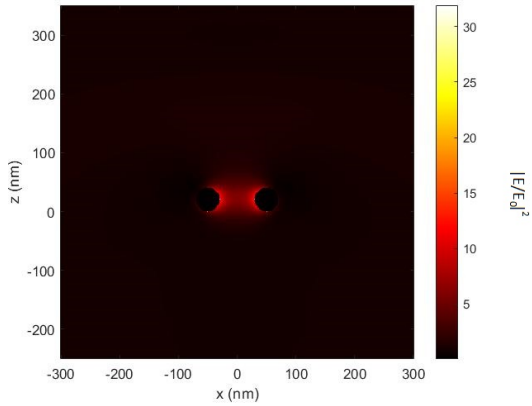

(b) Near-field enhancement of a torus with 100 nm outside diameter and 20 nm inside diameter simulated with a light wavelength of 540 nm.

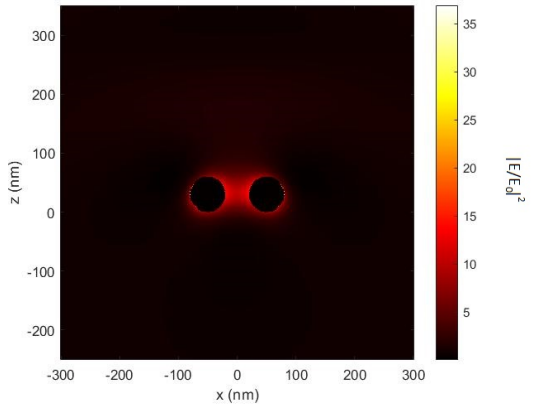

(c) Near-field enhancement of a torus with 100 nm outside diameter and 30 nm inside diameter simulated with a light wavelength of 540 nm.

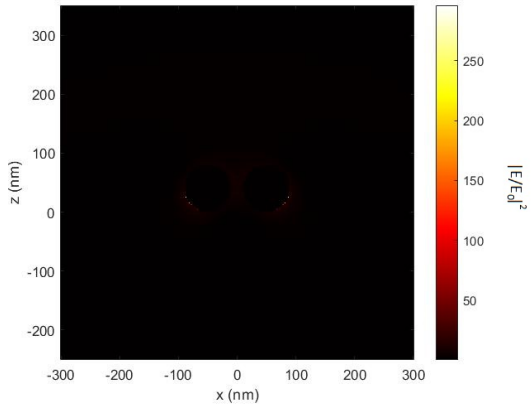

(d) Near-field enhancement of a torus with 100 nm outside diameter and 40 nm inside diameter simulated with a light wavelength of 540 nm.

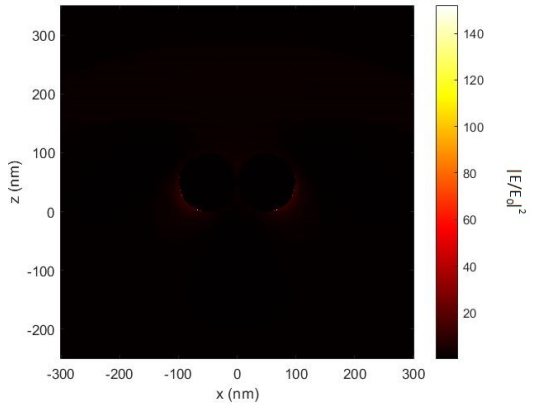

(e) Near-field enhancement of a torus with 100 nm outside diameter and 50 nm inside diameter simulated with a light wavelength of 540 nm.

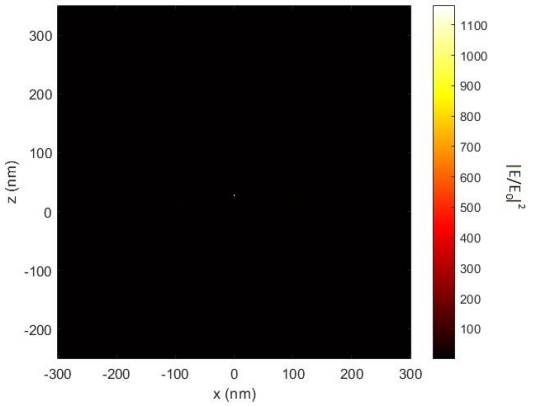

(f) Near-field enhancement of a torus with 100 nm outside diameter and 10 nm inside diameter simulated with a light wavelength of 540 nm.

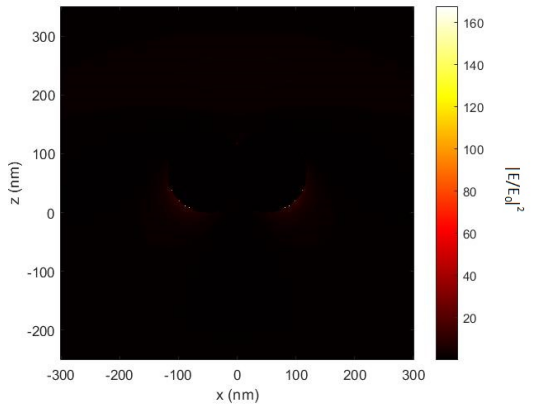

(g) Near-field enhancement of a torus with 100 nm outside diameter and 70 nm inside diameter simulated with a light wavelength of 540 nm.

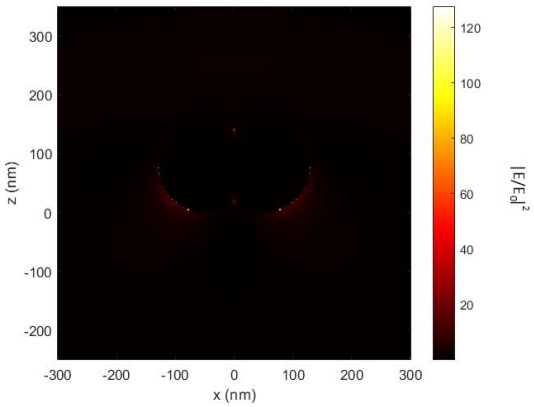

(h) Near-field enhancement of a torus with 100 nm outside diameter and 80 nm inside diameter simulated with a light wavelength of 540 nm.

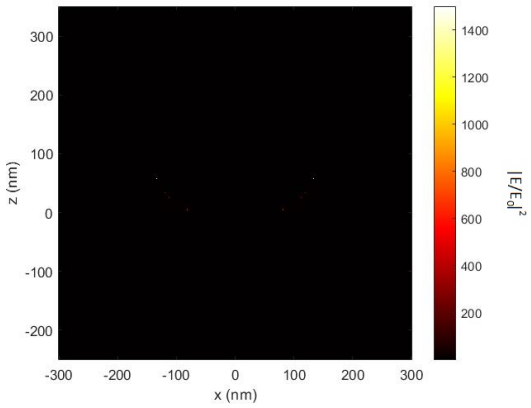

(i) Near-field enhancement of a torus with 100 nm outside diameter and 90 nm inside diameter simulated with a light wavelength of 540 nm.

Figure 58: Near-field enhancement of a torus with 100 nm outside diameter and varying inside diameters.

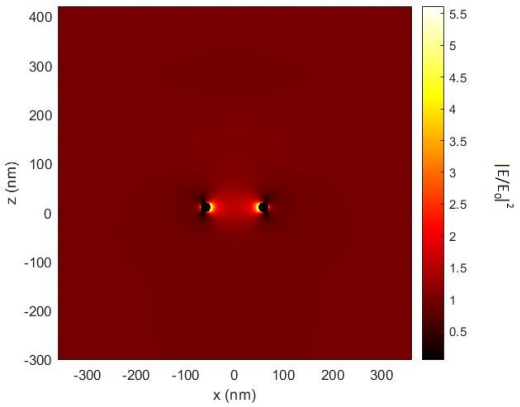

(a) Near-field enhancement of a torus with 120 nm outside diameter and 10 nm inside diameter simulated with a light wavelength of 540 nm.

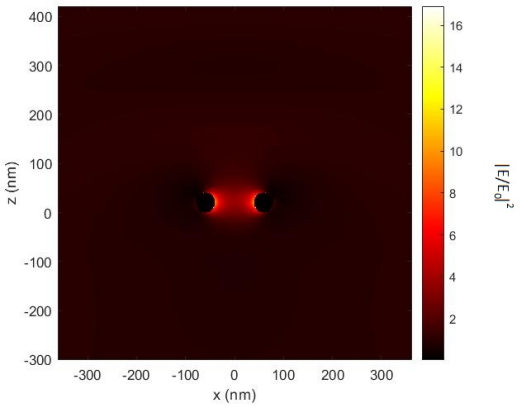

(b) Near-field enhancement of a torus with 120 nm outside diameter and 20 nm inside diameter simulated with a light wavelength of 540 nm.

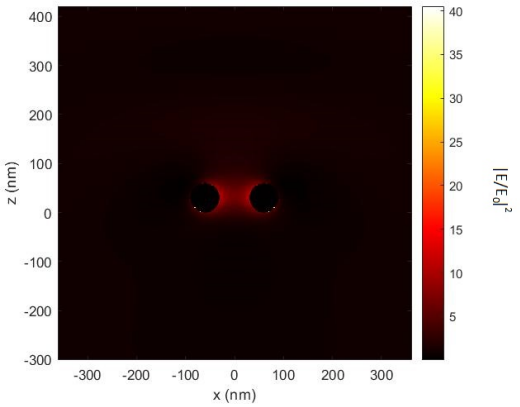

(c) Near-field enhancement of a torus with 120 nm outside diameter and 30 nm inside diameter simulated with a light wavelength of 540 nm.

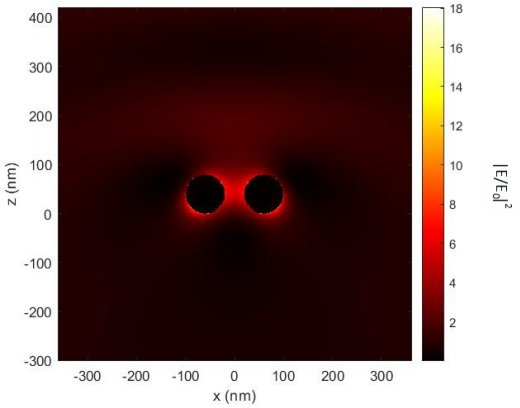

(d) Near-field enhancement of a torus with 120 nm outside diameter and 40 nm inside diameter simulated with a light wavelength of 540 nm.

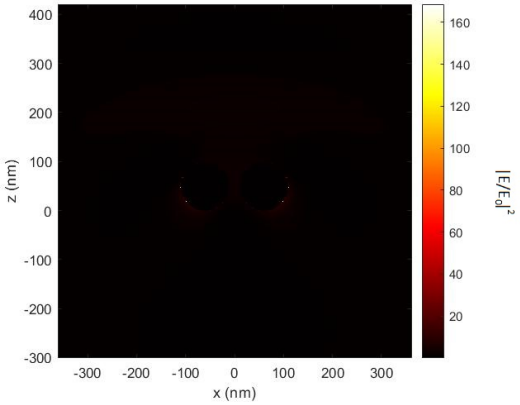

(e) Near-field enhancement of a torus with 120 nm outside diameter and 50 nm inside diameter simulated with a light wavelength of 540 nm.

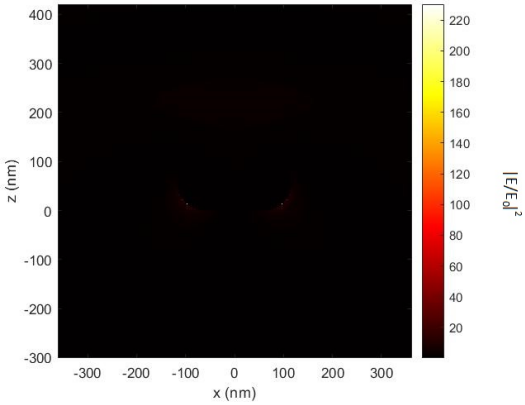

(f) Near-field enhancement of a torus with 120 nm outside diameter and 60 nm inside diameter simulated with a light wavelength of 540 nm.

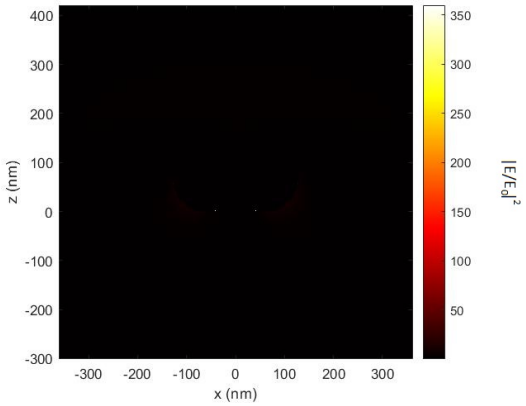

(g) Near-field enhancement of a torus with 120 nm outside diameter and 70 nm inside diameter simulated with a light wavelength of 540 nm.

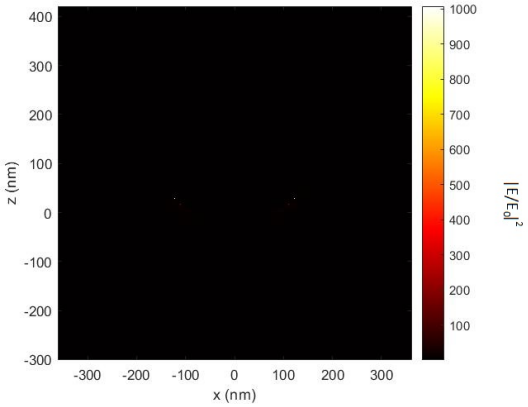

(h) Near-field enhancement of a torus with 120 nm outside diameter and 80 nm inside diameter simulated with a light wavelength of 540 nm.

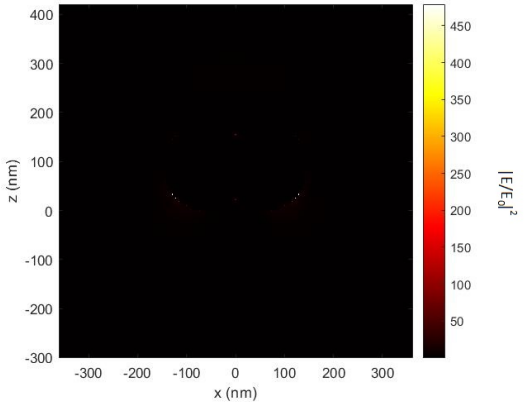

(i) Near-field enhancement of a torus with 120 nm outside diameter and 90 nm inside diameter simulated with a light wavelength of 540 nm.

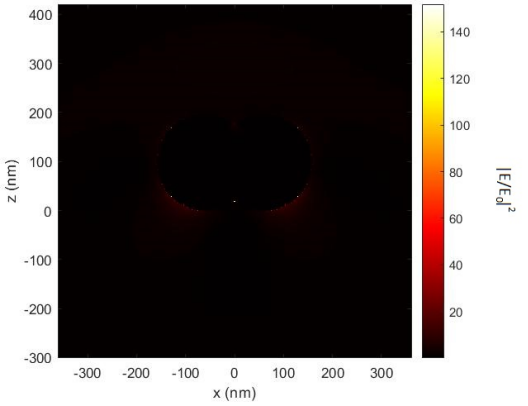

(j) Near-field enhancement of a torus with 120 nm outside diameter and 100 nm inside diameter simulated with a light wavelength of 540 nm.

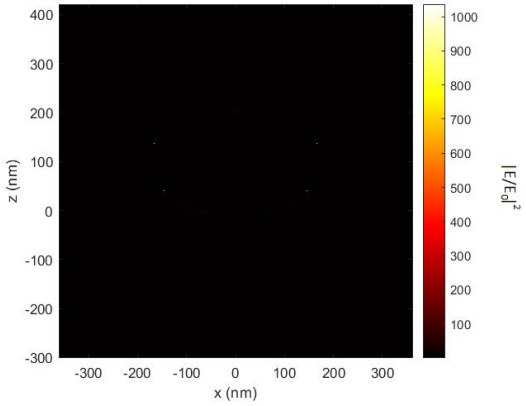

(k) Near-field enhancement of a torus with 120 nm outside diameter and 110 nm inside diameter simulated with a light wavelength of 540 nm.

Figure 59: Near-field enhancement of a torus with 100 nm outside diameter and varying inside diameters.

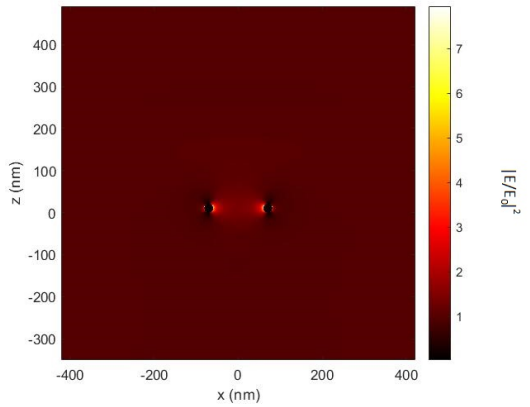

(a) Near-field enhancement of a torus with 140 nm outside diameter and 10 nm inside diameter simulated with a light wavelength of 540 nm.

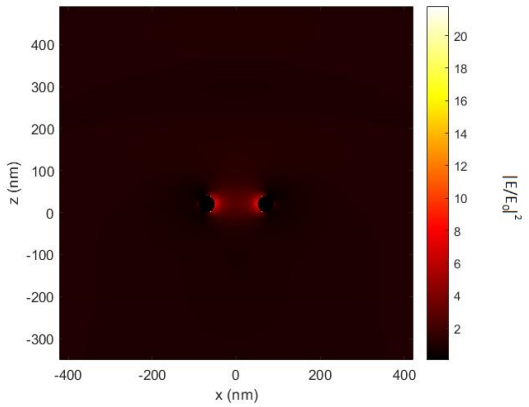

(b) Near-field enhancement of a torus with 140 nm outside diameter and 20 nm inside diameter simulated with a light wavelength of 540 nm.

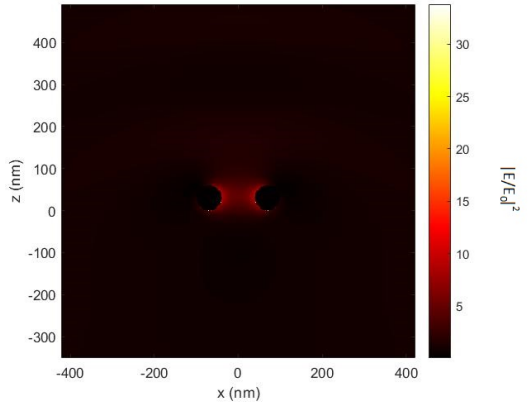

(c) Near-field enhancement of a torus with 140 nm outside diameter and 30 nm inside diameter simulated with a light wavelength of 540 nm.

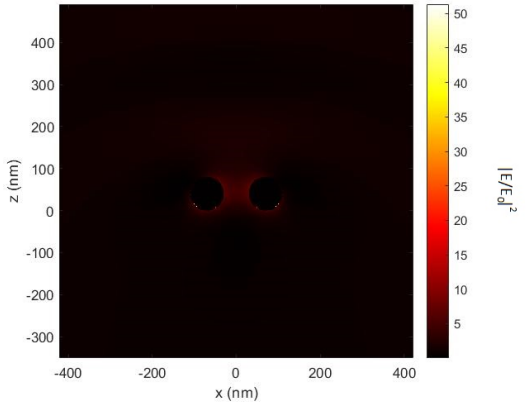

(d) Near-field enhancement of a torus with 140 nm outside diameter and 40 nm inside diameter simulated with a light wavelength of 540 nm.

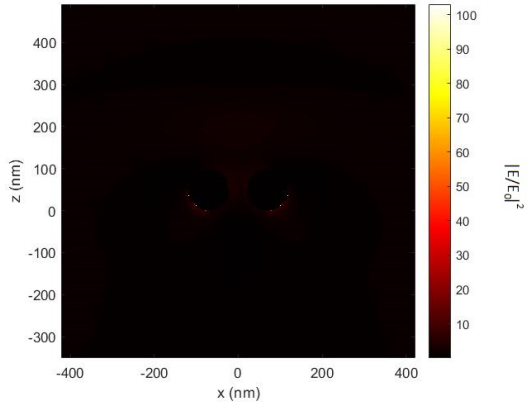

(e) Near-field enhancement of a torus with 140 nm outside diameter and 50 nm inside diameter simulated with a light wavelength of 540 nm.

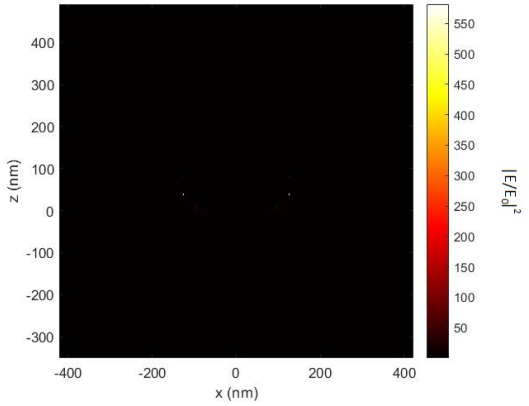

(f) Near-field enhancement of a torus with 140 nm outside diameter and 60 nm inside diameter simulated with a light wavelength of 540 nm.

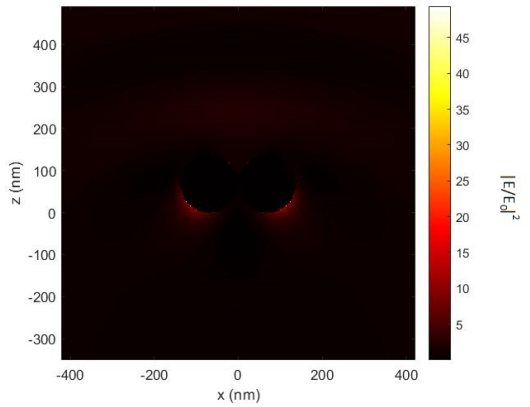

(g) Near-field enhancement of a torus with 140 nm outside diameter and 70 nm inside diameter simulated with a light wavelength of 540 nm.

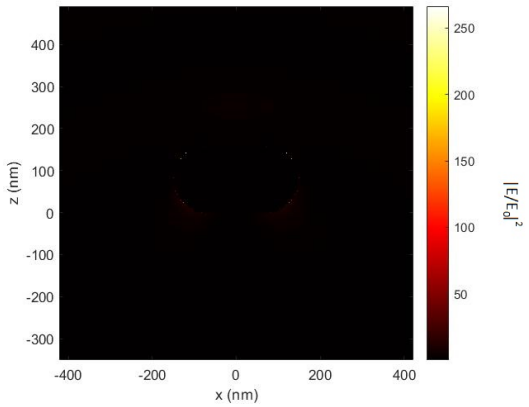

(h) Near-field enhancement of a torus with 140 nm outside diameter and 80 nm inside diameter simulated with a light wavelength of 540 nm.

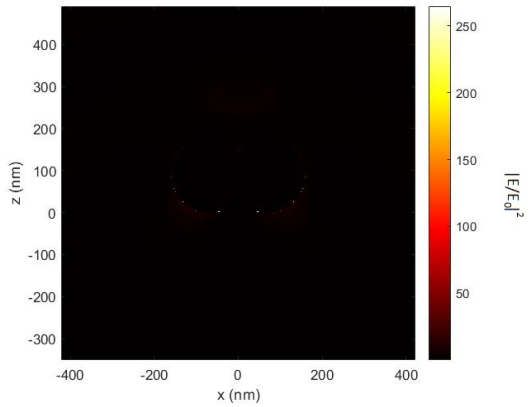

(i) Near-field enhancement of a torus with 140 nm outside diameter and 90 nm inside diameter simulated with a light wavelength of 540 nm.

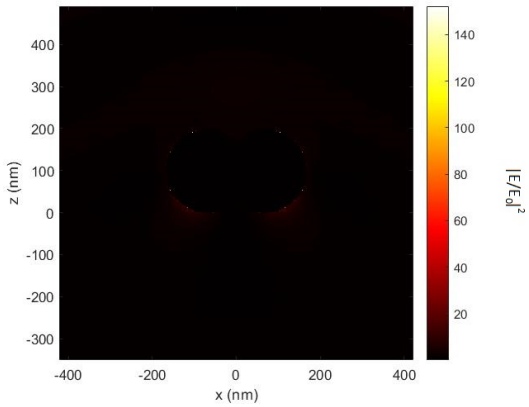

(j) Near-field enhancement of a torus with 140 nm outside diameter and 100 nm inside diameter simulated with a light wavelength of 540 nm.

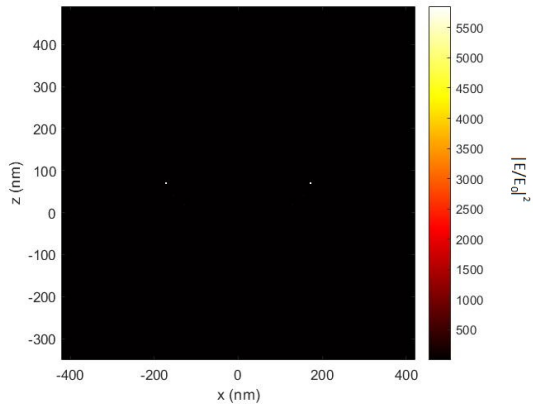

(k) Near-field enhancement of a torus with 140 nm outside diameter and 110 nm inside diameter simulated with a light wavelength of 540 nm.

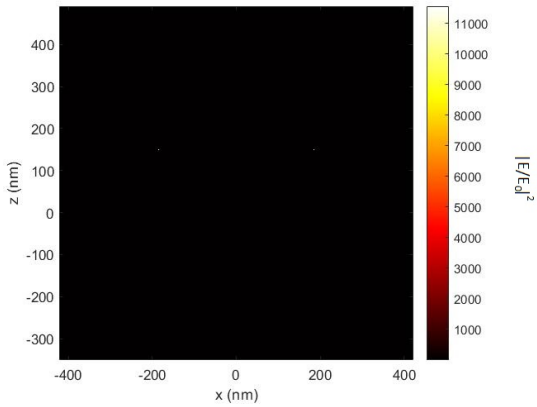

(l) Near-field enhancement of a torus with 140 nm outside diameter and 120 nm inside diameter simulated with a light wavelength of 540 nm.

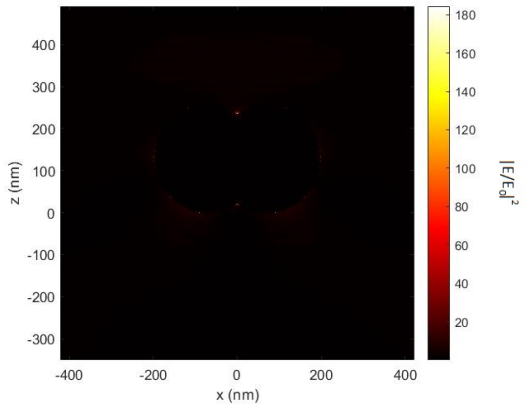

(m) Near-field enhancement of a torus with 140 nm outside diameter and 130 nm inside diameter simulated with a light wavelength of 540 nm.

Figure 60: Near-field enhancement of a torus with 140 nm outside diameter and varying inside diameters.

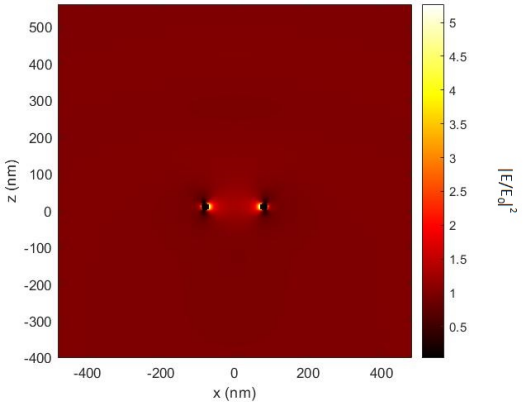

(a) Near-field enhancement of a torus with 160 nm outside diameter and 10 nm inside diameter simulated with a light wavelength of 540 nm.

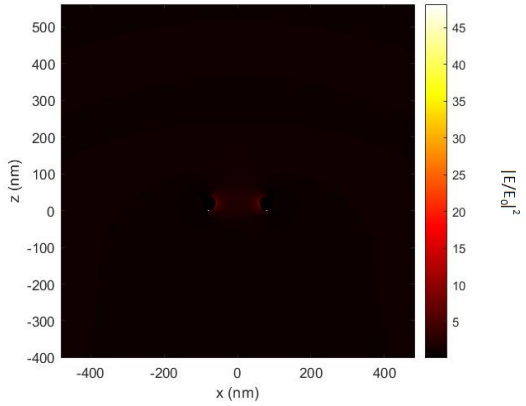

(b) Near-field enhancement of a torus with 160 nm outside diameter and 20 nm inside diameter simulated with a light wavelength of 540 nm.

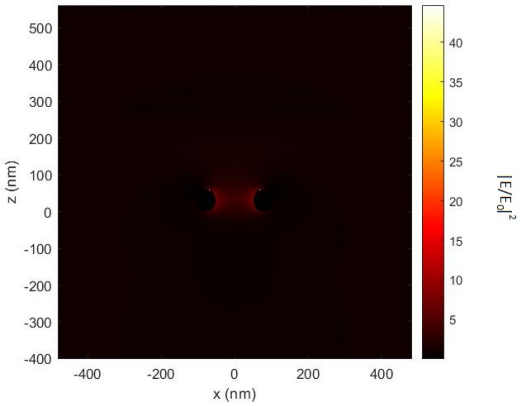

(c) Near-field enhancement of a torus with 160 nm outside diameter and 30 nm inside diameter simulated with a light wavelength of 540 nm.

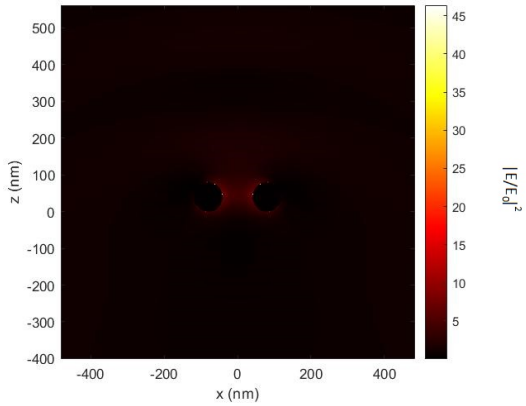

(d) Near-field enhancement of a torus with 160 nm outside diameter and 40 nm inside diameter simulated with a light wavelength of 540 nm.

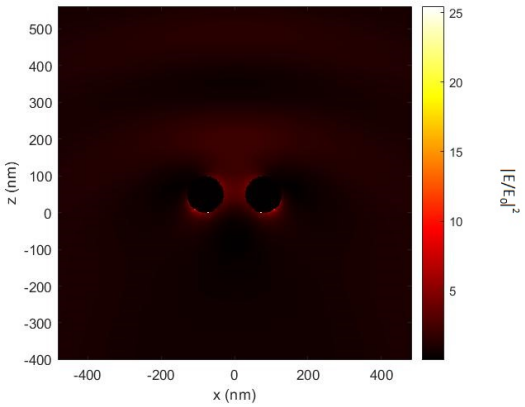

(e) Near-field enhancement of a torus with 160 nm outside diameter and 50 nm inside diameter simulated with a light wavelength of 540 nm.

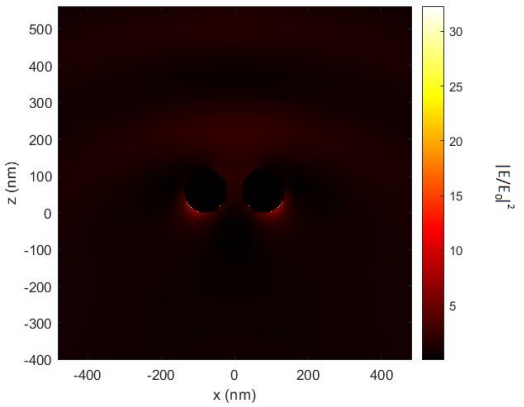

(f) Near-field enhancement of a torus with 160 nm outside diameter and 60 nm inside diameter simulated with a light wavelength of 540 nm.

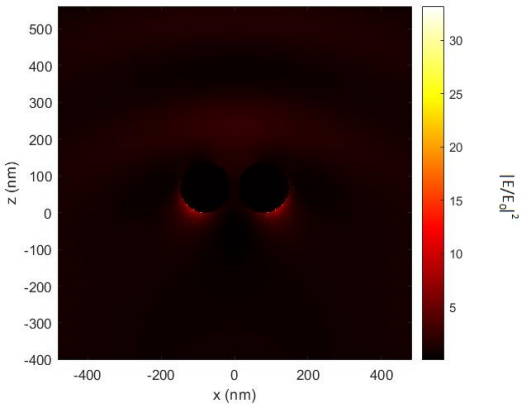

(g) Near-field enhancement of a torus with 160 nm outside diameter and 70 nm inside diameter simulated with a light wavelength of 540 nm.

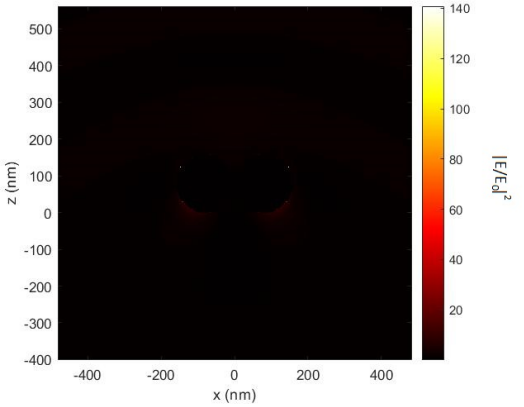

(h) Near-field enhancement of a torus with 160 nm outside diameter and 80 nm inside diameter simulated with a light wavelength of 540 nm.

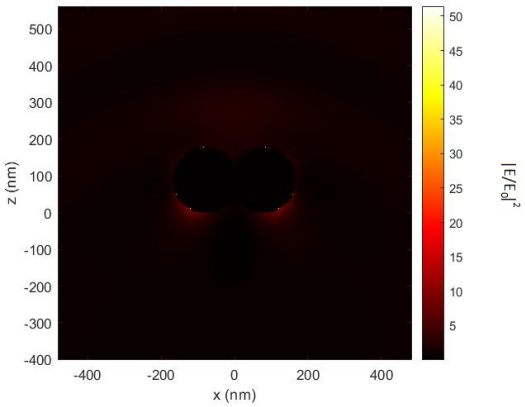

(i) Near-field enhancement of a torus with 160 nm outside diameter and 90 nm inside diameter simulated with a light wavelength of 540 nm.

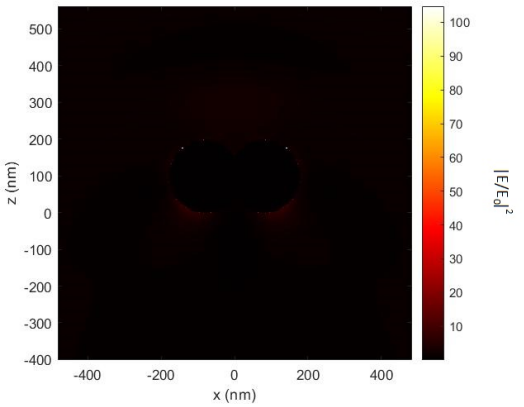

(j) Near-field enhancement of a torus with 160 nm outside diameter and 100 nm inside diameter simulated with a light wavelength of 540 nm.

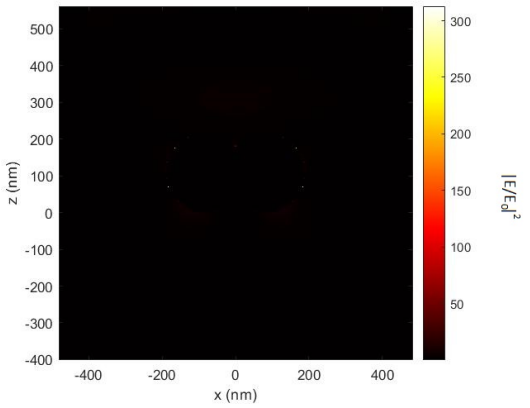

(k) Near-field enhancement of a torus with 160 nm outside diameter and 110 nm inside diameter simulated with a light wavelength of 540 nm.

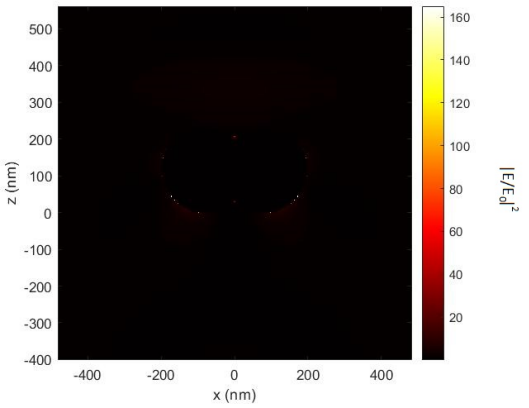

(l) Near-field enhancement of a torus with 160 nm outside diameter and 120 nm inside diameter simulated with a light wavelength of 540 nm.

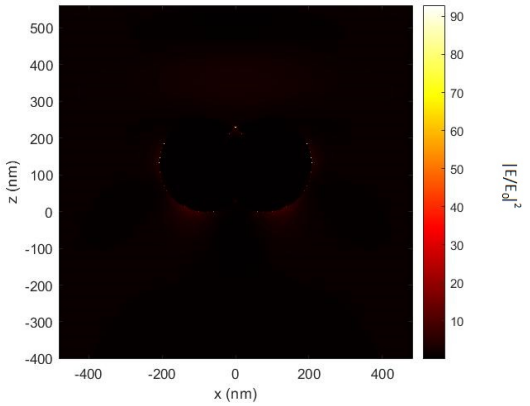

(m) Near-field enhancement of a torus with 160 nm outside diameter and 130 nm inside diameter simulated with a light wavelength of 540 nm.

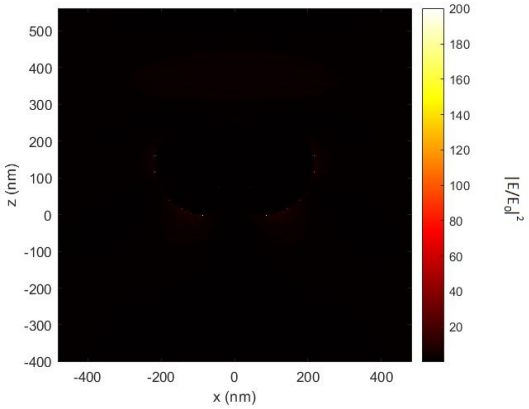

(n) Near-field enhancement of a torus with 160 nm outside diameter and 140 nm inside diameter simulated with a light wavelength of 540 nm.

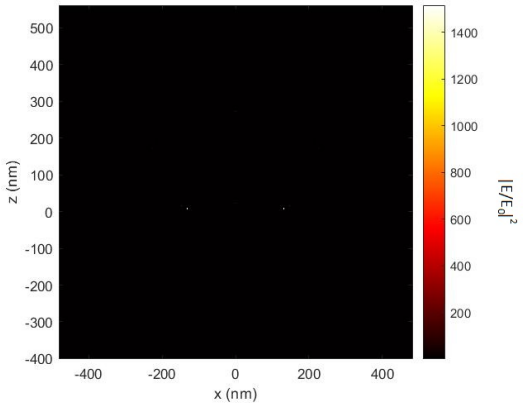

(o) Near-field enhancement of a torus with 160 nm outside diameter and 150 nm inside diameter simulated with a light wavelength of 540 nm.

Figure 61: Near-field enhancement of a torus with 160 nm outside diameter and varying inside diameters.

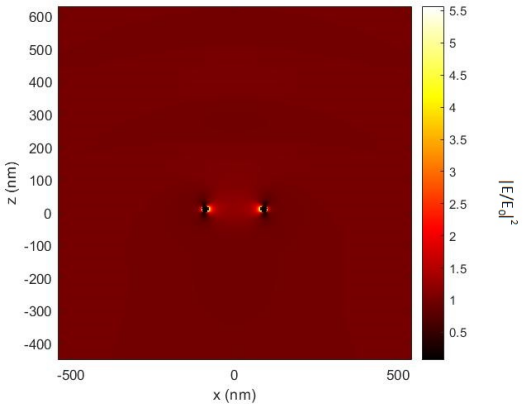

(a) Near-field enhancement of a torus with 180 nm outside diameter and 10 nm inside diameter simulated with a light wavelength of 540 nm.

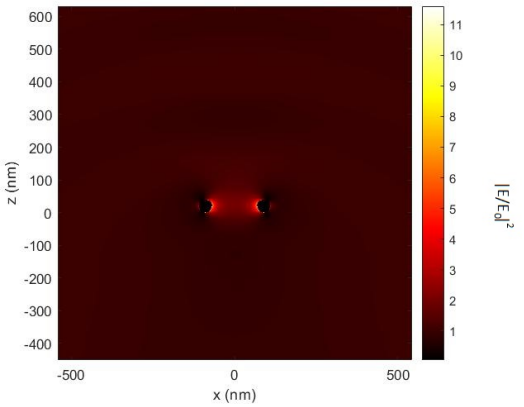

(b) Near-field enhancement of a torus with 180 nm outside diameter and 20 nm inside diameter simulated with a light wavelength of 540 nm.

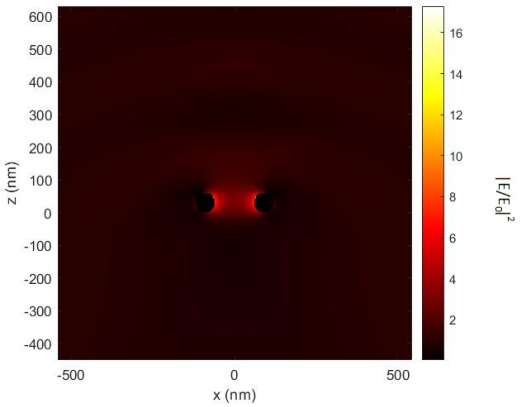

(c) Near-field enhancement of a torus with 180 nm outside diameter and 30 nm inside diameter simulated with a light wavelength of 540 nm.

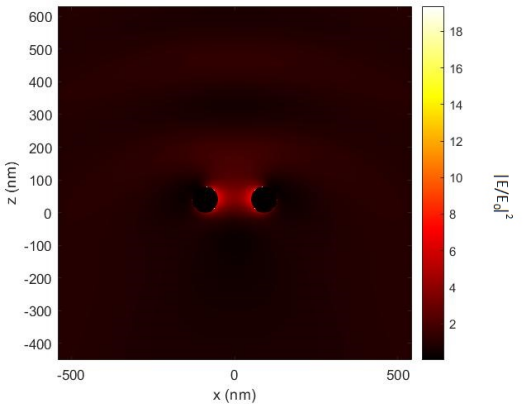

(d) Near-field enhancement of a torus with 180 nm outside diameter and 40 nm inside diameter simulated with a light wavelength of 540 nm.

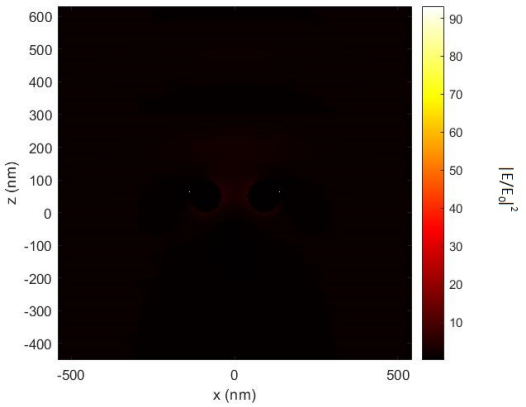

(e) Near-field enhancement of a torus with 180 nm outside diameter and 50 nm inside diameter simulated with a light wavelength of 540 nm.

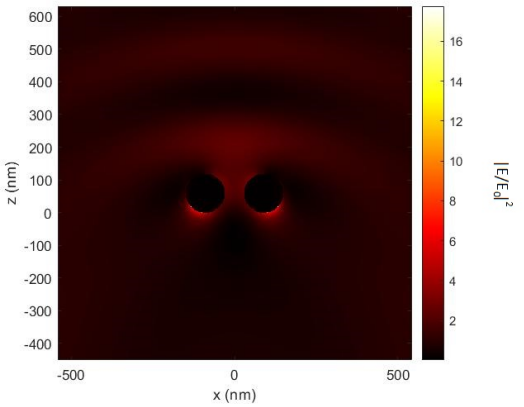

(f) Near-field enhancement of a torus with 180 nm outside diameter and 60 nm inside diameter simulated with a light wavelength of 540 nm.

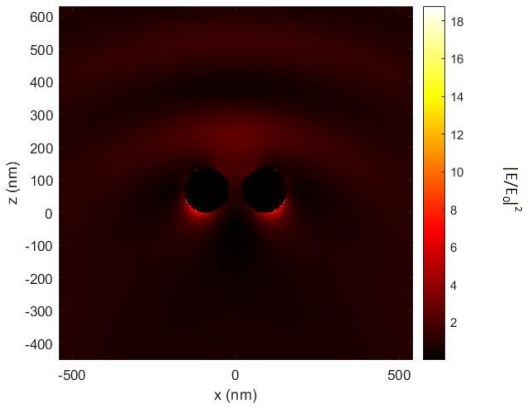

(g) Near-field enhancement of a torus with 180 nm outside diameter and 70 nm inside diameter simulated with a light wavelength of 540 nm.

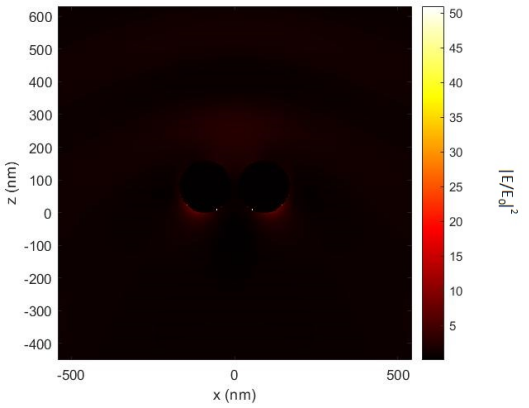

(h) Near-field enhancement of a torus with 180 nm outside diameter and 80 nm inside diameter simulated with a light wavelength of 540 nm.

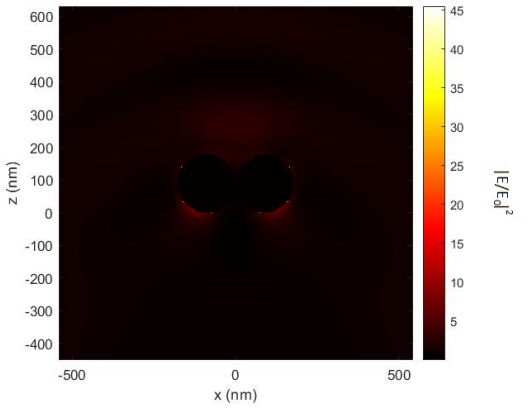

(i) Near-field enhancement of a torus with 180 nm outside diameter and 90 nm inside diameter simulated with a light wavelength of 540 nm.

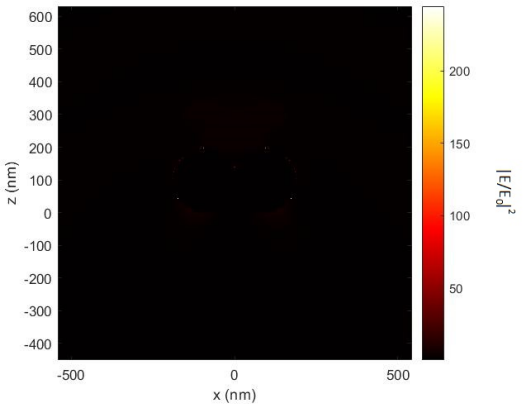

(j) Near-field enhancement of a torus with 180 nm outside diameter and 100 nm inside diameter simulated with a light wavelength of 540 nm.

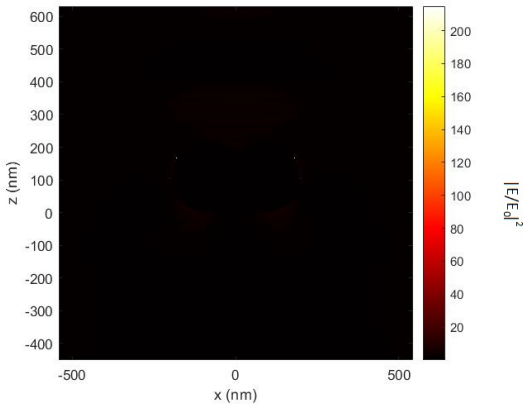

(k) Near-field enhancement of a torus with 180 nm outside diameter and 110 nm inside diameter simulated with a light wavelength of 540 nm.

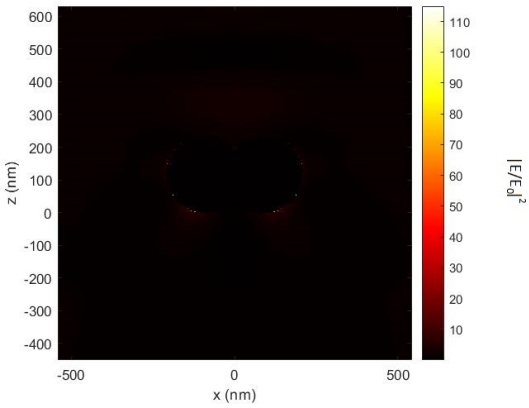

(l) Near-field enhancement of a torus with 180 nm outside diameter and 120 nm inside diameter simulated with a light wavelength of 540 nm.

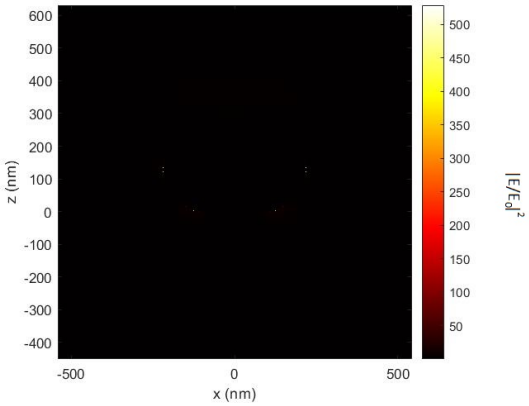

(m) Near-field enhancement of a torus with 180 nm outside diameter and 130 nm inside diameter simulated with a light wavelength of 540 nm.

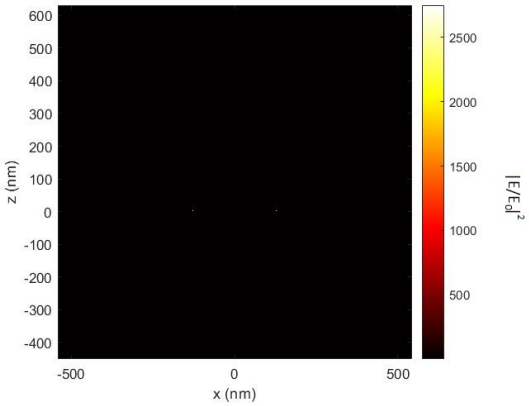

(n) Near-field enhancement of a torus with 180 nm outside diameter and 140 nm inside diameter simulated with a light wavelength of 540 nm.

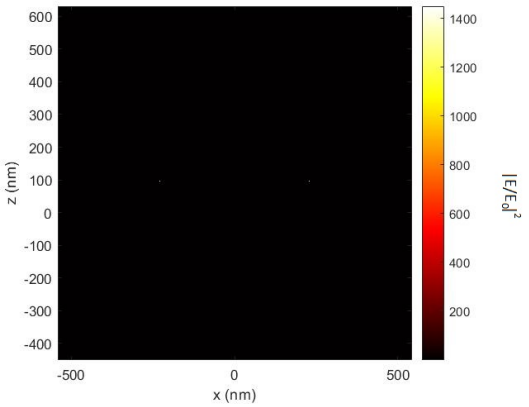

(o) Near-field enhancement of a torus with 180 nm outside diameter and 150 nm inside diameter simulated with a light wavelength of 540 nm.

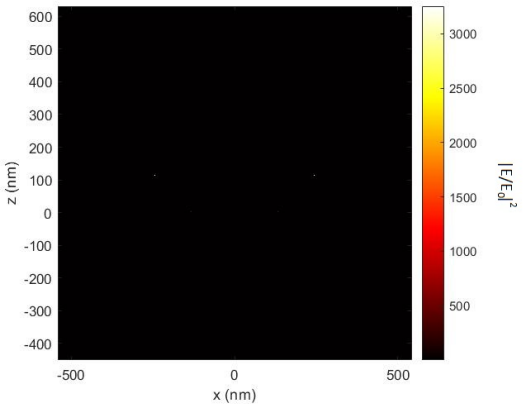

(p) Near-field enhancement of a torus with 180 nm outside diameter and 160 nm inside diameter simulated with a light wavelength of 540 nm.

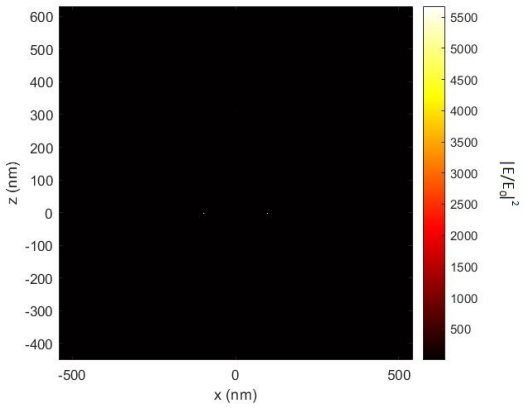

(q) Near-field enhancement of a torus with 180 nm outside diameter and 170 nm inside diameter simulated with a light wavelength of 540 nm.

Figure 62: Near-field enhancement of a torus with 180 nm outside diameter and varying inside diameters.